uOttawa

L'Université canadienne
Canada's university

Cardiac sympathetic innervation and PGP 9.5 expression by cardiomyocytes in rats after myocardial infarction.

Effects of central MR blockade.

Anastasia Drobysheva

This thesis is submitted to the Faculty of Graduate and Postdoctoral Studies as a partial fulfillment of the requirements for the M.Sc degree in Cellular and Molecular Medicine.

05.11.2013

Department of Cellular and Molecular Medicine
Faculty of Medicine
University of Ottawa

Abstract

Central mechanisms involving aldosterone - mineralocorticoid receptor (MR) activation mediate the increase in sympathetic tone after myocardial infarction (MI). We hypothesized that an increase in cardiac sympathetic activity (CSA) post MI facilitates cardiac sympathetic axonal sprouting, and that central MR blockade attenuates CSA and reduces cardiac sympathetic hyperinnervation post MI.

Western blotting and qRT-PCR were used to assess protein and gene expression, and fluorescent immunohistochemistry was used to study changes in sympathetic innervation. Tyrosine hydroxylase (TH) and Norepinephrine transporter protein content in the non-infarcted base of the heart remained unaltered. In contrast, protein gene product (PGP 9.5) protein was significantly increased 2 fold in the base of the heart, and 6 fold in the peri-infarct area at 1 wk post MI, and associated with increased ubiquitin expression. Cardiac myocytes rather than sympathetic axons were identified as the main source of elevated PGP 9.5 expression. At the infarct border sympathetic hyperinnervation was observed with a 4 fold increase in growth associated protein 43 (GAP 43), a 2 fold increase in TH and a 50% increase in PGP 9.5 positive fibers when compared to the epicardial side of the left ventricle in sham rats. Central infusion of the MR blocker eplerenone at 5 ug/day for 9 days post MI markedly attenuated the increase in TH, GAP 43 and PGP 9.5 nerve densities at the infarct border.

Central MR blockade may attenuate sympathetic hyperinnervation by several mechanisms, including decreasing CSA post MI, or affecting expression or function of nerve growth factor protein. Marked PGP 9.5 expression occurs in cardiomyocytes early post MI, which may contribute to the increase in ubiquitin and the early cardiac remodeling post MI.

Table of content

List of Tables

List of Figures

List of Abbreviations

ACh:	Acetylcholine
Angiotensin II	Ang II
BH_4:	Tetrahydrobiopterin
BP:	Blood pressure
CHF:	Congestive heart failure
CNS:	Central nervous system
CSA:	Cardiac sympathetic activity
CSNA:	Cardiac sympathetic nerve activity
DAG:	Diacylglycerol
EF:	Ejection fraction
ENaC:	Epithelial sodium channel
GAP 43:	Growth associated protein 43
HR:	Heart rate
ICV:	Intracerebroventricular
IP3:	Inositol triphosphate
LSG	Left stellate ganglion
LV:	Left ventricle
MAP	Mean arterial pressure
MI:	Myocardial infarction
MR:	Mineralocorticoid receptors
MSNA	Muscle sympathetic nerve activity
MW:	Molecular weight

NE :	Norepinephrine
NET:	Norepinephrine transporter
NGF:	Nerve growth factor
NOS:	Nitric oxide synthase
PGP 9.5:	Protein gene product
PKA:	Protein kinase A
PKC:	Protein kinase C
PKG:	Protein kinase G
PVN:	Paraventricular Nucleus
RAAS :	Renin-angiotensin-aldosterone system
RSG	Right stellate ganglion
RSNA:	Renal Sympathetic Nerve Activity
RV:	Right ventricle
SFO:	Subfornical Organ
SGX	Stellate ganglionectomy
SON:	Supraoptic Nucleus
ROS:	Reactive oxygen species
SE:	Standard error
SG:	Stellate ganglion
SIF:	Small intensity fluorescent cells
TH:	Tyrosine hydroxylase
UCH:	Ubiquitin carboxyl-terminal hydrolases
UPS:	Ubiquitin proteasome system

VIP: Vasoactive intestinal peptide

VMAT2: Vesicular monoamine transporter 2

Acknowledgements

Foremost, I would like to express profound gratitude to my supervisor **Dr. Frans Leenen**, for accepting me as a graduate student to be a part of his research team. Thank you for dedicating your time to teaching me and providing guidance and mentorship. His continuous support, encouragement and knowledge helped tremendously to carry out this project. He taught me how to analyze scientific literature, write in the language of science, interpret data, give presentations, multifunction productively, set priorities, use time wisely, and be critical. Thank you so much for that. Also, thank you for supporting me in aspiration to practice medicine in Northern America and giving me time to prepare for my board exams.

I want to express sincere gratitude to my co-supervisors, **Dr. James Van Huysse** and **Dr. Patrick Burgon** for valuable suggestions and critique at the advisory committee meetings.

Special thanks to **Roselyn White**, for kindness, friendship, positivity and encouragement. She introduced me to the lab, taught me multiple lab techniques and always was there when "things did not work". Thank you so much for that!

Danielle Oja, thank you for your positive attitude, encouraging spirit and help with formatting documents and handling academic formalities. Thank you for prompt replies, availability, organizing fun events and spa products from your garden!

Hongwei Wang, thank you for teaching me PCR technique and perfecting my Western blots, your patience and professionalism are so much appreciated.

Monir Ahmad, thank you for sharing your office with me, performing all surgeries in this research project and great conversations we had.

Bing Huang, thank you for your help with MR blockade experiment, your friendly smile and words of support.

Peter Rippstein, thank you for your kindness, support and sharing your knowledge and expertise on microscopy with me.

Dr. Sophie Jackson, thank you so much for introducing me to science, and generous hours of discussion, education and advice. It was in your lab in Cambridge where I learned how to use a pipette and took first steps in research!

Dr. Natalia Bagisheva, Dr. Anatoly Yarkov, Dr. Natalia Yashkina, thank you so much for your unwavering support throughout medical school and residency in Omsk, for providing inspiration and sharing your passion and devotion to patients and medicine.

Thanks to my lab mates, **Missalie, Naimeh, Katherine and Alex** for helping me with lab work, and sharing fun moments outside of the lab!

Sara Ahmadi, thank you for being my friend in the lab from day one. Thank you for being there during experiment troubleshooting, and awesome times we had at after work hours.

Larisa Romanova, thank you for being my person. **Kinna Degree Scearce**, thank you for being my sister. **Aaron Johnson**, thank you for being my friend. **Yulia Yamineva**, thank you for being my role model. **Antonina Kurtova**, thank you for your amazing heart. **Kristina Mikheeva**, thank you for being so amazing. **Binoy Kampmark**, thank you for believing in me. **Ioannis Apostolakos**, thank you for your wisdom. **Naya Dubanaeva**, thank you for being life-long friend. **Angela Degree Hernandez**, thank you for being my mom in the USA and giving your love to me.

I want to express cordial gratitude, love and appreciation to **my parents, grandmother Lena, and the rest of my family in Russia** for your unconditional love, patience, encouragement and supporting my ambitions and dreams. Special thank you to my family in Canada, **Arthur and Daniel Howe** for your love, understanding, patience and putting up with my busy schedule.

1. Introduction

1.1. Overview

Congestive heart failure (CHF) develops in many patients after acute myocardial infarction (MI) and remains the primary cause of post MI morbidity and mortality (Torabi et al. 2008). Multiple changes in the viable myocardium i.e. apoptosis of viable cells, interstitial fibrosis formation, cardiomyocytes hypertrophy and late-phase ventricular dilation are maladaptive and contribute to impairment of ventricular performance over time (Lal et al. 2004). Activation of the circulating and tissue-specific renin-angiotensin-aldosterone system (RAAS) and increased cardiac sympathetic activity play important roles in the development and progression of CHF post MI (Hayashi et al. 2003, Huang and Leenen 2009, Jugdutt et al. 2007, Westcott et al. 2009).

The knowledge regarding cardiac sympathetic activity (CSA) post MI and in CHF is rather limited, especially in humans. In moderate heart failure in humans initially there is a selective increase in CSA, which is then followed by augmented sympathetic outflow to skeletal muscle and kidneys. In severe heart failure cardiac norepinephrine (NE) spillover rate is increased three fold and total body spillover is increased 60% vs. healthy subjects (Rundqvist et al. 1997). In animal models there is evidence of increased CSA in both acute and chronic phases post MI. In rats, direct recordings from cardiac postganglionic sympathetic nerves demonstrate that cardiac sympathetic drive increases by 100% within first hours after MI (Schwenke et al. 2008). In conscious sheep cardiac sympathetic nerve activity (CSNA) was significantly increased by the second hour post MI, and remained elevated by 2 fold for at least one week (Jardine et al. 2005). Chronically at 8 weeks post MI in rats NE turnover rate was increased ~3 fold in the non-infarcted cardiac

left ventricle (LV), skeletal muscle, duodenum and whole kidney, but remained unaltered in spleen, liver and renal medulla (Patel et al. 2000). Increased CSA after MI may contribute to development of cardiac sympathetic hyperinnervation, since long-term subthreshold electrical stimulation in normal dogs produces increased nerve fiber density in the heart, and in dogs post MI augments cardiac sympathetic hyperinnervation (Swissa et al. 2004). In rodents sympathetic hyperinnervation occurs at the infarct border/peri-infarct area acutely (3-7 days) post MI (El-Helou et al. 2008, Li et al. 2004, Oh et al. 2006), and to a less extend in remote cardiac areas chronically (Oh et al. 2006, Yuan et al. 2009).

Post MI, a chronic increase in CSNA may be associated with increased tyrosine hydroxylase (TH) and norepinephrine transporter (NET) gene expression in the heart and stellate ganglia. The conversion of tyrosine to DOPA by TH is a rate-limiting step in NE synthesis, and regulation of TH molecules number and enzyme activity is the main mechanism for controlling NE synthesis in the heart (Dunkley et al. 2004, Kumer and Vrana 1996). The NET protein recycles NE by shifting it from the synapse back into axonal vesicles for storage and later use (Esler et al. 1990). Increased sympathetic nerve activity and membrane depolarization may be important factors in long-term regulation of TH enzyme activity and gene expression (Kilbourne et al. 1992). Depolarization is likely to upregulate NET expression via elevated catecholamine content rather than increased nerve activity, since sympathetic neurons exhibit elevated NE uptake, NET mRNA and protein in the presence of NE alone (Habecker et al. 2006). A 2-3 fold increase in NET and TH mRNA in stellate ganglia, and in NET and TH protein in the non-infarcted base of the heart was observed in rats 1 week post ischaemia-reperfusion.

TH and NET expression was normalized to the neuronal marker protein gene product (PGP 9.5) in order control for variation in innervation (Parrish et al. 2008). However, extra-neuronal expression of PGP 9.5 might take place in the heart and in patients with dilated cardiomyopathy cardiomyocytes exhibit strong PGP 9.5 immunoreactivity (Weekes et al. 2003). Whether an increase in CSA is associated with upregulation of TH and NET expression in cardiac sympathetic neurons post MI induced by permanent coronary artery ligation has not yet been studied.

There is strong evidence that central mechanisms play an essential role in controlling the sympathetic tone after MI. As one of the mechanisms elevated levels of circulating Angiotensin II (Ang II) initially activate the subfornical organ (SFO), and angiotensinergic neurons projecting from the SFO stimulate aldosterone synthesis and release. Via epithelial sodium channel (ENaC) and "ouabain", aldosterone may activate neurons in the paraventricular nucleus (PVN) of the hypothalamus, leading to sustained activation of angiotensinergic pathways and sympathetic hyperactivity (Huang and Leenen 2009). Central blockade of mineralocorticoid receptors (MR), "ouabain" or AT_1-receptors in rats post MI similarly inhibits sympathetic hyperactivity and circulatory and cardiac RAAS activation and attenuates cardiac remodeling and left ventricular dysfunction (Huang and Leenen 2005, 2009, Leenen et al. 1999b).

Effects of central MR blockade have been previously assessed on several parameters of sympathetic activity, such as plasma NE level, resting sympathetic tone and degree of sympathetic reactivity to stress (Huang and Leenen 2005, Lal et al. 2004). It is reasonable to expect attenuation of cardiac sympathetic hyperactivity post MI by central MR blockade.

The following topics will be addressed in the literature review:

a. MI and CHF
b. Sympathetic innervation of the heart and cardiac intrinsic nervous system
c. Synthesis, storage and re-uptake of NE. Regulation of TH enzyme activity and gene expression. Regulation of NET activity and gene expression.
d. Adrenergic receptors
e. Cardiac sympathetic hyperactivity post MI. Studies in humans. Studies in animal models.
f. Molecular studies on cardiac sympathetic activity, PGP 9.5 and Ubiquitin proteasome system.
g. Central mechanisms contributing to sympathetic hyperactivity post MI

1.2. Myocardial infarction and heart failure

Ischemic heart disease and acute MI are responsible for three-quarters of all cases of CHF in North America and Western Europe (Kasper et al. 2005). In recent decades the overall age- and sex-standardized rate of death from MI has declined by 38 %. However, at the same time, the rate for acute MI diminished only by 9 % (Tu et al. 2009). The increase in survival rates after MI has lead to increased number of patients who develop progressive heart failure after the acute cardiac event. In 896 patients with the hospital diagnosis of acute MI in 1998, 562 (67%) developed CHF and majority died in the next 6 years (Torabi et al. 2008). In Montreal the annual rate of admission for CHF increased from 92 per 10 000 population in 1990/91 to 124 per 10 000 population in 1997/98 ($p <$ 0.01). At the present time in Canada CHF is associated with the second highest total

number of hospital days and third highest number of patients affected (Tsuyuki et al. 2003). That makes it crucial to study specific mechanisms that promote cardiac remodeling and deterioration of ventricular function, leading to the development of CHF after MI. Several systemic and organ-specific mechanisms have been investigated in association with cardiac remodeling post MI. Activation of CSNA and circulating and tissue-based RAAS are thought to play a dominant role in the development of CHF post MI (Hayashi et al. 2003, Jugdutt et al. 2007, Packer 1992). There is a plethora of convincing evidence that post MI sympathetic nervous system activity is increased and likely to be involved in progressive deterioration of heart function (Graham et al. 2002, Huang and Leenen 2009, Kasama et al. 2011, Westcott et al. 2009).

1.3. Sympathetic innervation of the heart

The activity of the heart is regulated by the autonomic nervous system through its sympathetic and parasympathetic divisions. In addition, the heart possesses an intrinsic nervous system that originates from intracardiac ganglia and may play an important role in integrating neuronal information from various sources (Crick et al. 2000). In the cardiac sympathetic division of the autonomic nervous system, preganglionic autonomic neurons are located in the lateral gray horns of the superior five or six thoracic segments of the spinal cord, while postganglionic ones are located in the paravertebral ganglia (Moore and Dalley 1999). Analysis of central nervous system (CNS) cell groups that project to stellate preganglionic neurons shows that several key areas are involved, including the caudal raphe nuclei, rostal ventromedial medulla, rostal ventrolateral medulla, paraventricular and lateral hypothalamic areas and a complex system of spinal

neurons (Jansen et al. 1995). Analysis of all sympathetic ganglia from superior cervical ganglion through the 10th thoracic ganglion indicated that the majority of the somata are located in the stellate ganglion (SG) complex, which is a fusion of inferior and middle cervical ganglia and first three thoracic ganglia. In humans, the SG complex is composed of a fusion of the inferior cervical ganglion and first thoracic ganglion, and the anatomy of the SG in rats closely resembles the one in humans (Abdi and Yang 2005). The SG complex is located on the lateral surface of the longus colli muscle at the level of 7th cervical vertebrae (Fig I1), posterior to the neck of the first rib, and just below the subclavian artery (Yasunaga and Nosaka 1979).

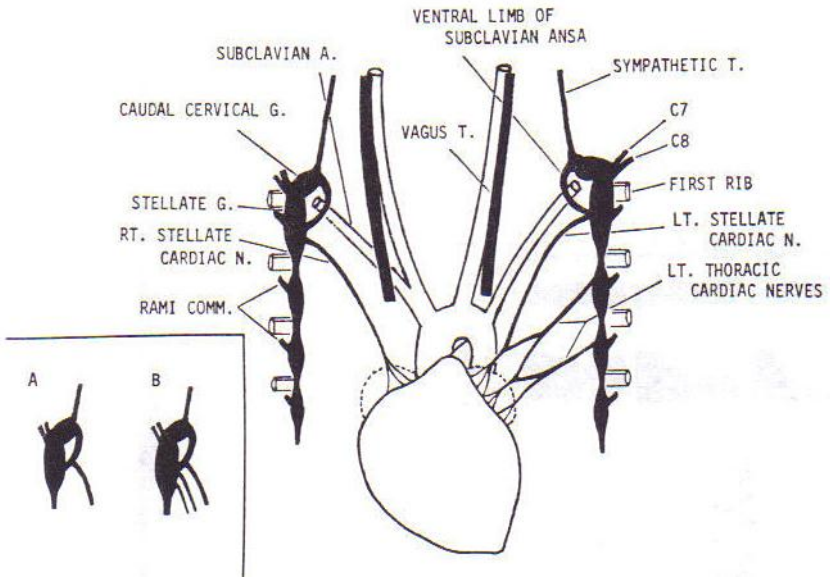

Fig. I.1. Sympathetic innervation of the heart. A schematic illustration of the ventral view of the rat heart demonstrating distribution of cardiac sympathetic nerves and the location of stellate ganglia. Inserts, A and B show variations of the cardiac nerves arising from stellate ganglia. Adapted from Yasunaga and Nosaka 1979.

Bilateral stellate ganglionectomy in rats results in 90-100% reduction in cardiac NE content, indicating the removal of almost all cardiac noradrenergic cells (Pardini et al. 1989). The results of unilateral ganglionectomy indicate that the LV receives bilateral innervation from both left and right SG complex, while the right ventricle (RV) receives innervation mostly from the left SG complex (Pardini et al. 1989). Postganglionic fibers from the right SG through innervation of the sino-atrial node appear to play a more important role in affecting the heart rate (HR), whereas postganglionic fibers from the left SG predominantly affect ventricular function. In dogs, right stellate ganglionectomy notably reduced resting HR and the increase in HR during exercise (Schwartz and Stone 1979). Direct stimulation of left SG resulted in pronounced elevation of systolic blood pressure (BP) without changes in HR, while stimulation of right SG increased both BP and HR (Randall and Rohse 1956).

Targeted bilateral stellate ganglia ablation with cholera-toxin B conjugated to ribosomal inactivating protein sapropin significantly diminished several parameters of cardiac sympathetic activity such as resting HR, HR responses to graded exercise and mean arterial pressure (MAP) and HR responses to increasing doses of sodium nitroprusside (Lujan et al. 2009).

Postganglionic sympathetic fibers enter the base of the heart to form a complex interconnecting network with parasympathetic postganglionic fibers called the cardiac plexus. Some efferent fibers of the cardiac plexus synapse with neurons of the intrinsic nervous system, while others bypass the intracardiac ganglia and innervate various cardiac tissues directly (Crick et al. 2000). The fillets which contain both sympathetic and parasympathetic fibers penetrate the heart by branches that remain in the epicardium,

branches that go to the myocardium and branches that go to the endocardium (San Mauro et al. 2009). At least four different targets of cardiac sympathetic nerves have been described: the sino-atrial node, the conducting system, cardiac myocytes and coronary vessels (Wallis et al. 1996).

1.3.1. Cardiac intrinsic nervous system

In addition to the extrinsic noradrenergic sympathetic innervation of the heart from stellate ganglia, neurons within the cardiac intrinsic nervous system in humans also possess noradrenergic functionality (Hoover et al. 2009). Ganglia containing intrinsic cardiac neurons and interconnecting nerves in a human heart are located predominantly within the epicardial fat on posterior surfaces of the atria and superior surfaces of the ventricles, forming five ganglionated plexuses in the atria and five in the ventricles, with approximately 14000 neurons per heart (Weihe et al. 2005). In an immunohistochemical study on atria samples obtained from heart biopsies from humans, the vast majority of the intrinsic cardiac neurons possess dual immunoreactivity for the cholinergic marker choline acetyltransferase and the nitrergic marker neuronal nitric oxide synthase (NOS) (Hoover et al. 2009). Nitric oxide may facilitate acetylcholine release from the cardiac cholinergic nerves, as well as act directly on cardiomyocytes and activate guanylate cyclase with subsequent formation of cyclic GMP. A small number of these neurons also expressed TH and vesicular monoamine transporter 2 (VMAT2), which indicates dual adrenergic/cholinergic phenotype and the potential for catecholamines synthesis and storage. In addition, some nerve fibers within intracardiac ganglia had positive immunoreactivity for vasoactive intestinal peptide (VIP), calcitonin gene-related peptide

and substance P. It is likely that these peptidergic nerves originate from sensory neurons located outside the heart (Hoover et al. 2009). Human postmortem heart samples also showed the existence of a dual cholinergic/noradrenergic phenotype in human intracardiac ganglia (Weihe et al. 2005). The study demonstrated co-expression of TH, VMAT2, aromatic L-amino acid decarboxylase and dopamine-β-hydroxylase by cardiac intrinsic neurons, indicating a full potential for NE synthesis, storage release and re-uptake. Hoover et al. (2009) observed dual cholinergic/noradrenergic phenotype in a small number of the intrinsic cardiac neurons, while Weihe et al. (2005) reported it in the major subpopulation (40-50%) of cardiac neurons.

Studies which assessed noradrenergic markers in the rodent intrinsic cardiac nervous system provided more variable results. In rats, all neurons showed immunoreactivity to a general neuronal marker PGP 9.5, choline acetyltransferase and neuropeptide Y, and a small subpopulation of neurons also expressed NOS. Calcitonin-gene related peptide, VIP, and TH immunoreactivity was observed in the nerve fibers within ganglia, but never in the neuronal bodies (Richardson et al. 2003). TH immunoreactivity, however, was also identified in a population of small cells (5-10 μm diameter), called small intensity fluorescent cells (SIF) which form groups surrounding intracardiac ganglia. Expression of TH by SIF cells of rats was also described in several other studies (Forsgren et al. 1990, Slavikova et al. 2003). Forsgren et al. (1990) suggested that SIF cells could potentially be noradrenergic, based on positive co-localization with dopamine-β-hydroxylase. Slavikova et al. (2003) described SIF cells as potentially dopaminergic/serotoninergic, based on positive co-localization of TH and tryptophan hydroxylase and negative co-localization for TH and dopamine-β-hydroxylase. The latter

study also described large neurons (20-40 μm diameter) within the cardiac intrinsic nervous system with catecholaminergic phenotype. These large cells could have a potential to synthesize both NE and epinephrine, based on co-expression of TH, dopamine-β-hydroxylase and phenylethanolamine N-methyltransferase (Slavikova et al. 2003). In mice, a large population of cholinergic intrinsic cardiac neurons that co-express enzymes required for NE synthesis and re-uptake (TH, dopamine-β-hydroxylase and NE transporter) was also described (Hoard et al. 2008). Collectively, these findings indicate that in rodents the intrinsic cardiac nervous system has complex neurochemical properties with potential for local NE synthesis.

1.4. Synthesis, storage and re-uptake of Norepinephrine

Preganglionic sympathetic neurons use acetylcholine (ACh) as neurotransmitter at the level of paravertebral ganglia, whereas postganglionic neurons originating in stellate ganglia use the neurotransmitter NE at nerve terminals. Pathway for catecholamine biosynthesis proceeds in the following direction:

$$\text{Tyrosine} \xrightarrow[\text{Tyrosine hydroxylase}]{} \text{DOPA} \xrightarrow[\text{Aromatic L-amino acid decarboxylase}]{} \text{Dopamine} \xrightarrow[\text{Dopamine-ß-hydroxylase}]{} \text{Norepinephrine}$$

In the sympathetic neuron, tyrosine is actively delivered into the axoplasm from the extracellular fluid by high and low affinity amino acid transporters (Haider et al. 2010). TH and aromatic L-amino acid decarboxylase are axoplasmatic enzymes, whereas dopamine-β-hydroxylase is located within amine storage vesicles, where it catalyzes the conversion of dopamine to NE (Klimaschewski et al. 1996). Dopamine is transported into

the vesicles against a large concentration gradient by the vesicular monoamine transporter, which is expressed as an integral protein of the vesicular lipid bilayer membrane (Eiden et al. 2004). Supplying aromatic L-amino acid decarboxylase and dopamine-β-hydroxylase with additional substrate leads to increased product formation, i.e. these steps are not rate limiting in NE synthesis, and these enzymes are unlikely to be major potential sites for regulatory control. In contrast, conversion of tyrosine to DOPA by TH is rate-limiting and the regulation of TH molecules number and activity represents principal means for controlling NE synthesis in the heart (Dunkley et al. 2004, Kumer and Vrana 1996).

Under normal conditions, most of the NE released by sympathetic nerves is taken back up by the nerves where it is metabolized or re-utilized (Esler et al. 1990). The NET protein, which belongs to the large gene family of Na^+/Cl^- dependent neurotransmitter transporters, shifts NE from the synapse back into its vesicles for storage and later use. In healthy individuals cardiac NE re-uptake is highly efficient and approximately 90% of released NE is cleared by NET (Wehrwein et al. 2008). Cardiac NE spillover accounts only for 2-3 % of total body NE release to plasma (Esler et al. 1990). NET protein is a polypeptide that possesses 12 transmembrane domains, cytoplasmic NH_2 and COOH terminal and a large hydrophilic loop between domains 2 and 3 that contains three sites for N-glycosylation (Melikian et al. 1996). N-glycosylation site is highly conserved in the transporter proteins family, which implies an essential role of glycosylation for synthesis and function of the protein. Unglycosylated human NET with molecular weight (MW) of 46 kDa shows reduced protein stability, surface trafficking and transport activity in comparison with glycosylated 80 and 54 kDa forms of NET (Melikian et al. 1996).

1.4.1. Regulation of TH enzyme activity and gene expression

It is conventionally considered that hydroxylation of tyrosine is regulated by two mechanisms: short-term direct regulation of enzyme activity (feedback inhibition by catecholamines and phosphorylation) and medium- to long-term regulation of gene expression, transcriptional regulation, mRNA stability, alternative mRNA splicing, translational regulation and enzyme stability (Fitzpatrick 2000, Kumer and Vrana 1996). Since different tissues possess their own unique TH regulation mechanisms, only major ones potentially applicable to cardiac sympathetic neurons will be discussed.

TH enzyme activity is regulated by two distinct catecholamine-binding sites: high affinity dopamine binding site (K_D=4nM), located in the active enzyme site at the N-terminal domain, and low affinity dopamine binding site (K_D=60-90nM) with unknown location (Gordon et al. 2009). These sites are called dopamine binding, but epinephrine and NE bind to TH at both sites with similar affinities (Gordon et al. 2008). For many years, the primary mechanism involving short-term regulation of TH activity was associated with feedback inhibition by the strong binding of catecholamines to the high affinity site. In vitro catecholamines form a complex with the active site iron and inhibit enzyme activity by decreasing V_{max} and increasing K_M for the obligate co-factor tetrahydrobiopterin (BH_4). Phosphorylation of TH at Ser40 decreases the affinity for bound catecholamines (K_D ~ 78-208nM), which can now easily dissociate from the enzyme and allow the ferric ion to be reduced by the co-factor BH_4 and return the enzyme to the fully active state (Kumer and Vrana 1996, McCulloch et al. 2001). TH phosphorylation and dissociation of catecholamines from high affinity dopamine site were considered to be the primary mechanism involved in fast and short-term increase of

enzyme activity. Recently a low affinity dopamine binding site was discovered, which might be a first-level response mechanism for regulating TH activity at the basal cell conditions, leaving TH phosphorylation as an additional recourse for prompt increase in NE synthesis. In vivo under basal conditions only a small portion of TH is phosphorylated (in rat brain phosphorylation of Ser40 is 0.02-0.05 mol pSer40 TH/mol total TH), and since the K_D for high affinity dopamine binding site in the low nM range, the high affinity dopamine binding site is almost fully saturated (Gordon et al. 2008, Salvatore et al. 2000). The K_D of the low affinity dopamine binding site approximates the concentration of neuronal cytosolic catecholamines (≤100 nM), making it possible for the low affinity site to regulate TH activity under basal cell conditions by responding to changes in cytosolic catecholamine levels (Gordon et al. 2009, Salvatore et al. 2000). Catecholamines can bind to the low affinity site when their levels in the cytosol increase, providing TH with feedback inhibition, or easily dissociate from it regardless of phosphorylation at Ser40, and dissociation increases TH activity 9-12 fold. Increasing TH activity further by phosphorylation of Ser40 may only be necessary when higher than physiological levels of NE synthesis are required (Gordon et al. 2008). In addition, there is strong evidence that extracellular signal-regulated kinases phosphorylate TH at Ser31 and that protein kinase A (PKA) phosphorylates TH at Ser40 under depolarizing conditions in a Ca^{2+}-dependent manner (Dunkley et al. 2004, Salvatore et al. 2001).

TH phosphorylation at Ser40 can maintain TH activation for over 48 hours when adrenal chromaffin cells are stimulated by nicotine, suggesting that TH phosphorylation might actually be involved in prolonged regulation of TH activity and maintenance of catecholamine synthesis (Bobrovskaya et al. 2007). These mechanisms for TH

activation/inactivation via feedback inhibition and TH phosphorylation are likely to be general for different cells producing catecholamines, but have not yet been specifically assessed in cardiac sympathetic neurons.

In cardiac sympathetic neurons elevated nerve activity and membrane depolarization appear to be major triggers which increase TH activity. Acute nerve stimulation in vivo results in the immediate 4-8 fold increase of TH activity in sympathetic neurons and their end organs (Rittenhouse and Zigmond 1990). Even though the exact mechanism for increased activity immediately after stimulation was not assessed, it is likely to involve TH phosphorylation and dissociation of catecholamines from high affinity site since alterations in gene expression are time consuming.

Elevated nerve activity and membrane depolarization may also upregulate transcription of TH gene and increase TH mRNA and protein content in sympathetic neurons in vitro and in vivo (Biguet et al. 1989, Kilbourne et al. 1992, Spiegel et al. 1989, Zigmond et al. 1980). Electrical stimulation of superior cervical ganglia for 90 min in vivo leads to 2.5 fold increase of TH mRNA content 48 hours later, and to 2 fold increase of TH activity and protein content 72 hours later (Biguet et al. 1989, Zigmond et al. 1980). Effects of long-term stimulation and membrane depolarization on TH expression in sympathetic ganglia have not yet been assessed. A depolarization responsive element in the TH gene was mapped to the region containing the cAMP responsive element. Stimulation of the cell results in adenylyl cyclase activation, an increase in second messenger cAMP, activation of PKA, and subsequent phosphorylation and activation of CREB. Phosphorylated CREB in turn activates transcription of the TH gene (Kumer and Vrana 1996).

1.4.2. Regulation of NET activity and gene expression

Binding of both Na^+ and Cl^- ions to NET is needed prior to NE binding to the transporter, and electrochemical energy from inward gradient of Na^+ facilitates transport of neurotransmitter into the cell. This secondary active cotransport depends on the proper function of the Na^+/K^+-ATPase, which maintains Na^+ concentration gradient across the plasma membrane (Mandela and Ordway 2006). Drugs which block ATP synthesis (dinitrophenol, cyanide), or Na^+/K^+-ATPase pump blockers such as "oubain" can inhibit NET function. Importantly, ischaemia can result in inadequate ATP synthesis, which interferes with Na^+/K^+-ATPase pump activity and produces NET dysfunction.

NET activity in cardiac sympathetic neurons can be regulated by several intracellular and extracellular signalling proteins. Transporter trafficking and surface expression is under control of phosphorylation/dephosphorylation mechanisms, and NET phosphorylation via protein kinase C (PKC) is the most studied intracellular pathway in regulation of NET activity. Phosphorylation of NET alters the equilibrium between plasma membrane and cytoplasmic fraction of the transporter, significantly decreases cell surface expression and subsequent NE re-uptake. Other messenger systems, like cAMP/PKA, cGMP/Protein kinase G (PKG) are also involved in NET phosphorylation, but effects appear to be cell and species specific (Blakely and Bauman 2000, Mandela and Ordway 2006, Ordway et al. 2005). Interaction of NET and syntaxin 1A may be required for protein kinase regulation of NE re-uptake. Activation of PKC interrupts NET/syntaxin 1A complex and downregulates NET activity (Sung et al. 2003).

Similarly to TH, NET gene expression in sympathetic neurons might also be affected by increased nerve activity and membrane depolarization. Brief depolarization (40 mM

K^{+} f for 5 min) in vitro of cervical sympathetic neurons increases NE uptake by stimulating cell surface trafficking of NET (Savchenko et al. 2003). Prolonged depolarization of sympathetic neurons for several days with 30 mM K^{+} stimulates NE re-uptake and NET mRNA. It is likely that depolarization stimulates NET expression via elevated catecholamine content (as a result of increased TH expression and activity), since stimulating catecholamine production in the absence of depolarization elevates NE uptake, NET mRNA and protein in sympathetic neurons (Habecker et al. 2006).

In addition to NE, several other neurotransmitters and hormones such as nerve growth factor (NGF), natriuretic peptide, insulin, Ang II and nitric oxide have been shown to influence NET gene expression in vitro. However, most studies used P12 cells derived from pheochromocytoma of the rat adrenal medulla and it is not clear if results are applicable to sympathetic neurons (Mandela and Ordway 2006).

1.5. Adrenergic receptors

NE is an agonist for adrenergic receptors in the heart. At the present time nine subtypes of adrenoreceptors have been discovered in various tissues and classified as β-1, β-2, β-3, α-1A, α-1B, α-1D, and α-2A, α-2B and α-2C (Brum et al. 2006). Cardiomyocytes express β-1, β-2, α-1 receptors, and expression of β-3 adrenoreceptors and atypical cardiostimulatory β-adrenoreceptors has been reported in various species, including humans (Gauthier et al. 2000, Kaumann and Molenaar 1997, Myslivecek and Trojan 2003).

Signal transduction is carried out via binding of adrenoreceptors to one or more guanosine triphosphate binding proteins or G-proteins that couple receptors to the second

messengers in the cell. For example, β-adrenoreceptors bind to Gαs subunit and stimulate adenylate cyclase, thus increasing cAMP second messenger concentration that activates PKA and subsequent protein phosphorylation, producing highly specific physiological action (Costanzo 2002).

In the human heart β-1 adrenoreceptors are predominantly expressed in contrast to β-2 (ratio 80-70:30-20 in the ventricles) (Wallukat 2002). In rat cardiomyocytes, the proportion of β-2-adrenoceptors (30–40%) is greater than that in the human heart (Xiao et al. 2006). Cardiac β-2 adrenoreceptors are located not only postsynaptically, but also presynaptically and they regulate the amount of NE released for a given level of nerve firing.

In comparison to β-receptors, expression of α-1 receptors in the heart is limited, and the ratio of β-receptors to α- receptors is 10:1 in human myocardium (Leenen 1999). Adrenoreceptors α-1A and α-1B couple to the Gq family of heterotrimeric G proteins, which in turn activate phospholipase C. Signal transduction pathway involves hydrolysis of inositol phospholipids by phospholipase C to generate two second messengers, inositol triphosphate (IP3) and 1, 2 diacylglycerol (DAG). IP3 is a regulator of intracellular calcium responses, while DAG activates PKC, which then can stimulate calmodulin-dependent protein kinases and activate L-type calcium channels (Woodcock et al. 2008). Activation of α-1 receptors results in augmented contractility, as well as in changes in electrophysiological properties of the heart through increasing the moycyte calcium level. Under normal conditions α-1 receptors are not major regulators of cardiac function, however, they may play an important role in pathologic conditions such as ischaemia and heart failure when β-1 receptor signaling is compromised (Woodcock et al. 2008).

Effects of catecholamines on cardiac myocytes are also associated with cellular hypertrophy and apoptosis. In in vitro studies in cultured cardiac myocytes tonic exposure to NE increases the number of apoptotic myocytes via stimulation of the β1-receptor pathway (Brum et al. 2006, Communal et al. 1999, Singh et al. 2001). Excessive β-1 receptor signaling leads to progressive hypertrophy and heart failure, as was demonstrated in transgenic mice with heart specific overexpression of β-1 receptors (Colucci et al. 2000). In contrast, β-2 receptor stimulation opposes apoptosis. It has been proposed that anti-apoptotic mechanism of β-2 receptors involves coupling with pertussis toxin-sensitive protein, presumably G_i (Communal et al. 1999, Patterson et al. 2004). In vitro treatment of rat cardiomyocytes with muscarinic agonist carbachol, which activates Gi, inhibits NE-stimulated apoptosis (Communal et al. 1999). Consequences of overexpression of β-2 receptors in the heart are "dose-related". Mice that express β-2 receptors at 60 fold have hyperdynamic cardiac function and normal survival, while mice that overexpress the receptor at 350 and 100 fold develop delayed cardiomyopathy, characterized by myocyte hypertrophy, myocardial fibrosis, LV chamber dilation and reduced contractile function (Simpson 1983). This study suggests that chronic stimulation of β-1 and β-2 receptors can cause deleterious cardiac transformation. In the failing heart the contribution of β-2 adrenergic pathways is more considerable than in the normal heart, because β-1 receptors are selectively downregulated at both mRNA and protein levels, resulting in approximate 50:50 ratio of β-1 to β-2 subtypes (Brum et al. 2006). A major current debate is whether changes in β- receptor expression and transduction associated with heart failure are actually adaptive or maladaptive, due to anti-apoptotic

properties of β-2 adrenergic pathways and higher degree of β-2 receptor stimulation necessary to induce adverse alterations (Bisognano et al. 2000).

Overexpression of α-1A receptors results in increased cardiac contractility, demonstrating inotropic actions of α-1A receptor pathway (Lin et al. 2001). It was proposed that α-1A receptor stimulation may produce important pro-survival effects and protect against maladaptive cardiac remodeling and CHF (Woodcock et al. 2008). Transgenic mice overexpressing α-1A receptors show enhanced inotropy and diminished LV remodeling, preserved cardiac function, and reduced acute heart failure mortality in both post-MI and pressure-overload models (Du et al. 2004, Lin et al. 2001). In contrast, α -1B receptor overexpression appears to have deleterious effects, since it produced severe dilated cardiomyopathy and death of transgenic animals from CHF. Altered cardiac gene expression of sarcomeric components was noted in mice overexpressing α -1B receptors, resulting in significant increase in α-Myosin heavy chain and titin mRNA, and a significant decrease in β- Myosin heavy chain mRNA (Lemire et al. 2001).

1.6. Cardiac sympathetic hyperactivity post MI

Global indices of sympathetic neural activity, such as plasma NE levels only provide information regarding general sympathetic drive and do not reflect the pattern of regional adrenergic outflow. In addition plasma NE concentration depends not only on the rate of nerve firing, but also on the clearance of neurotransmitter from plasma (Esler and Kaye 2000).

1.6.1. Studies in humans

Sympathoexcitation after MI can be defined as an augmentation of sympathetic nerve firing activity, and the rate of NE spillover into the venous drainage of individual organs is usually proportional to the rate of their sympathetic nerve firing (Esler et al. 1990). At times of high sympathetic nerve activation, the amount of NE entering the blood increases dramatically (Klabunde 2005), which manifests in patients post-MI by increased concentrations of NE in the blood (Jewitt et al. 1969, McAlpine et al. 1988, Omland et al. 1993).

Sympathetic drive to various organs and tissues exhibits heterogenic behavior in both physiological and pathological conditions (Esler and Kaye 2000), which emphasizes the importance of assessment of regional sympathetic neural activity, for instance CSNA post-MI. In clinical research two methods of quantifying regional sympathetic nervous system activity have been widely used (Esler and Kaye 2000):

1) Microneurography technique, which measures sympathetic nerve firing rates to skeletal muscle and skin
2) Isotopic dilution method, which measures rates of organ-specific norepinephrine spillover to plasma, for example cardiac or renal neurotransmitter spillover into vascular beds.

In regards to cardiac sympathetic activity majority of studies performed on humans were done on patients with heart failure, and there is limited information concerning cardiac sympathetic drive post-MI. In moderate human heart failure at first there is a selective increase in cardiac adrenergic drive, which is then followed by the augmented

sympathetic outflow to kidneys and skeletal muscle, which appears as CHF progresses (Rundqvist et al. 1997). In severe heart failure cardiac NE spillover rate increases by three fold, and total body spillover increases by 60% increase in comparison with healthy subjects (Kaye et al. 1994).

In most post-MI studies in humans muscle sympathetic nerve activity (MSNA) was evaluated for the direct assessment of sympathetic nerve activity. A significant increase in MSNA was described 2-4 days after MI (Graham et al. 2002). Sympathetic hyperactivity persisted for at least next 6 months and was inversely correlated with LV ejection fraction (EF).

1.6.2. Studies in animal models

Animal models permit use of different techniques, such as recording direct signals from cardiac or renal nerves, calculating NE turnover rates in different organs and studying regional changes in gene expression. Multiple studies evaluated general and renal sympathetic drive at various time points post-MI in animals, but only a few studies evaluated cardiac sympathetic activity. Moreover, changes in CSNA have been mostly researched in the acute phase post MI, and very little information is available regarding its time course.

Single-fiber CSNA in anesthetized cats increases during coronary occlusion (Brown 1967, Malliani et al. 1969). Direct nerve recordings during transient 90s coronary occlusion show that ischemia provokes immediate increased firing of afferent cardiac sympathetic nerves, followed within seconds by increased firing of efferent cardiac sympathetic nerves, which is connected with the existence of excitatory cardiac reflex

(Malliani et al. 1969). Direct recordings from cardiac postganglionic sympathetic nerves in rats within first hours after left anterior descending (LAD) artery ligation show that cardiac sympathetic drive increases by 100% (Schwenke et al. 2008). In conscious sheep CSNA increased significantly by the second hour after MI, and remained elevated by two fold for at least one week (Jardine et al. 2005). Sheep which developed fatal ventricular fibrillation in the first hour post MI had a significant increase in CSNA burst size preceding the event (Jardine et al. 2007).

Some data regarding cardiac sympathetic activity in the chronic post-MI state is available from NE turnover studies. In rats, NE turnover rate was increased ~3 fold in the non-infarcted cardiac LV, skeletal muscle, duodenum and whole kidney, but remained unaltered in spleen, liver and renal medulla at 8 weeks post MI (Patel et al. 2000). Blockade of sympathetic ganglionic traffic with hexamethonium eliminated regional heterogeneous increase in the sympathetic tone. This data supports the concept that chronic heart failure evokes a central-nervous system mediated increase in basal sympathetic tone that exhibits regional heterogeneity (Patel et al. 2000).

A general parameter of sympathetic activity, plasma NE level, has been measured by several researchers during the acute post MI state. Notable four-fold increase in plasma NE level has been reported 24 hours after the cardiac injury (Kolettis et al. 2007, Oikonomidis et al. 2010). There is a possible correlation between the size of MI injury, subsequent velocity of progression into LV failure and time course of plasma NE level. Rats with MI size of approximately 30% of LV area present with mild to moderate heart failure at 2-4 weeks post MI, and no increase in plasma NE level (Basu et al. 1996, Ganguly et al. 1997). In the same time frame more severe heart failure develops with MI

size reaching 45-50% of LV area, associated with increase in plasma NE concentration between one to three fold at 2 and 4 weeks post-MI (Mircoli et al. 2002, Soeki et al. 2008). Elevation of plasma NE concentration in the chronic MI state has been reported from 6 weeks to a year after the cardiac injury in rats (Lal et al. 2004, Shi et al. 2009, van Veldhuisen et al. 1994, Zhang and Cheng 2000). Animals with smaller MI sizes of about 30% develop more severe heart failure by 8 weeks, and then show one-fold increase in plasma NE level (Basu et al. 1996, Ganguly et al. 1997).

1.7. Molecular studies on cardiac sympathetic activity

A chronic increase in CSNA and NE release can also lead to an increase in NE synthesis and changes in neuronal gene expression. Since membrane depolarization up-regulates TH and NET gene expression in sympathetic neurons in vitro and in vivo (Spiegel et al. 1989, Zigmond et al. 1980), cardiac sympathetic hyperactivity may upregulate TH and NET expression in the heart and stellate ganglia after MI. A 2-3 fold increase in NET and TH mRNA in stellate ganglia, and in NET and TH protein in the non-infarcted base of the heart was observed in rats 1 week post ischaemia-reperfusion (Li et al. 2004, Parrish et al. 2008). In transgenic AOGEN rats which lack sympathetic hyperactivity post MI, the increase in TH and NET mRNA and protein in stellate ganglia and the heart was abolished at 1 wk post ischaemia-reperfusion (Parrish et al. 2010).

A significant decrease in TH, but not NET protein content was described in the LV below the ligation (Parrish et al. 2008), and this may be explained by the differential regulation of inflammatory cytokines. Lack of neuronal gp130 receptors in transgenic mice prevented the depletion of TH in cardiac sympathetic nerves below the ligation,

suggesting that inflammatory cytokines may act through gp130 receptor and contribute to local depletion of TH post MI (Parrish et al. 2010).

An important limitation in the above studies is that PGP 9.5 was used as the only standard control to normalize TH and NET expression to variations in tissue innervation density. Even though PGP 9.5 is an abundant cytoplasmic neuronal protein, it is not stably expressed, and its expression is not exclusive to neural tissue. Firstly, reactive oxygen species (ROS) generation is increased during ischaemia-reperfusion injury (Raedschelders et al. 2012), and PGP 9.5 gene expression can be notably downregulated by oxidative stress (Shen et al. 2006).

Secondly, extra-neuronal expression of PGP 9.5 might take place in the heart. Fibroblasts in human cutaneous wounds can express PGP 9.5 protein during the healing process (Olerud et al. 1998). Cardiomyocytes in patients with dilated and ischaemic cardiomyopathy exhibit strong PGP 9.5 immunoreactivity (Weekes et al. 2003), and associated with markedly high levels of cardiac ubiquitinated proteins.

1.7.1. PGP 9.5 and Ubiquitin proteasome system

PGP 9.5 belongs to the family of ubiquitin carboxyl-terminal hydrolases (UCH), and functions as deubiquitinating enzyme in the ubiquitin proteasome system (UPS) pathways. UPS accounts for 80-90% of intracellular protein degradation, and regulates two distinct cellular processes: protein quality control and biological control. Protein quality control involves clearance of misfolded, dysfunctional or damaged proteins. Biological control involves highly specific degradation or preservation of regulatory proteins. UPS can regulate cell cycle, cell signaling, protein turnover and apoptosis

(Sohns et al. 2010). For example, by increasing the concentration of signaling proteins such as Bax, p53, $p27^{kip1}$ and hypoxia inducible factor 1a UPS may promote apoptotic cell death, but inhibit it via tagging caspases or TNF-receptor associated factors for degradation (Sohns et al. 2010).

Several consecutive and highly regulated processes are involved in the protein degradation by the UPS. At first, the substrate must be tagged by the covalent attachment of multiple ubiquitin molecules. The ubiquitin activating enzyme, E1 uses the energy of ATP to generate a high energy thiol ester intermediate E1-ubiquitin. Then the activated ubiquitin is transferred from E1 to a thiol group on one of the several E2 ubiquitin conjugating enzymes. Lastly, E2 ubiquitin conjugating enzyme binds to the E3 –a ubiquitin ligase that identifies a substrate protein destined for degradation (Glickman and Ciechanover 2002). Ubiquitin is then transferred to the lysine 48 residue on the substrate protein, or on the ubiquitin molecule previously coupled to that protein. Polyubiquitinated proteins are then produced, and transferred to the 26S proteasome, where they are degraded into peptides and ubiquitin (Rodriguez et al. 2009).

Ubiquitin ligases precisely regulate the UPS by targeting specific substrates for ubiquitination and subsequent degradation by the 26S proteasome (Rodriguez et al. 2009). The role of several E3 ubiquitin ligases was identified in the ischaemia-reperfusion injury. MDM2 ubiquitin ligase inhibits p53 transcriptional activity by facilitating its proteasomal degradation, and reduces cardiomyocyte apoptosis after the ischaemic stress (Toth et al. 2006). Highly expressed in cardiac muscle CHIP ligase binds heat-shock proteins and is essential in protecting the heart against ischaemia-reperfusion

injury (Zhang et al. 2005). MAFbx/atrogin-1 ubiquitin ligase, on the other hand, enhances apoptosis via regulating JNK signaling (Xie et al. 2009).

The 26S proteasome is a macromolecular structure consisting of a 20S proteolytic core and two 19 S regulatory particles made of a base and a lid. The 20S barrel shaped proteolytic core is composed of two pairs of homologous rings each containing seven a and β subunits. The β subunits have three proteolytic activities: trypsin-like, chymotrypsin-like, and caspase-like activities (Powell and Divald 2010). In eukaryotes, a subunits don't possess direct proteolytic activity, but play an essential gaiting function by blocking the access of proteins to the central proteolytic core when the proteasome is inactivated (Groll and Huber 2003). Cardiac ischaemia-reperfusion injury is associated with proteasomal dysfunction. In rats, cardiac ischaemia-reperfusion for 30 min significantly decreases caspase-like, trypsin-like and chymotrypsin-like proteasome activities, leading to increased levels of ubiquinated proteins (Bulteau et al. 2001). Cardiac oxidative phosphorylation is significantly decreased during ischaemia, and since proteasomal protein degradation requires energy, ATP depletion is likely to be the major factor to account for proteasomal dysfunction (Powell and Divald 2010).

Multiple deubiquitinating enzymes, including PGP 9.5, commonly referred to as UCH-L1, play several important roles in the function of UPS. Firstly, it hydrolyses a peptide bond between C-terminal glycine of ubiquitin and lysine on the target protein, thus generating a free mono-ubiquitin molecule available for another catalytic cycle (Fang et al. 2010). Secondly, UCH-L1 can bind and stabilize mono-ubiquitin, which ensures its stability and elongates half – life (Osaka et al. 2003). Thirdly, in its dimer

form UCH-L1 can function as ubiquitin ligase and directly target a protein for degradation via polyubiquitination (Liu et al. 2002).

1.8. Cardiac sympathetic innervation post MI

Hypoxic injury to sympathetic nerves after MI leads to Wallerian degeneration, followed by axonal regeneration i.e. axonal sprouting (Chen et al. 2007). Proliferation of Schwann cells and axons starts at the edges of necrotic myocardial injury, and then proceeds towards the center of the scar, resulting in hyperinnervation of the scar area (El-Helou et al. 2008, Vracko et al. 1990, Wernli et al. 2009).

Oh et al. (2006) studied the time course of cardiac sympathetic hyperinnervation in mice by quantifying TH and growth associated protein 43(GAP 43) immunoreactivity in the peri-infarct and remote areas of the LV at 3 hours, 3 days, 1 wk, 1 and 2 months post MI. GAP 43 is an abundant neuronal protein in the axonal growth cone and is associated with axonal sprouting (Chen et al. 2007). Increase in cardiac sympathetic nerve fiber density peaked between 3 hours and 1 wk post MI with a 4 fold increase of GAP 43 and a 9 fold increase in TH immunoreactivity in the peri-infarct area. Chronically at 1 and 2 months post MI GAP 43 immunoreactivity in the peri-infarct zone was not different from corresponding areas of sham rats, but an increase in TH immunoreactivity persisted. In remote areas of the LV TH and GAP 43 nerve densities were increased 4 and 2 fold respectively at 1 and 2 months post MI. Changes in sympathetic innervation were mostly localized to the epicardial outer loop of the heart. No ChAT immunoreactivity was present in the heart ventricles (Oh et al. 2006).

In rats post MI similar findings have been reported. After permanent coronary artery ligation TH immunoreactivity increased 5 fold at the infarct border area at 7 days post MI, but was only slightly elevated vs. control at 28 days post MI (Hasan et al. 2006). At one week post ischaemia-reperfusion PGP 9.5, TH and NET immunoreactivity revealed extensive denervation in the LV below the infarct zone, conservation of sympathetic innervation in the base of the heart and regions of hyperinnervation along the infarct border (Li et al. 2004). Presence of nerve fibers within the scar tissue was also demonstrated by El-Helou et al. (2007) with neurofilament-M fiber immunoreactivity and GAP 43 protein expression at 1 wk post MI. At 4 wks post MI 2 to 5 fold increases in TH and GAP 43 immunoreactivity were reported in the remote areas of the LV (Lee et al. 2012, Lee et al. 2010, Yuan et al. 2009).

Collectively these findings indicate that cardiac sympathetic hyperinnervation is most pronounced acutely at the infarct border within the first week post MI, and to a less extent in remote cardiac areas chronically.

Several mechanisms may contribute to cardiac sympathetic hyperinnervation post MI. Firstly, the family of neurotrophins, including NGF, neurotrophin-3, neurotrophin-4/5 and brain-derived neurotrophic factor play a crucial role as neural chemoattractants in the heart and are strongly implicated in the development of sympathetic hyperinnervation post-MI (Kimura et al. 2012). Pronounced upregulation of NGF expression occurs within hours post MI at the infarct site and at the infarct border, and to a lesser extent in the non-infarcted LV (Oh et al. 2006, Zhou et al. 2004). The source of the increased NGF mRNA and protein in the heart after MI is still under investigation. Zhou et al. (2004) showed that within first hours post MI at the infarct zone concentration of NGF increases by 3

fold, likely as a result of release from necrotic tissues, which is followed by 10 fold NGF expression upregulation at 1 wk post MI. Hasan et al. (2006) demonstrated that macrophages and myofibroblasts synthesize NGF mRNA and protein at the infarct border/peri-infarct area, suggesting that inflammatory process contributes to infarct border hyperinnervation. ATP-sensitive potassium channel agonists prevent excessive sympathetic nerve sprouting, most likely by attenuating expression of endothelin-1, which upregulates NGF expression (Kang et al. 2009).

Secondly, in normal dogs long-term subthreshold electrical stimulation of left stellate ganglion also produces increased ventricular nerve fiber density. Sympathetic hyperinnervation induced by electric stimulation in normal dogs and in dogs post MI was significantly more pronounced than one induced by infusion of NGF, indicating that CSNA may also play a crucial role in promoting cardiac sympathetic hyperinnervation post MI (Cao et al. 2000, Swissa et al. 2004).

1.9. Central mechanisms contributing to sympathetic hyperactivity post MI

Immuno-histochemical detection of Fos family proteins, Fra-like immunoreactivity showed clear increases in the magnocellular neurons of the supraoptic nucleus (SON) and PVN, and to a lesser extent in the parvocellular neurons of the PVN at 2 and 4 weeks in rats post MI. Immuno-histochemical detection of Fos family of transcriptional factors has become a sensitive marker of long-term neuronal activation including neurons involved in cardiovascular homeostasis (Vahid-Ansari and Leenen 1998). Direct electrophysiological recordings in heart failure in rats 4-6 wks post MI showed that the

neuronal activity in the PVN is significantly increased 2-3 fold (Basu et al. 1996, Zhang et al. 2002).

After myocardial injury several mechanisms can potentially lead to activation of brain nuclei involved in cardiovascular homeostasis. Firstly, post MI plasma concentrations of Ang II rise within first hours (Leenen et al. 1999a). Plasma Ang II may activate CNS pathways via AT_1- receptors stimulation in circumventricular organs which have incomplete blood-brain barrier such as the SFO or organum vasculosum of the lamina terminals (Lindley et al. 2004). They may send signals by neuronal projections to downstream nuclei such as PVN and SON and cause sustained activation and consequent sympathetic hyperactivity (Davern and Head 2007). Secondly, plasma aldosterone levels rapidly increase during post MI acute phase and aldosterone can cross blood-brain barrier and activate central mechanisms directly via MR (Huang and Leenen 2009). Thirdly, post MI cardiac vagal and sympathetic afferent fibers that carry mechano and chemo – sensitive information to the CNS become activated (Zhu et al. 2004).

Regarding the sequence of central mechanisms that leads to sympathetic hyperactivity post MI there is strong evidence that elevated levels of circulating Ang II activate SFO and PVN via AT_1- receptors. Angiotensinergic neurons projecting from the SFO stimulate aldosterone production and release from magnocellular neurons in the SON, followed by the "ouabain" release in the PVN (Huang and Leenen 2009). The increase of aldosterone content in the hypothalamus after MI appears to reflect an augmentation in its local production. Chronic blockade of aldosterone synthesis by intracerebroventricular (icv) infusion of aldosterone synthase inhibitor prevents the increase of hypothalamic aldosterone, but does not affect plasma aldosterone (Huang et al. 2009).

MR belong to the steroid hormone receptor group of the nuclear receptor superfamily of ligand-activated transcription factors. After binding a ligand in the cellular cytoplasm, the MR + ligand complex migrates to the nucleus where it directly interacts with hormone-responsive elements of the target genes (Shen and Young 2012). The intrinsic affinity of MR for aldosterone, cortisol and corticosterone is similar. Since circulating concentrations of glucocorticoids is ~ 100-1000 fold higher than that of aldosterone, cellular regulation exists to ensure the specificity of mineralocordicoid signalling. In epithelial tissues the specificity of signal is accomplished via the co-expression of MR and 11β-hydroxysteroid dehydrogenase type 2 (11β-HSD2), which possesses dehydrogenase activity and inactivates cortisol and corticosterone by converting them to their 11-dehydro forms (Gomez-Sanchez 2010). In the brain, autoradiographic studies demonstrated retention of both steroids in the hippocampus, circumventricular organs, and several of the brain stem nuclei, and preferential binding of aldosterone in the cortex, thalamus and brainstem (Birmingham et al. 1984). Even though the majority of MR receptors are predominantly occupied by physiological concentrations of cortisol and corticosterone, several possible mechanisms exist in the brain to confer MR ligand specificity for aldosterone. The co-expression of MR and 11β-HSD2 may lower glucocorticoid concentration in cells, and this phenomena was demonstrated in the in neurons of tractus solitarii in the brain, which might be involved in central regulation of blood pressure (Geerling et al. 2006). Intracellular factors, such as co-regulators of transcription and differential expression of chaperone and scaffolding proteins that associate with MR might also be involved in conferring the MR specificity (Gomez-Sanchez 2010)

Sympathoexcitatory and pressor responses to icv infusion of aldosterone can be prevented by either MR or ENaC blockade, which strongly suggests a pathway linkage between brain aldosterone and ENaC (Huang and Leenen 2009). By mechanisms not fully understood, activation of central MR by aldosterone appears to lead to the increase in "ouabain" release in the CNS. In rats, chronic icv infusion of aldosterone increases "ouabain" content in the hypothalamus, and the increase can be blocked by ENaC blocker benzamil or MR blocker spironolactone (Huang and Leenen 2009, Wang et al. 2003). "Ouabain" might bind to the cardiac glycoside binding domain on the a-subunit of the Na^+/K^+ -ATPase enzyme and inhibit its activity and related Na^+ gradient-dependent transport processes. Hypothalamic increase in "ouabain" is likely to enhance AT_1 receptor stimulation, because sympathoexcitatory effects induced by aldosterone or ouabain injected in the PVN or cerebral ventricles can be abolished by an AT_1 receptor blocker (Gabor and Leenen 2009, Huang and Leenen 1996). PVN contains angiotensinergic projections to presympathetic neurons in the spinal cord, which play a major role in control of sympathetic tone (Lind et al. 1984, Unger et al. 1981).

In rats post MI central blockade of MR receptors, Na^+ channels, "ouabain" or AT_1-receptors similarly inhibits sympathetic hyperactivity, circulatory and cardiac RAAS activation and attenuates cardiac remodeling and left ventricular dysfunction (Huang and Leenen 2005, 2009, Leenen et al. 1999b). Indeed, sympathetic hyper-reactivity to stress, increase of plasma NE and impairment of arterial baroreflex can be prevented by central blockade of MR or ENaC with icv infusion of MR blocker or benzamil (Huang and Leenen 2005, Lal et al. 2004). Continuous icv infusion of MR blocker spironolactone for 4 wks in rats post MI markedly ameliorates the impairment of baroreflex regulation of

renal sympathetic nerve activity (RSNA) and HR, and attenuates the increase in resting RSNA (Francis et al. 2001).

Icv infusion of aldosterone synthase inhibitor FAD286 prevents the increase in hypothalamic aldosterone content and notably improves LV function in rats post-MI (Huang et al. 2009), suggesting that hypothalamic aldosterone is the major ligand that binds to brain MR receptors. In turn, chronic icv infusion of Fab fragments to bind "ouabain" after MI also prevents sympathetic hyper-reactivity and normalizes plasma NE level, exaggerated resting RSNA and impairment of arterial and cardiopulmonary baroreflex control of RSNA and HR (Huang et al. 2000). Lastly, in rats post MI sympathetic hyperactivity can be largely prevented by chronic blockade with icv infusion of AT_1- receptor blocker losartan, accentuating the role of the central RAAS system in producing sympathetic hyperactivity in heart failure (Zhang et al. 1999). Transgenic rats that express antisense RNA against brain angiotensinogen mRNA post MI preserve normal sympathoexcitatory response to stress and normal arterial baroreflex in comparison with Sprague-Dawley rats (Wang et al. 2004). Also, transgenic rats exhibit marked attenuation of cardiac remodeling and lesser decrease in LV function, which emphasizes the role of excessive sympathetic drive post-MI in deteriorating ventricular performance.

These findings suggest that brain RAAS activity which generates excessive sympathetic drive after cardiac injury is likely secondary to activation of MR and increases in "ouabain" release, since central blockade of MR, brain Na+ channels, or "ouabain" produces similar effects in decreasing various parameters of sympathetic hyperactivity in rats with heart failure post MI.

The effects of central treatment on CSA post MI have not been studied yet, but recently it was demonstrated that icv infusion of losartan for 5 hrs normalizes elevated CSNA in CHF induced by rapid ventricular pacing (Ramchandra et al. 2012).

1.10. Rational for study

At 1 wk post ischaemia-reperfusion injury, TH and NET gene and protein expression were found increased in both stellate ganglia and the base of the heart (Parrish et al. 2008), which is consistent with cardiac sympathetic hyperactivity. However, changes in expression of enzymes involved in cardiac NE synthesis and re-uptake post MI by permanent coronary artery ligation have not yet been assessed. We aimed to evaluate the evolution of TH and NET expression in stellate ganglia and the heart post-MI induced by permanent coronary artery ligation during the transition from acute to chronic post-MI time points. In addition, we aimed to clarify the origin of TH and NET mRNA and proteins in the heart. It is assumed that stellate ganglia neurons are the main source of cardiac TH and NET proteins, i.e. proteins are synthesized in the stellate ganglia and then transported to the heart via axons. Intracardiac ganglia, however, may also express NET and TH, and small intensity fluorescent cells have been shown to express TH. The contribution of these locally produced proteins in total TH and NET contents in the heart is unclear (Hoard et al. 2008, Richardson et al. 2003).

There is extensive evidence for increased cardiac sympathetic innervation shortly after MI (described in “Cardiac sympathetic innervation post MI” of literature review). Cardiac hyperinnervation may be influenced by increased CSNA, since long-term subthreshold electrical stimulation of left stellate ganglia in normal dogs increases nerve

fiber density in the heart, and in dogs post MI augments cardiac sympathetic hyperinnervation (Swissa et al. 2004). We aimed first to describe the pattern of sympathetic innervation in rats at 10 days post MI, and then assess the effect of central MR blockade on cardiac sympathetic hyperinnervation. It is reasonable to expect attenuation of CSNA by central MR blockade, since it prevents generalized sympathetic hyperactivity post MI. Thus, central MR blockade by decreasing CSNA may attenuate or prevent sympathetic hyperinnervation post MI.

Our last goal was to study changes in PGP 9.5 expression and the possibility of extra-neuronal PGP 9.5 expression in the heart post MI. Assessment of PGP 9.5 expression post MI was necessary in order to evaluate if it can be used it as a neuronal control. PGP 9.5 expression by cardiomyocytes in association with UPS dysfunction was previously described in human dilated and ischaemic cardiomyopathy (Weekes et al. 2003). We wanted to investigate this phenomenon in rats post MI, and study effects of central MR blockade on possible extra neuronal PGP 9.5 expression and UPS activity.

1.11. Hypothesis

1) Increased CSNA post MI upregulates TH and NET expression in stellate ganglia and the heart and facilitates sympathetic hyperinnervation in the heart post MI.
2) Central MR blockade attenuates the effects of CSNA in the heart and reduces cardiac sympathetic hyperinnervation post MI.

1.12. Objectives

1). Study the time course of TH and NET gene and protein expression in stellate ganglia and the heart during the transition from acute to chronic post-MI states.

2). Study the origin of TH and NET mRNA and proteins in the heart, and evaluate the potential role of intracardiac ganglia in TH and NET protein synthesis.

3). Describe changes in cardiac sympathetic innervation at 10 days post MI, and then assess effects of central MR blockade on cardiac sympathetic hyperinnervation.

4). Evaluate possible extra-neuronal PGP 9.5 expression and associated UPS activity in rats post MI, and assess effects of central MR blockade on PGP 9.5 expression and UPS.

2. Materials and Methods

Surgical procedures (left anterior descending coronary artery ligation, stellate ganglionectomy), echocardiography and assessment of LV hemodynamics were performed by Dr. Monir Ahmad. Placement of icv cannulas and osmotic minipumps were performed by Dr. Bing Huang. Primers and plasmids for TH, NET, PGP 9.5 and PGK were developed by Dr. Hong-Wei Wang. Quality control experiments for Western blotting and Immunohistochemisty were performed by Roselyn White. Tissue collection, qRT-PCR, Western blotting and Immunohistochemisty experiments were performed by Anastasia Drobysheva.

Animals: Male Wistar rats (Charles River, Montreal, Canada) 10-12 wks old, weighting 200-250 grams were housed on a 12h:12h light-dark cycle at constant room temperature (22ºC) and humidity (30%) and given free access to regular rat chow (120 μmol Na^+/g) and tap water. All experiments were approved by the University of Ottawa Animal Care Committee and comply with the *Guide for the Care and Use of Laboratory Animals* published by the US National Institutes of Health (NIH Publication, 8th edition, 2011). Experiments were performed after acclimatization of animals for 1 week. All surgeries were performed under sterile conditions and isoflurane inhalation. Chemicals were purchased from Sigma (Oakville, ON, Canada) unless noted otherwise.

2.1. Experimental protocols.

2.1.1. Experiment 1

Time course of TH, NET and PGP 9.5 expression in stellate ganglia, LV and RV in rats post MI.

Animals were randomly divided into two groups, for permanent coronary artery ligation (n=10) or sham operation (n=8). Left anterior descending coronary artery ligation was performed to induce MI as described in "Surgical procedures". Sham operated animals underwent thoracotomy without coronary artery ligation. At different time points after the surgery (1 wk, 4 wks and 12 wks) LV dimensions and function were assessed by echocardiography and Millar catheter. Rats were then euthanized and tissues collected as described in "Tissue collection". TH, NET and PGP 9.5 protein expression was assessed by Western blotting technique, and gene expression was assessed by the qRT-PCR. Three time points were selected to represent acute changes (1 wk., to make comparison with ischaemia-reperfusion model), early (4wks) and late (12 wks) chronic changes. Specific time points were chosen based on former studies that applied established methods of assessment of CSNA, such as direct recordings from cardiac sympathetic nerves and NE turnover technique (as described in "Cardiac sympathetic hyperactivity post MI" chapter of literature review).

2.1.2. Experiment 2

Origin of NET, TH and PGP 9.5 mRNA and proteins in the heart.

Animals were randomly divided into 2 groups, for bilateral stellate ganglionectomy (n=5), and sham operation (thoracotomy) without stellate ganglionectomy (n=4). Stellate ganglionectomy was performed as described in "Surgical procedures". One wk after the surgery animals were sacrificed and tissues collected as described in "Tissue collection". This time point was selected because Pardini et al. (1989) showed that 7 days after bilateral stellate ganglionectomy cardiac NE was reduced by 90%-100%. TH, NET and

PGP 9.5 mRNA and protein levels were assessed by qRT-PCR and Western blotting technique.

2.1.3. Experiment 3

Cardiac sympathetic innervation in rats 10 days post MI. Extra-neuronal PGP 9.5 expression and UPS.

Animals were randomly divided into two groups, for permanent coronary artery ligation (n=10) or sham operation (n=8). The time point of 10 days post MI was selected since previous studies show that cardiac nerve sprouting and sympathetic hyperinnervation is pronounced at 1 wk post MI (Oh et al. 2006, Zhou et al. 2004).

At 10 days post MI, LV function was assessed by Millar catheter before rats were euthanized by transcardiac perfusion with 0.1 M PBS (pH 7.4) under pentobarbital sodium anesthesia (100 mg/kg, intra peritoneal). Hearts were removed immediately, and free wall of the LV was separated on ice. The LV was then divided into 2 halves. The first half of the LV was fixed for 24 h at 4 ºC in 4% paraformaldehyde for immunohistochemistry, then rinsed in PBS, and cryoprotected in 30% sucrose for 48 h at 4 ºC. The second half of the LV was separated on ice into non-infarcted base and peri-infarct area (3 mm zone adjacent to MI border) for Western blotting. Tissues were snap frozen in liquid nitrogen and stored in -80ºC freezer.

PGP 9.5, GAP 43 and TH fluorescent double staining was performed to visualize sympathetic axons in the heart post MI. GAP 43 is a dominant neuronal protein in the axonal growth cone and is associated with axonal sprouting (Chen et al. 2007). PGP 9.5 is an abundant cytoplasmic neuronal protein, and was included in the assay to study both sympathetic innervation and possible extra-neuronal PGP 9.5 expression. TH is

conventionally used in immunohistochemical experiments as a marker of sympathetic innervation (Burgi et al. 2011, Zhou et al. 2004), thus colocalization of TH with PGP 9.5 or GAP 43 shows that PGP 9.5 and GAP 43 proteins are contained within the sympathetic axons of the heart.

Extra neuronal PGP 9.5 expression was evaluated with analysis of PGP 9.5 immunoreactivity in various regions of the LV. Fluorescent double staining with vimentin (marker for fibroblasts and macrophages) and alpha-sarcomeric Actin (marker for cardiac myocytes) was performed to characterize the origin of extra-neuronal PGP 9.5 expression. PGP 9.5, GAP 43 and ubiquitin protein expression in the peri-infarct area and the base of the LV was assessed by Western blotting technique.

2.1.4. Experiment 4

Effects of central MR blockade on cardiac sympathetic hyperinnervation, PGP 9.5 expression and UPS 10 days post MI.

MI and sham surgeries were performed as in the first experiment. At one day post MI, an icv cannula was placed into the left cerebral ventricle and the upper end of cannula was connected to Alzet osmotic minipump (model 2002, Alza; Palo Alta, CA) for a 9-day infusion at a flow rate of 0.5µl/h. Animals were randomly divided into groups (n=8/group) for treatment with eplerenone or vehicle as follows:

1) MI group with an icv infusion of the MR blocker Eplerenone 5 ug/day, dissolved in aCSF with 4% acetonitrile.
2) MI group with an icv infusion of vehicle, aCSF with 4% acetonitrile.
3) Sham operated group with icv cannulation surgery only.

The time point of 10 days post MI was selected since previous studies show that cardiac nerve sprouting and sympathetic hyperinnervation is pronounced at 1 wk post MI (Oh et al. 2006, Zhou et al. 2004). The rate of icv infusion of Eplerenone was based on previous studies (Huang et al. 2010). At the end of day 10 infusion LV dimensions and function were assessed, and then animals were sacrificed. LV for immunohistochemistry and Western blotting were collected as described in the third experiment. PGP 9.5, GAP 43 and TH fluorescent double staining was performed to visualize sympathetic axons in the heart post MI.. PGP 9.5, GAP 43 and ubiquitin protein expression in the peri-infarct area, in the base of the LV and in the RV was assessed by Western blotting technique.

2.2. Surgical procedures

2.2.1. Left anterior descending coronary artery ligation: Animals were given premedication with buprenorphine (0.05 mg/kg, SC), and then anaesthetized with 2% Isoflurane in Oxygen. An endotracheal tube was inserted and connected with a respirator (model 683; Harvard Rodent Ventilator) with room air. Left thoracotomy was performed in the left fourth intercostal space, and the left anterior descending coronary artery was permanently ligated 2–3 mm from its origin with a 6-0 silk suture passed 1-2 mm deep through the myocardium with the atraumatic needle. Positive end-expiratory pressure was then applied to inflate the lung before the chest was closed in layers. Anesthetic was stopped and the animals remained ventilated until they started to breathe independently. The mortality during surgery and in subsequent 48-h period was ~ 30%. Animals with MI < 20% were excluded from the study.

2.2.2. Stellate ganglionectomy: Animals were given premedication with buprenorphine (0.05 mg/kg, SC), and then anaesthetized with 2% Isoflurane in Oxygen. An endotracheal tube was inserted and connected with a respirator (model 683; Harvard Rodent Ventilator) with room air. After a midline skin incision, left thoracotomy was performed in the 2nd intercostal space and the incision was retracted. Surgical microscope was used to locate the left stellate ganglion on the lateral surface of the longus colli muscle at the level of 7th cervical vertebrae, posterior to the neck of the first rib. Left stellate ganglion was excised, and all ganglion axons were isolated and cut. After hemostasis, the chest was closed in layers. To remove the right stellate ganglion, the same procedure was performed on the right side at the end of the surgery. Skin was closed using clamps. Anesthetic was stopped and the animals remained ventilated until they started to breathe independently. The mortality during surgery and in subsequent 48-h period was ~ 0%.

2.2.3. Placement of icv cannula and osmotic minipump: Under isoflurane inhalation, rats were placed in a stereotaxic frame, and the skull was leveled between the bregma and lambda. A little burr hole was made in the rat skull, and one arm of a right-angled guide cannula (23 gauge) was introduced into the left cerebral ventricle and fixed to the skull of the rat with acrylic cement. The location of the left cerebral ventricle was established according to the rat atlas of Paxinos and Watson, 0.5 mm posterior to the bregma, 1.4 mm lateral to the bregma, and 3.5 mm ventral from the dura. The upper end of cannula was connected to an osmotic minipump implanted subcutaneously at the back of the neck via PE-50/60 tube. The skin incisions were sutured after the cannulation was done. Penicillin G (30 000 IU IM Derapen, Ayerst Laboratories, Montreal, CA) was injected after surgery. The accuracy of the icv cannula placement was assessed after animals were

euthanized and brains were collected. Data from animals with incorrectly placed cannula were excluded from the analyses.

2.3. Echocardiography

Echocardiography was performed under mild isoflurane anesthesia (2% Isoflurane + 2Litre/Min Oxygen) with a Vevo 770 echocardiography system (VisualSonics). A 25-MHz transducer was placed on the left hemithorax of the rat to take recordings. Using the 2-D parasternal long-axis imaging plane as a guide, a left ventricular M-mode tracing was obtained just below the tips of the mitral leaflets. Simultaneous M-mode recording of intraventricular septum thickness, posterior wall thickness, and chamber size was performed for 4 cardiac cycles. LV EF was then calculated.

2.4. Assessment of LV Hemodynamics

Under mild isoflurane anesthesia (2% Isoflurane + 2Litre/Min Oxygen) 2 F high-fidelity micromanometer catheter (SPR-407; Millar Institute, Houston, TX) was inserted into the LV via the right carotid artery. The Millar catheter was connected to a Harvard Data Acquisition system interfaced with a PC with AcqKnowledge III software (ACQ 3.2) for measurement of LVEDP, LVPSP, dP/d*t*max, and minimal first derivative of change in pressure over time (dP/d*t*min).

2.5. Tissue Collection

Rats were euthanized by transcardiac perfusion with 0.1 M PBS (pH 7.4) under pentobarbital sodium anesthesia (100 mg/kg, intra peritoneal). Stellate ganglia were

collected immediately under surgical microscope and snap frozen in liquid nitrogen. The hearts were removed and the LV was separated from the RV at the interventricular septum on ice. Left and right ventricles were weighted for hypertrophy assessment. The LV was opened and spread out, and the infarcted and noninfarcted areas were traced onto transparent sheet. LV infarct size was measured by planimetry from endocardial surface and expressed as a percentage of total LV area with the Image –Pro 6.2 software. Tissues were then snap frozen in liquid nitrogen and transferred with stellate ganglia to -80 ºC freezer for storage.

2.6. Molecular biology assays

2.6.1. qRT-PCR

Total RNA isolation: 100 mg of tissue from the base of the LV (area above the ligation) and the base of the right ventricle were homogenized in TRIzol Reagent buffer (Invitrogen, Burlington, ON, Canada) by using a Polytron. Stellate ganglia were homogenized in 0.3 ml TRIzol Reagent by using a pestle (Bel-Art-Products, Pequannock, NJ) driven by a Pellet Pestle Motor, and another 0.7 ml TRIzol was added thereafter. Homogenized samples were incubated at room temperature for 10 min to allow a complete dissociation of nucleoprotein complexes. Chloroform was then added to the samples at 0.2 ml per 1ml of Trizol to separate the RNA in an aqueous phase. Samples were shaken vigorously for 30 seconds and centrifuged at 12000 x g for 20 minutes at 4 °C. After centrifugation, the mixture separated into a lower red phenol-chloroform phase an interphase and a colorless upper aqueous phase containing total RNA. The aqueous phase was then collected and total RNA was precipitated from aqueous phase by 0.5 ml

isopropyl alcohol per 1 ml Trizol used for the initial homogenization. Samples were incubated at room temperature for 15 min, proceeding with centrifugation for 20 minutes at 12000 x g at 4 °C. The RNA pellet was then washed with 1000 µl 75% ethanol and centrifuged for 5 min at 7500 x g at 4 °C. RNA pellet was air dried and dissolved in RNase free water. RNA integrity was verified on agarose gel (Fig M1) and the quantity and purity of RNA was measured by Nano-drop Spectrophotometer (ND-1000, USA). The dissolved RNA was stored at -80 °C.

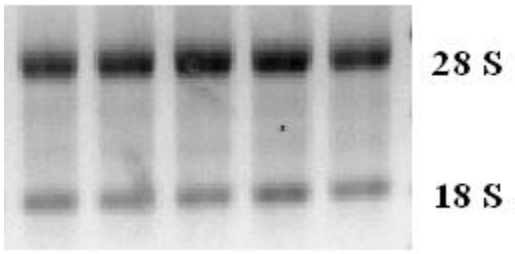

Figure M1. RNA native agarose gel. RNA extracted from stellate ganglia was run on 1% agarose gel for quality control.

DNase I treatment: To eliminate potential genomic DNA contamination, RNA was treated with DNase I using Ambion's DNA-*free*^{TM} kit (Ambion, Austin, TX) before reverse transcription reaction. Treatment was carried out on 5µg of RNA from the heart, or on the total amount of RNA from stellate ganglia. The recombinant DNase I (0.5 µl for stellate ganglia and 1 µl for adrenal) was combined with 0.1 volume of 10 x DNase I buffer for a total volume of 50 µl. Samples were then incubated at 37 °C for 30 minutes. After the incubation period, 0.1 volume of DNase Inactivation Reagent was added to samples. Samples were then kept at room temperature for a couple of minutes and vortexed 2-3 times during incubation. After centrifugation at 12,000 x g for 2 min at 4 °C, the supernatants were collected into clean 1.5 ml eppendorff tubes. For RNA

concentration, 2.5 volume of 100% ethanol and 1/10 volume of sodium acetate (NaAc, 3M PH 5.3) were added and the mixture was then left overnight at -20 °C. Next morning samples were centrifuged at 12000 x g at 4 °C for 20 minutes. RNA pellet was then washed with 1000 µl 75% ethanol, centrifuged for 5 min at 7500 x g at 4 °C, air dried and dissolved in RNase free water. Quantity and purity of RNA was measured by Nano-drop Spectrophotometer (ND-1000, USA).

cDNA synthesis: 1µg DNase I treated RNA was used for the first strand cDNA synthesis. Oligo$(dT)_{12-18}$ primers (1 µl, 500µg/ml) and dNTP Mix (1 µl, 10 mM) were combined with 1µg of RNA to a total volume of 12 µl. The mix was incubated at 65 °C for 5 min and then quickly chilled on ice for 2 minutes. DDT (2 µl, 0.1 M) , 5x First-Strand Buffer (4 µl), and RNaseOUT (1 µl, 40 units/ µl) were added to the mix, which was then kept up for 2 minutes at 42 °C. After that 200 U SuperScript ™ II RNase H-Reverese Transcriptase was added, and the mix was incubated at 42ºC for 50 minutes. To inactivate the reaction, samples were incubated for 15 minutes at 70 ºC and then stored at -20 °C. All the reagents for cDNA synthesis were from Invitrogen, Burlingtone, ON, Canada.

Real-time PCR: Real-time PCR amplifications were performed with a Roche Light Cycler by using Fast Start DNA Master SYBR Green I (Roche Diagnostics, Penzberg, Germany). One microliter of the RT product from each sample was used as a template. The specific TH, NET, PGP 9.5 and PGK primer sequences used are listed in Table M1. All primers were ordered from Integrated DNA Technologies. The real-time PCR conditions were optimized by Dr. Wang previously as follows: an initial step of 95°C for 10 min followed by 45 cycles of denaturation at 95°C for 5 s, and annealing of primers to

the target for 5 s at 62°C for the PGP 9.5 and PGK primers, and 62°C for 7 s for the TH and NET primers. The extension step was performed at 72°C. The specificity of real-time PCR products was documented with a melting curve analysis. In addition, high-resolution gel electrophoresis was performed to confirm the amplification of a single product of the appropriate size for each gene.

Table M1. Primer sequences for detection of TH, NET, PGP and PGK mRNA transcripts

Gene	Sense sequence	Antisense sequence
TH	5'-CAGGGCTGCTGTCTTCCTAC-3'	5'-GGGCTGTCCAGTACGTCAAT-3'
NET	5'-GCTGACCAGCACCATCAAC-3'	5'-GGGTGACAGCACATGTGAAG-3'
PGP	5'CCAGTTCAGAGGACTCTCTG-3'	5'-GCCTCTGAAGTTCACACTGG-3'
PGK1	5'-GCTGCAGAACTCAAATCTCT-3'	5'-TGTGTGCAGTCCCAAAAGCA-3'

TH – tyrosine hydroxylase, NET –Norepinephrine transporter, PGP 9.5 – protein gene product 9.5, PGK 1- phosphoglycerate kinase 1

The specificity of real-time PCR products was documented with a melting curve analysis. In addition, high-resolution gel electrophoresis was performed to confirm the amplification of a single product of the appropriate size for each gene.

External Standard generation: Concentration of TH, NET, PGP 9.5 and PGK plasmids was measured by UV absorbance (OD260, Nano-drop). A series of 10 fold dilution from 100 pg/µl to 0.001 pg/µl of the DNA plasmids containing cDNA of the gene of interest were used to generate a standard curve. The optimized PCR program for

each gene was used to generate standard curves. Real-time PCR efficiencies for TH, NET, PGP and PGK amplification were 1.99, 1.99, 1.89 and 1.92, respectively. NET standard amplification curve (Fig M2, M3), melting curve (Fig M4) and gel electrophoresis (Fig M5) are provided as an example.

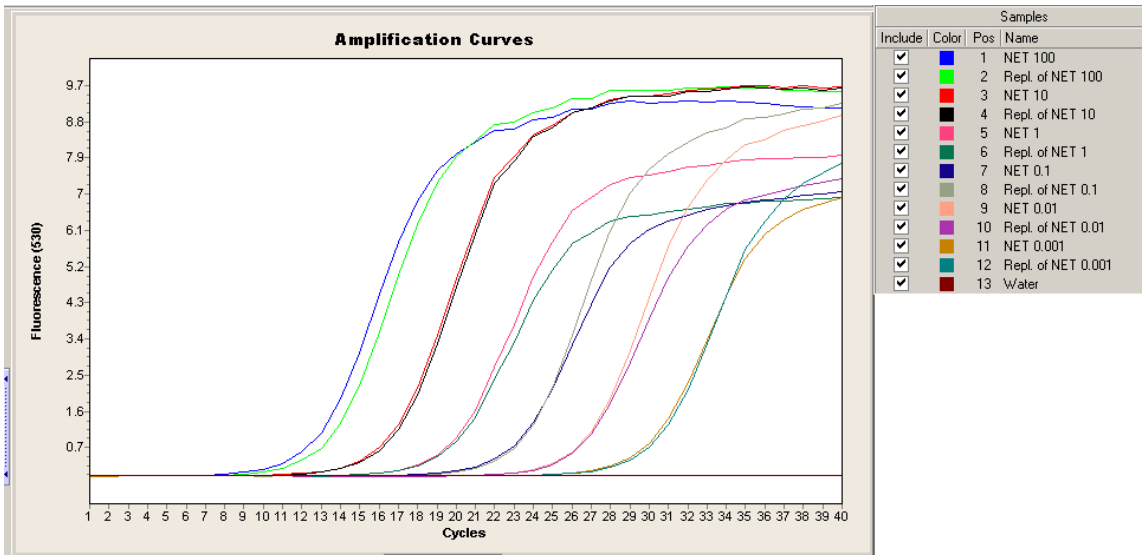

Figure M2. NET standard amplification curve. A serial 10 fold dilution from 100pg/µl to 0.001 pg/µl of the DNA plasmids containing the NET DNA fragment was used to generate a standard curve.

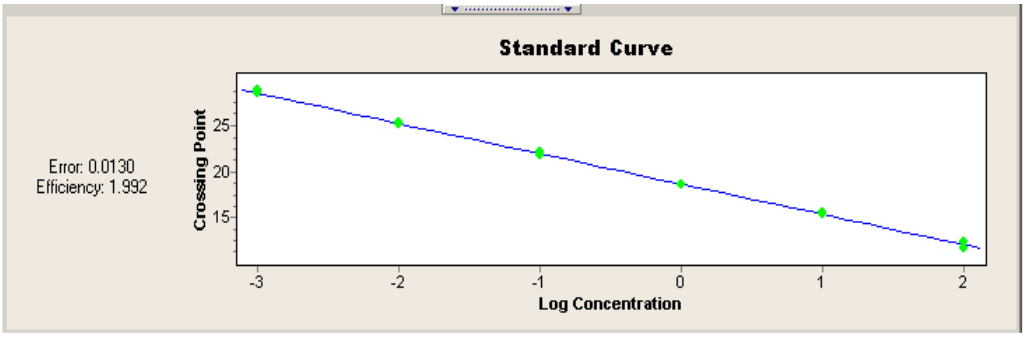

Figure M3. NET standard curve. A linear standard curve was obtained from the serial 10 fold dilutions of NET cDNA from 100 pg/µl to 0.001 pg/µl. Efficiency 1.99.

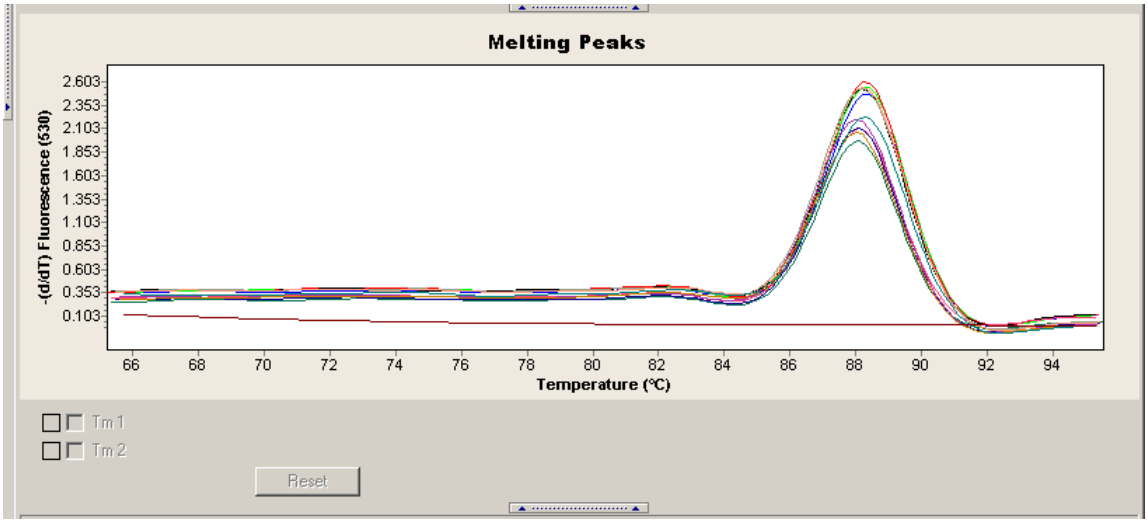

Figure M4. NET Melting curve. Melting cutve of a duplicated NET PCR product at a serial 10 fold dilution from 100 pg/µl to 0.001 pg/µl cDNA.

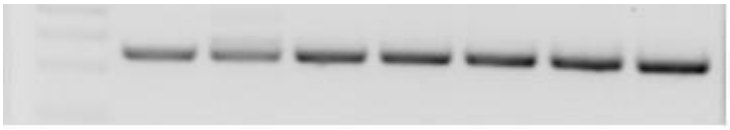

Figure M5. Agarose gel of PCR product for NET. Amplified NET PCR product at a serial 10 fold dilution from 100 pg/µl to 0.001 pg/µl cDNA.

Quantification of mRNA by real-time qPCR

Absolute quantification method was used to establish TH, NET, PGP 9.5 and PGK cDNA concentration, and then normalization of TH, NET and PGP 9.5 expression was accomplished by using the constitutively expressed reference gene, phosphoglycerokinase1 (PGK1), as an internal control. External standards for absolute quantification method were generated by using a series of dilution of TH, NET, PGP 9.5 and PGK as described above.

2.6.2. Western Blotting

Protein extraction: 100 mg of tissue from the base of the LV (area above the ligation) and the base of the RV were homogenized in 2 ml of lysis buffer (20mM Tris-HCl, 137 mM NaCl, 2 mM EDTA , 10 mM NaF, 0.5% Igepal and 10% glycerol, pH 8) with added protease inhibitor cocktail (Sigma, 10ul/ml buffer) by using a Polytron. Stellate ganglia were homogenized in 100 ul of lysis buffer with protease inhibitor cocktail by using a pestle (Bel-Art-Products, Pequannock, NJ) driven by a Pellet Pestle Motor. To solublize proteins, tightly closed tubes containing tissue homogenates were left on the rotary mixer in the cold room for 1 hour. Samples were then centrifuged for 20 min at 12000g at 4 °C, supernatants collected, aliquoted and stored at -80 °C. Protein concentration in samples was quantified by the Bradford method.

Gel electrophoresis: The mini-PROTEAN 3 system (Bio-rad) was utilized for hand casting the gels and performing protein electrophoresis. SDS page gels were cast according to the Instruction manual, resolving gel was 10 % acrylamide, and stacking gel was 4% acrylamide. After gels polymerized, they were placed into the inner chamber of the mini-tank module, and module was filled with the 1X Running buffer (25 mM Tris base, 190 mM Glycine and 0.1% SDS, pH 8.3). Just prior to loading, samples were diluted 1:1 with 2x Laemmli buffer mixed with 5% *b*-mercaptoethanol, and incubated at 70°C for 10 min. Protein ladder (dual color, Bio-rad) and samples were loaded into the gel wells with gel-loading pipette tips with the assistance of the sample loading guide. Power supply (Bio-rad Power Pac 200) was attached to the module, and electrophoresis was performed at 150V for approximately 1.5 hours till proteins were well separated

throughout the gel. TH, NET and ubiquitin proteins were fractionated on separate gels and transferred to different membranes.

Transfer: Protein transfer was carried out with the Mini Trans Blot Electrophoretic Transfer cell (Bio-rad). Transfer buffer (25 mM Tris, 192 mM glycine, 20% v/v methanol, pH 8.3) was prepared on the day of the transfer and chilled to 4 °C to improve heat dissipation. Polyvinylidene difluoride membrane (Bio-Rad) was first activated in methanol for 30 sec, and then equilibrated in the chilled transfer buffer for 10 min. Gels were carefully removed from the glass plates and were also equilibrated in the in the chilled transfer buffer for 10 min. After that the transfer "sandwich" was assembled according to the instruction manual, and placed into the transfer tank. Bio-ice cooling unit was inserted on the side of the tank, and small stirring bar was placed at the tank bottom. The tank was then filled with the chilled transfer buffer and positioned on the stirring plate so that the stirring bar could distribute chilled buffer throughout the unit. After the power supply was attached (Bio-rad Power Pac 300), protein transfer was carried out in at 4 °C in the cold room, at 300 mA for 1.5 hours. At the end of the transfer the "sandwich" was disassembled, and membranes were rinsed in dd H_2O. Protein transfer was confirmed with the Ponceau S dye (Sigma).

Immunoblotting: Prior to immunoblotting, membranes were first rinsed in 1X TBS-T buffer (50 mM Tris, 150 mM NaCl, pH 7.4 plus 0.5% Tween 20), and then blocked with TBS-T containing filtered 5% skim milk powder for 1 hour at room temperature.

Membranes for TH, NET, PGP 9.5 and β-Actin immunoblotting were cut below 37kDa. Upper parts of membranes (250-37 kDa) containing TH and NET proteins were incubated overnight at 4°C with polyclonal rabbit anti-TH (Chemicon #AB152, 1: 500)

and polyclonal rabbit anti-NET (Chemicon #AB5066P, 1:1000). Lower parts of both membranes containing PGP 9.5 protein (~ 26kDa) were incubated separately overnight at 4°C with mouse monoclonal anti-PGP (Vector # VP-P983, 1:40). Membrane containing ubiquitin and ubiquitin-bound proteins was incubated overnight at 4°C with polyclonal rabbit anti-Ubiquitin (Abcam #ab7780, 1:1000). All incubation steps were performed on the rocker platform with gentle agitation. Membranes were then washed with TBS-T buffer 4 times for 5 min, and incubated for 1 h at room temperature with goat anti-rabbit HRP conjugate for NET, TH and ubiquitin (1:5000, Santa Cruz #sc 2004) and sheep anti-mouse HRP conjugate for PGP 9.5 (1:10,000 Amersham #NXA93). Following incubation, membranes were washed with TBS-T buffer 6 times for 5 min, and immunoreactive bands were visualized by chemiluminescence (Western Lighting ECL, PerkinElmer). Membranes containing NET, TH proteins (250-37 kDa area) and ubiquitin were re-blocked overnight at 4°C with 5% non-fat dry milk diluted in TBS-T and then incubated for 1 hour at room temperature with monoclonal mouse anti-β–actin (1:10,000 Sigma #A2228). After washing with TBS-T buffer 4 times for 5 min, membranes were incubated with sheep anti-mouse HRP conjugate (1:10,000, Amersham #NXA93). Membranes were then extensively washed with TBS-T buffer and immunoreactive bands were visualized by chemiluminescence. Alpha Innotech Fluorochem HD camera system was used to expose and take images of the membranes.

Loading concentration: Optimal loading concentration was established to be 5 ug and 15 ug of total neuronal protein from stellate ganglia for TH and NET quantification respectively, and 20 ug of total cardiac protein for TH, NET and ubiquitin. To establish the optimal concentration for protein loading from a particular tissue, western blotting

was performed for the series of ascending protein concentrations and immunoreactive bands were visualized by chemiluminescence. Intensity of the bands was then quantified with AlphaEaseFC software, and protein concentration was plotted against the corresponding band intensity. Western blotting showing ascending TH protein concentration from the left stellate ganglia and graphic analysis of TH protein concentration vs. band intensity are provided as an example (Fig M6, M7).

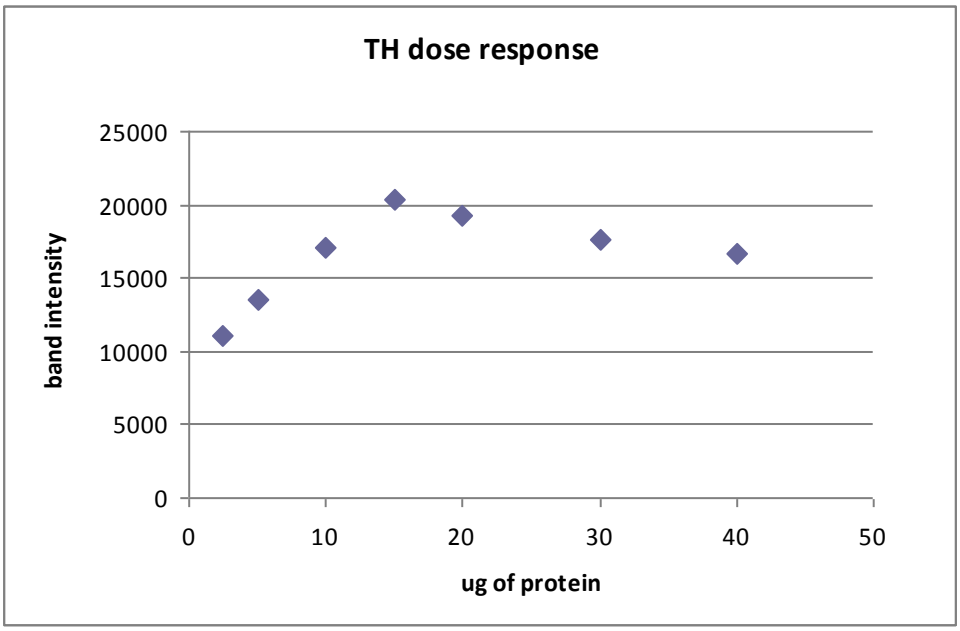

Figure M6. TH dose response in LSG. Loading protein concentration is plotted against corresponding band intensity.

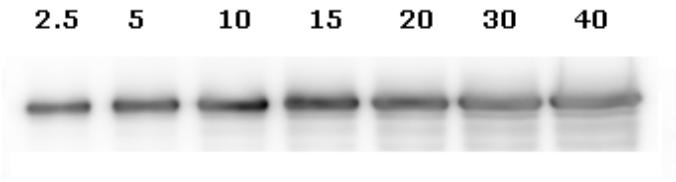

Figure M7. Western blotting of ascending concentration of TH protein (ug) from LSG for the dose response experiment.

Quality control: Prior to immunoblotting, western blotting using positive control (adrenal, brain) and negative control (liver) were performed for TH and NET antibodies respectively. In addition, NET antibody was pre-absorbed with the excess of NET peptide, and western blotting with pre-absorbed antibody showed a significant decrease in the intensity of NET bands in comparison with original antibody.

Analysis: Intensity of the bands was quantified with AlphaEaseFC image analysis software. Normalization of TH, NET, PGP 9.5, ubiquitin and ubiquitin-bound proteins expression was accomplished by using the constitutively expressed reference gene, β–actin, as an internal control. Expression of ubiquitinated proteins with approximate molecular weights of 30 kDa, 40 kDa, 50 kDa, 60 kDa, 100 kDa, 250 kDa was quantified separately. Various forms of NET protein (native NET 46 kDa, poorly glycosylated NET 54 kDa and active glycocylated NET 80 kDa) were quantified separately and together as a total NET for protein analysis.

2.6.3. Immunohistochemistry: PGP 9.5, GAP 43 and TH fluorescent doublestaining

LV and RV were cut longitudinally into 10 μm sections that were thaw mounted onto charged slides. Sections were then washed in PBS 3 times for 5 min, and rinsed with 1% sodium borohydride for 20 min to reduce fixative-induced autofluorescence. After 3 washes for 5 min in PBS, sections were blocked with 10% normal donkey serum in PBS (Jackson immunoresearch) at room temperature for 1h.

Protocol A: TH, GAP 43 or PGP 9.5 doublestaining

Sections were incubated with anti-TH sheep polyclonal antibodies (1:1000, Abcam, ab113) overnight at 4°C. All further steps were performed in the darkened room, and

incubations were carried out protected from light. Sections were rinsed 3 times for 5 min in PBS, and incubated for 1 h at room temperature with Dylight™ 594-conjugated AffiniPure Donkey anti-sheep IgG with minimal cross reaction to rabbit and rat serum proteins (1:500, Jackson immunoresearch, 713-515-147). Sections were rinsed 3 times for 5 min in PBS, and then incubated with anti-PGP 9.5 rabbit polyclonal antibody (1: 400, Ultraclone CL95101) overnight at 4°C or anti-GAP 43 rabbit polyclonal antibody (1: 500, Abcam ab16053). Following incubation, sections were rinsed 3 times for 5 min in PBS, and incubated for 1 h at room temperature with Alexa Fluor 488-conjugated AffiniPure Donkey anti-rabbit IgG with minimal cross reaction to sheep and rat serum proteins (1:800, Jackson immunoresearch, 711-545-152). Slides were then rinsed 3 times for 5 min in PBS.

Protocol B: PGP 9.5 and alpha-sarcomeric Actin doublestaining

Sections were incubated with anti-PGP 9.5 rabbit polyclonal antibody (1: 400, Ultraclone CL95101) overnight at 4°C. All further steps were performed in the dark room, and incubations were carried out protected from light. Sections were rinsed 3 times for 5 min in PBS, and incubated for 1 h at room temperature with Dylight™ 594-conjugated AffiniPure Donkey anti-sheep IgG with minimal cross reaction to rabbit and rat serum proteins (1:500, Jackson immunoresearch, 713-515-147). Sections were rinsed 3 times for 5 min in PBS, and then incubated with anti-alpha sarcomeric actin (1: 200, Abcam, ab 28052) overnight at 4°C. Following incubation, sections were rinsed 3 times for 5 min in PBS, and incubated for 1 h at room temperature with Dylight™ 594-conjugated AffiniPure Donkey anti-mouse IgG with minimal cross reaction to rabbit and

rat serum proteins (1:500, Jackson immunoresearch, 715-515-151). Slides were then rinsed 3 times for 5 min in PBS.

Sections for both protocols were cover slipped with Dako Fluorescent mounting medium, examined using an Olympus BX fluorescent microscope with the 10X objective, and then captured with a Spot camera (RT color) and Application software (Diagnistic instruments, Inc.).

Quality control: Immunohistochemical detection revealed strong specific signal for the TH antibody positive control (adrenal) and PGP 9.5 antibody positive control (brain) (Fig M8, M9). Negative control tissue for both TH and PGP 9.5 antibodies (liver) showed no fluorescent signal. Heart sections were also incubated only with anti-TH and anti-PGP primary antibodies, and only with Dylight™ 594-conjugated AffiniPure Donkey anti-sheep IgG and Alexa Fluor 488-conjugated AffiniPure Donkey anti-rabbit IgG secondary antibodies. No fluorescent signal was obtained from the sections incubated separately with primary and secondary antibodies.

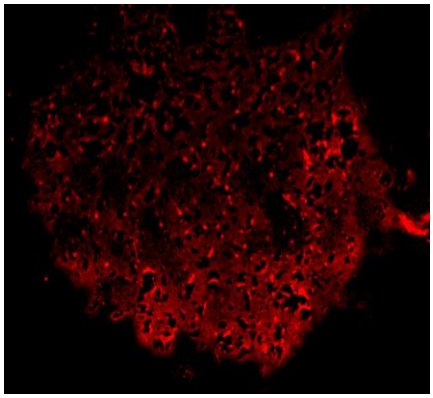

Figure M8. Positive control (medulla of the rat adrenal gland) for the TH antibody shows specific fluorescent signal at 20X magnification.

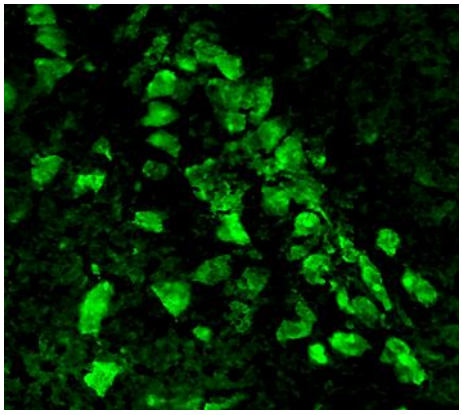

Figure M9. Positive control (neurons in the rat cortical brain region) for the PGP 9.5 antibody shows specific fluorescent signal at 40X magnification.

Analysis: Composite images of the base of the LV were used to create a representative section of the area of interest. Base of the LV and infarct border areas of LV were assessed separately and compared with corresponding areas in the control group. Six sections from each animal located at least 200 μm apart were analyzed from each heart and averaged together. TH, GAP 43 and PGP 9.5 innervation density was determined by the threshold discrimination using Image J. All pictures were first converted to black and white images, and then the auto brightness/contrast tool was applied. The threshold was adjusted manually to ensure that only specific staining was included in the quantification. Since the heart ventricles have 2 layers of muscle at different angles, sections included some nerve fibers cut longitudinally and some nerve fibers cut cross-sectionally (Lorentz et al. 2010). Innervation density was expressed as the percent of area that was above the threshold. Overlay of images was performed using Adobe Photoshop.

2.7. Statistical Analysis

Data represent means ± standard error (SE). Differences between two groups were compared by unpaired *t*-test. Differences between three groups were compared by two-way ANOVA. When the F values were significant for main effect, a Duncan's method was applied for multiple comparisons as a post-hoc analysis. The level of statistical significance was set at $p \leq 0.05$.

3. Results

3.1. The time course of TH, NET and PGP 9.5 expression in stellate ganglia and the heart post MI.

Average infarct sizes measured by the planimetry method were 30-35 % at 1, 4 and 12 wks post MI. Mean body weight was similar in MI rats and sham-operated rats. Hypertrophy of right and left ventricles was evident in MI rats at four and twelve wks, but not yet at one wk post MI. There were no significant differences in HR between the groups (Table R1).

Table R1. MI size and hypertrophy indices.

	One wk post MI		Four wks post MI		Twelve wks post MI	
	SHAM	MI	SHAM	MI	SHAM	MI
N	8	10	12	8	8	10
MI size (% LV)	-	32%	-	35%	-	30%
Body weight (BW)	307 ± 5	286 ± 7	419 ± 6	442 ± 11	624 ± 25	622 ± 24
LV (mg/100g BW)	242 ± 6	263 ± 8	220 ± 6	257 ± 11*	198 ± 5	227 ± 11*
RV (mg/100g BW)	74 ± 2	74 ± 4	69 ± 3	95 ± 12*	42 ± 4	57 ± 5*
HR	398 ± 8	405 ± 9	396 ± 9	370 ± 8	382 ± 8	371 ± 8

Data = mean ±SE. * $p < 0.05$, *vs. sham*

Echocardiography showed substantial decrease in systolic function in MI rats at 1, 4 and 12 wks post MI with a significant decrease in EF. LV Hemodynamics by Millar Catheter demonstrated that MI groups had a significant increase in LVEDP, decrease in

LVPSP, dP/d*t*max, and dP/d*t*min at all time points studied, but no significant changes over time in these parameters were present (Fig R1).

Figure R1. LV function measured by echocardiography and Millar catheter.

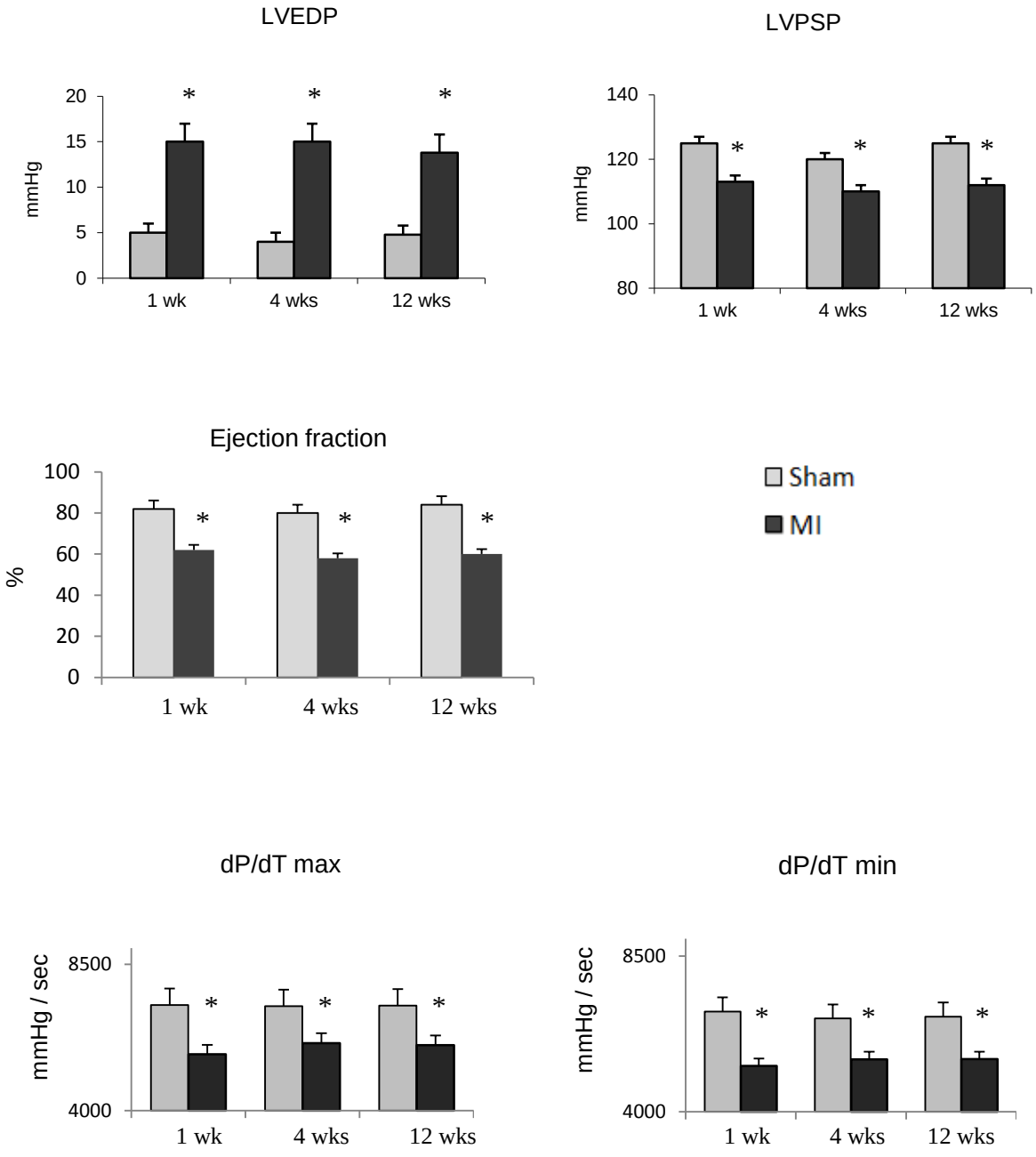

Data = mean ±SE, n= 8-12/group. * *p < 0.05, vs. sham*

3.1.1. Stellate ganglia

No changes in PGP 9.5 mRNA content were noted at 1 and 4 wks post MI, but at 12 wks post MI PGP 9.5 mRNA was significantly decreased ~ 2 fold in both LSG and RSG (Fig R2-3; Table R2-3). No changes in PGP 9.5 protein level were present.

No significant changes were found in TH and NET mRNA and TH protein in left and right stellate ganglia at all three post MI time points. Various forms of NET expressed in stellate ganglia (native NET 46 kDa, poorly glycosylated NET 54 kDa and active glycosylated NET 80 kDa) were quantified separately and together as total NET for protein analysis. In left stellate ganglia, no significant changes were observed in NET protein expression at 1 and 4 wks post MI (Fig R4-6). In contrast, at 12 wks post MI NET 80 protein content was increased ~ 2 fold, with no significant changes in NET 46, NET 54 and total NET expression (Fig R4, R7; Table R4). In right stellate gangia, there were no significant changes present in NET protein expression at all time points studied (Fig R8-11; Table R5).

Figure R2. TH, NET and PGP 9.5 mRNA in LSG at 1, 4 and 12 wks post MI.

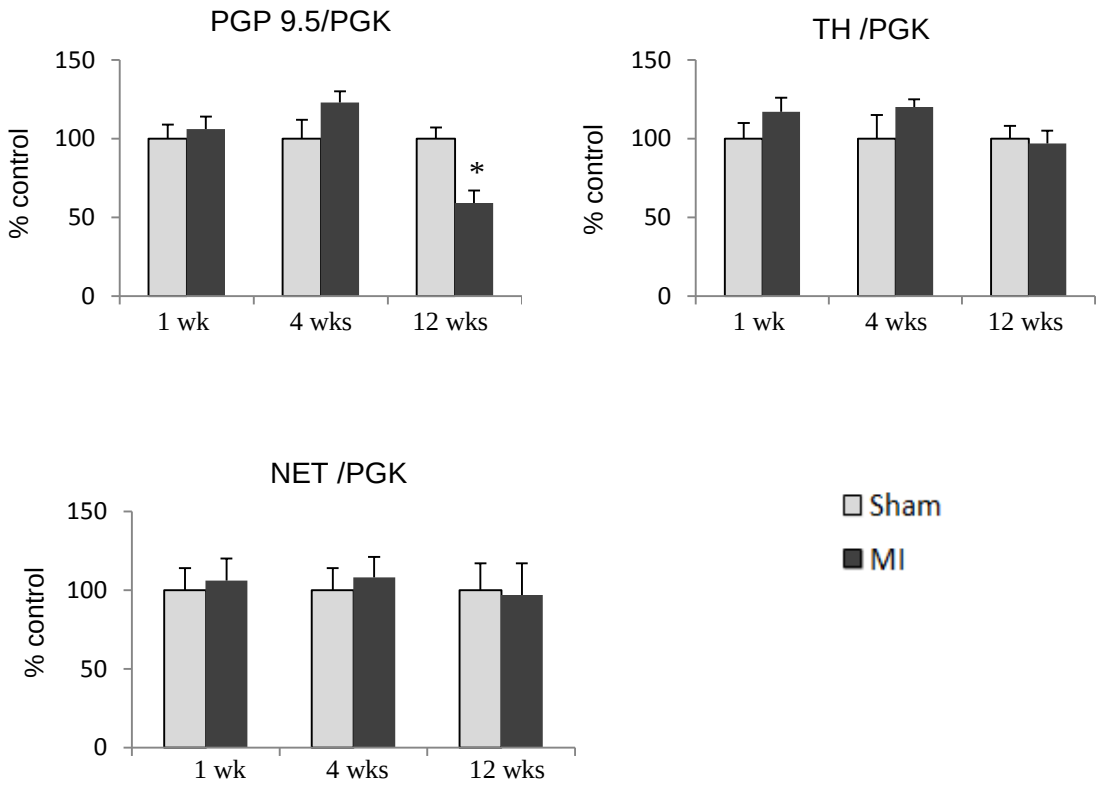

PGP 9.5, TH and NET mRNA expression was normalized to PGK. Data is shown as percentage of control group (100%). Data = mean ± SE, n = 4-6/group. ** $p < 0.05$, vs. sham*

Table R2. TH, NET and PGP 9.5 mRNA in LSG at 1, 4 and 12 wks post MI.

	PGP 9.5/PGK		**TH/PGK**		**NET/PGK**	
	Sham	**MI**	**Sham**	**MI**	**Sham**	**MI**
1 wk	3.82±0.35	4.05±0.32	1.15±0.12	1.35±0.13	1.55±0.22	1.65±0.23
4 wks	3.45±0.43	4.26±0.29	1.01±0.15	1.21±0.03	1.94±0.27	2.09±0.27
12 wks	0.98±0.07	0.58±0.05*	1.32±0.10	1.29±0.10	1.07±0.19	1.00±0.23

Data = mean ±SE, n= 4 - 6/group. ** $p < 0.05$, vs. sham*

Figure R3. TH, NET and PGP 9.5 mRNA in RSG at 1, 4 and 12 ws post MI.

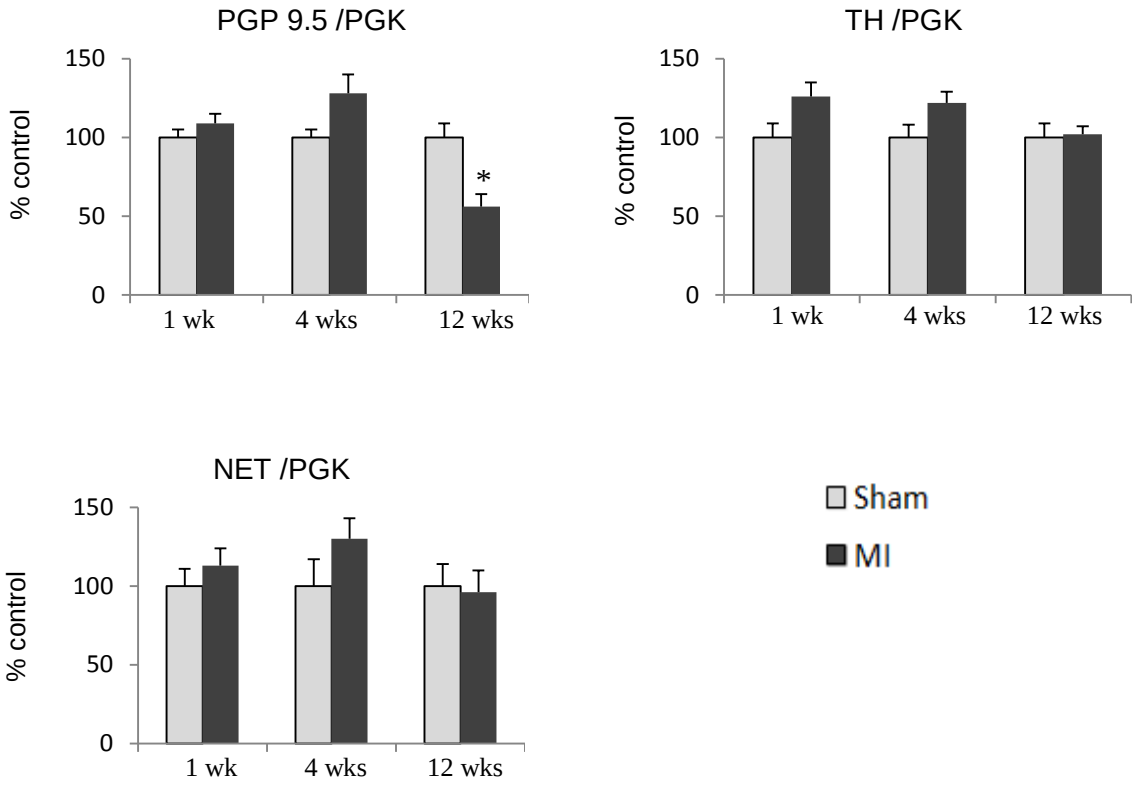

PGP 9.5, TH and NET mRNA expression was normalized to PGK. Data is shown as percentage of control group (100%). Data = mean ± SE, n = 4-6/group. ** $p < 0.05$, vs. sham*

Table R3. TH, NET and PGP 9.5 mRNA in RSG at 1, 4 and 12 wks post MI.

	PGP 9.5/PGK		TH/PGK		NET/PGK	
	Sham	MI	Sham	MI	Sham	MI
1 wk	3.55±0.15	3.90±0.25	1.23±0.11	1.55±0.14	1.25±0.14	1.42±0.15
4 wks	3.63±0.18	4.61±0.53	0.80±0.06	0.98±0.07	1.45±0.25	2.00±0.25
12 wks	1.15±0.11	0.65±0.05*	1.72±0.16	1.76±0.06	1.18±0.16	1.14±0.16

Data = mean ±SE, n = 4-6/group. ** $p < 0.05$, vs. sham*

Figure R4. TH, NET and PGP 9.5 proteins in LSG at 1, 4 and 12 wks post MI.

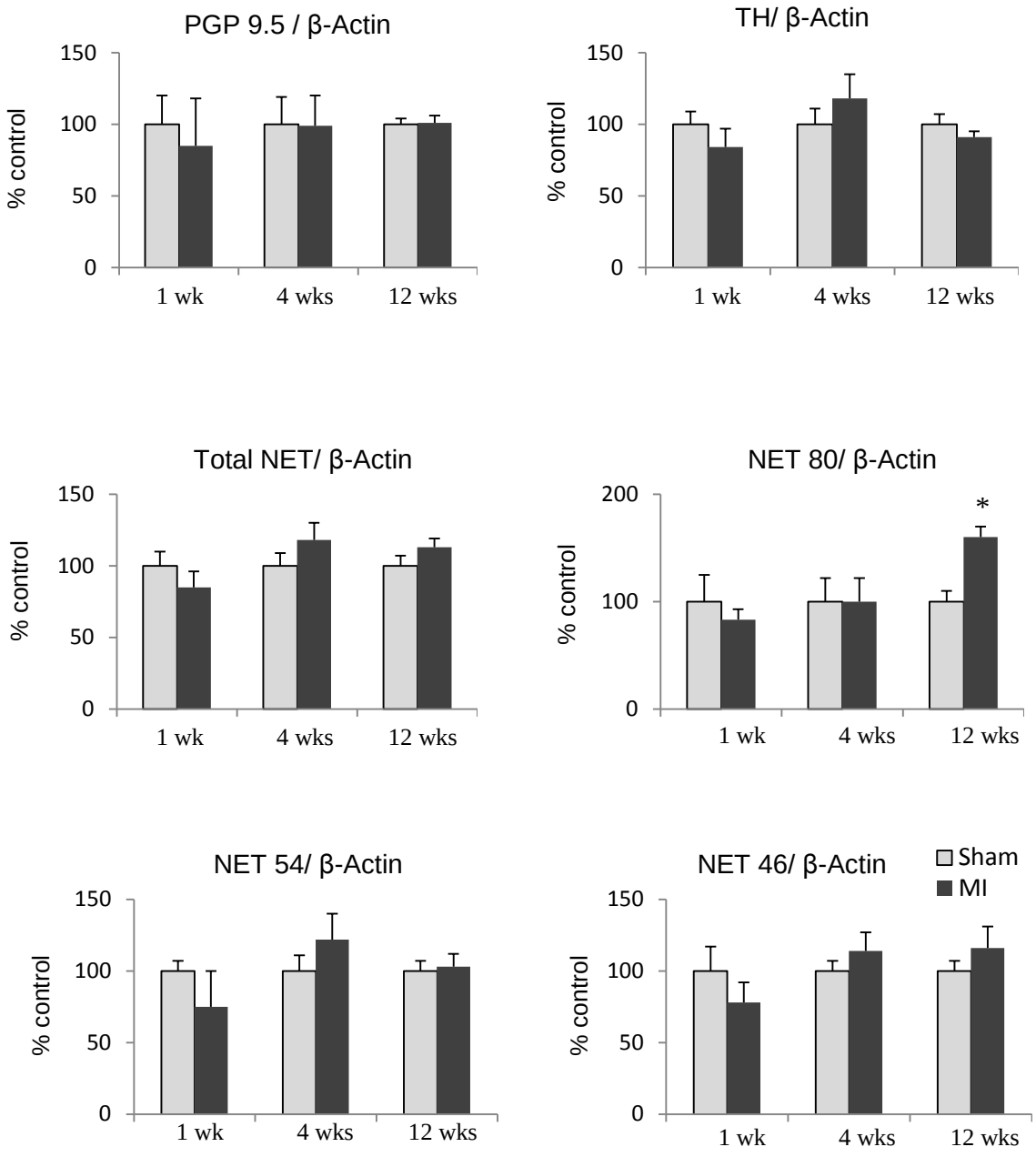

TH, NET and PGP 9.5 proteins were normalized to β-Actin. Various forms of NET expression are shown separately: 46 kDa native protein, partially glycosylated 54 kDa protein, active fully glycosylated 80 kDa protein and total NET. Data is shown as percentage of control group (100%). Data = mean ± SE, n = 4 - 6/group. *$p < 0.05$, *vs. sham*

Figure R5. Western blot from LSG showing TH, NET, PGP 9.5 and β-Actin proteins at 1 week post MI.

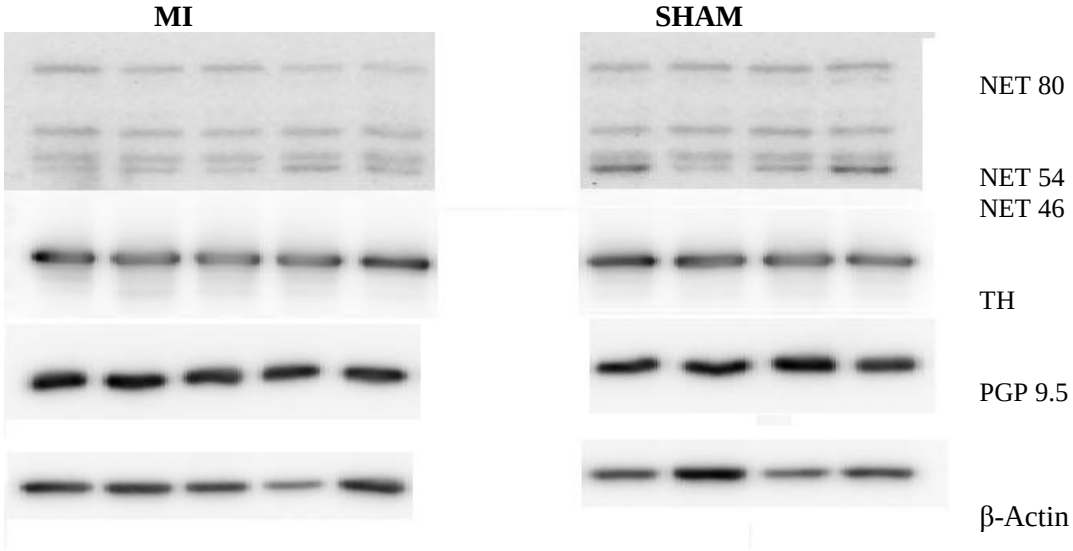

Figure R6. Western blot from LSG showing TH, NET, PGP 9.5 and β-Actin proteins at 4 wks post MI.

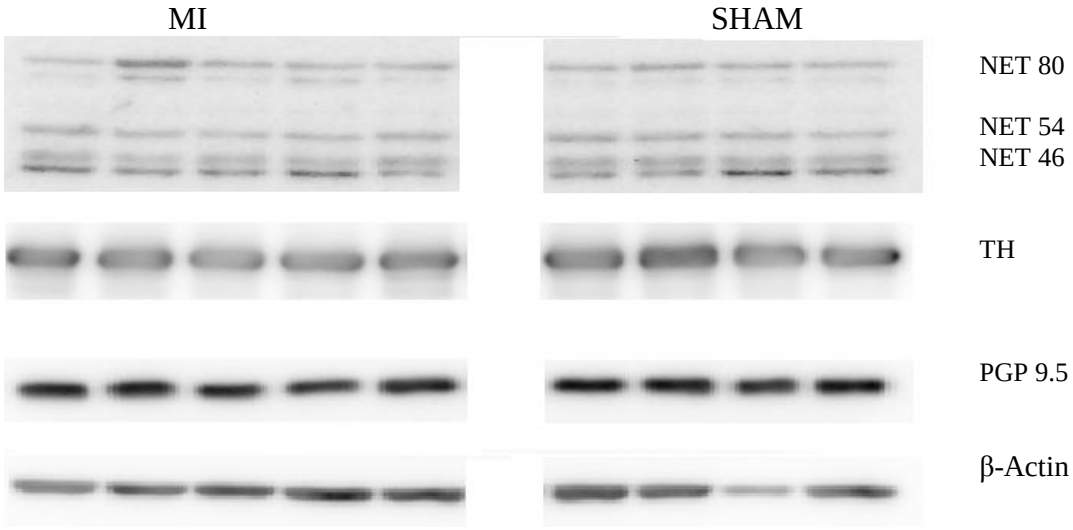

Figure R7. Western blot from LSG showing TH, NET, PGP 9.5 and β -Actin proteins at 12 wks post MI.

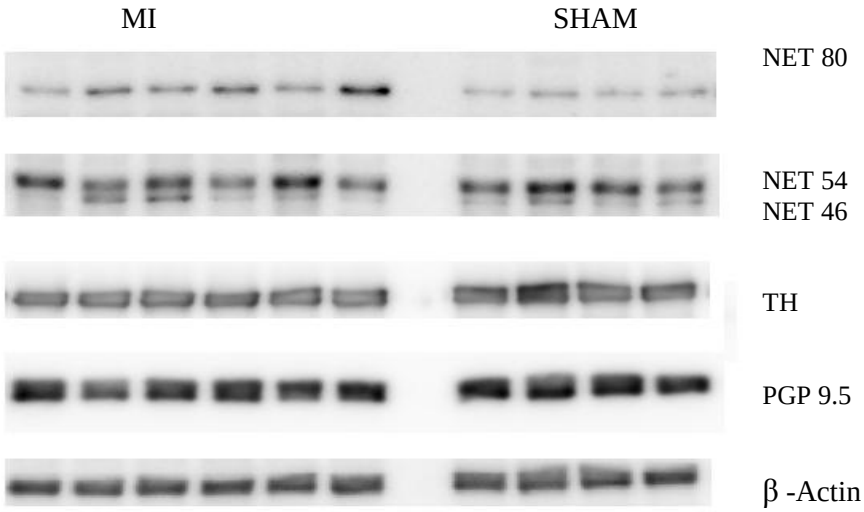

Table R4. TH, NET and PGP 9.5 protein content in LSG at 1, 4 and 12 wks post MI.

	PGP 9.5/ β-Actin		TH/ β -Actin		Total NET/ β -Actin	
	Sham	MI	Sham	MI	Sham	MI
	3.94 ±0.80	3.38 ± 1.10	5.75 ±0.50	4.83 ± 0.63	0.45±0.04	0.37 ±0.04
4 wks	0.68 ±0.13	0.67 ± 0.14	0.99±0.11	1.17± 0.21	0.33±0.03	0.39±0.05
12 wks	3.72 ±0.13	3.75 ± 0.19	3.81 ± 0.27	3.47 ±0.04	3.20 ±0.21	3.60 ± 0.22

	NET 46/ β -Actin		NET 54/ β -Actin		NET 80/ β -Actin	
	Sham	MI	Sham	MI	Sham	MI
1 wk	0.18±0.03	0.14 ± 0.02	0.16 ± 0.01	0.12 ± 0.03	0.12 ± 0.03	0.10 ± 0.01
4 wks	0.14 ±0.01	0.16 ± 0.02	0.09±0.01	0.11±0.02	0.09±0.02	0.09±0.02
12 wks	0.97 ±0.07	1.13 ± 0.17	1.94 ± 0.13	1.99 ± 0.18	0.69 ± 0.07	**1.11 ±0.11***

Data = mean ±SE, n= 4 - 6/group. **p < 0.05, vs. sham*

Figure R8. TH, NET and PGP 9.5 proteins in RSG at 1, 4 and 12 wks post MI.

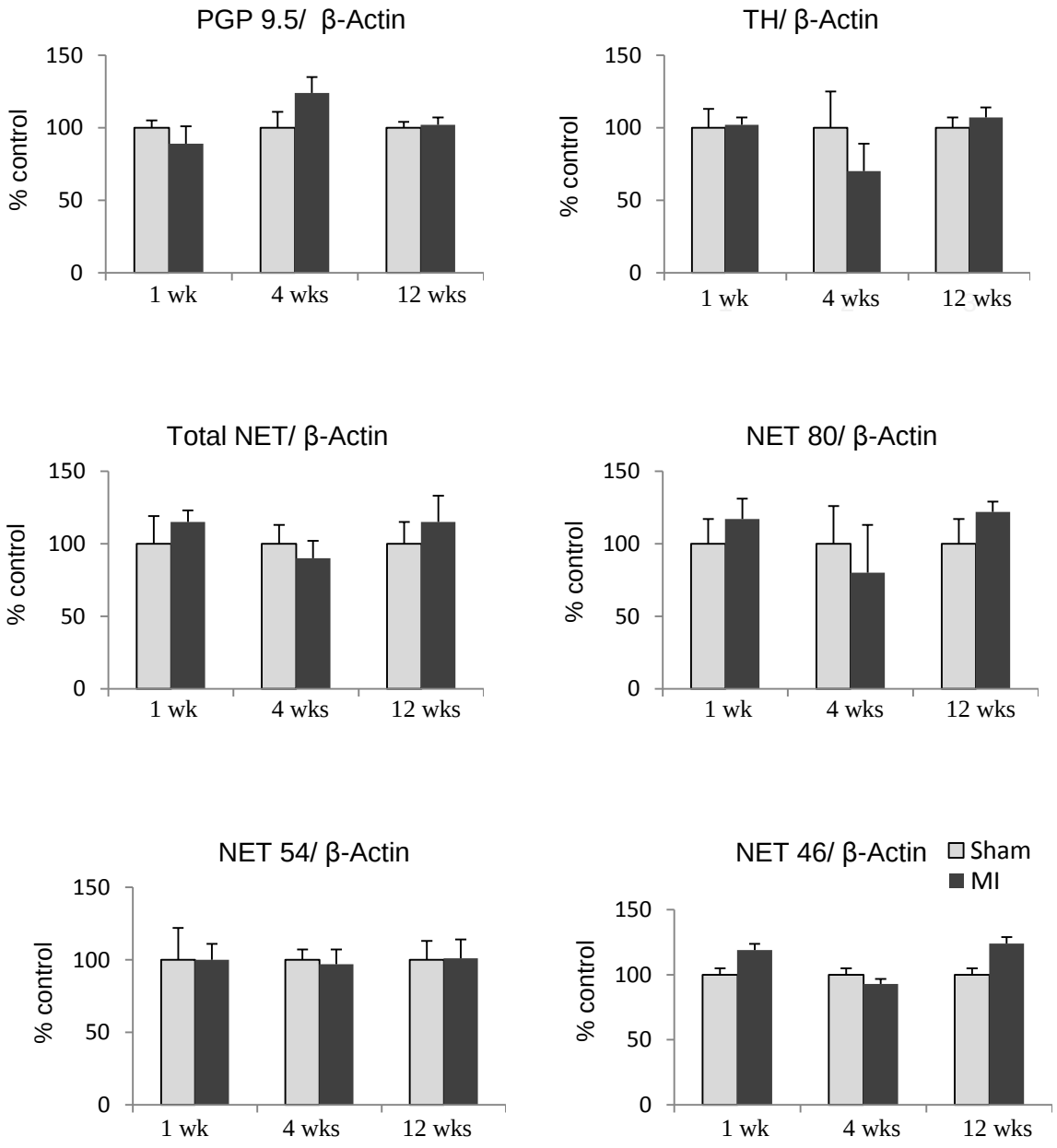

TH, NET and PGP 9.5 proteins were normalized to β-Actin. Various forms of NET expression are shown separately: 46 kDa native protein, partially glycosylated 54 kDa protein, active fully glycosylated 80 kDa protein and total NET. Data is shown as percentage of control group (100%).Data = mean ±SE, n = 4-6/group. * $p < 0.05$, *vs. sham*

Figure R9. Western blot from RSG showing TH, NET, PGP 9.5 and β-Actin proteins at 1 wk post MI.

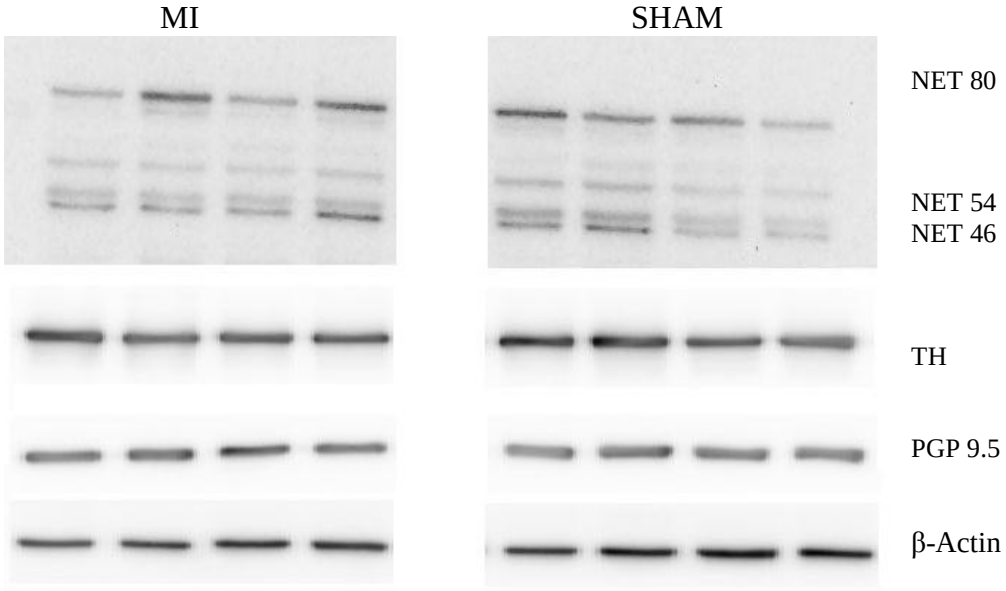

Figure R10. Western blot from RSG showing TH, NET, PGP 9.5 and β-Actin proteins at 4 wks post MI.

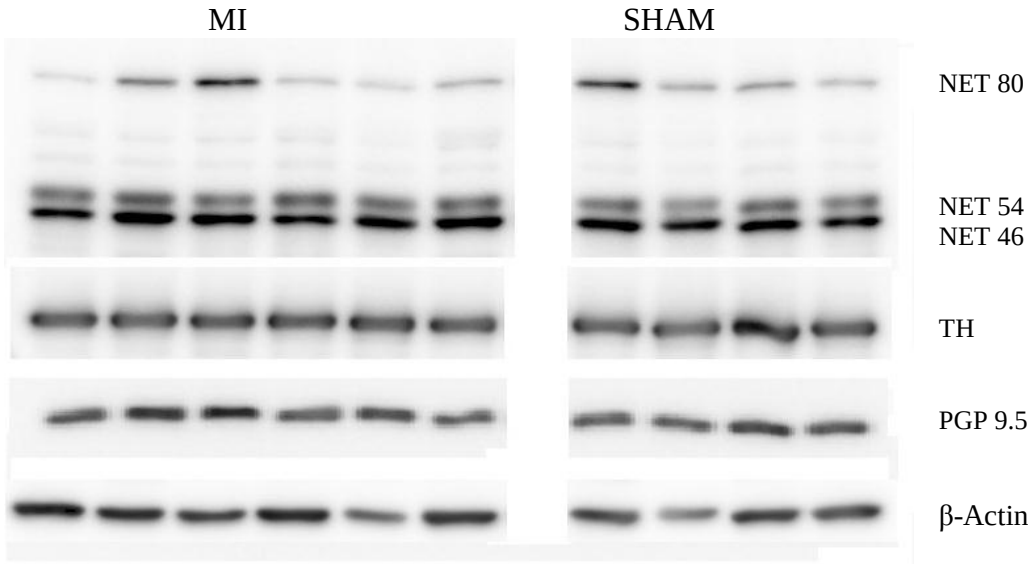

Figure R11. Western blot from RSG showing TH, NET, PGP 9.5 and β-Actin proteins at 12 wks post MI.

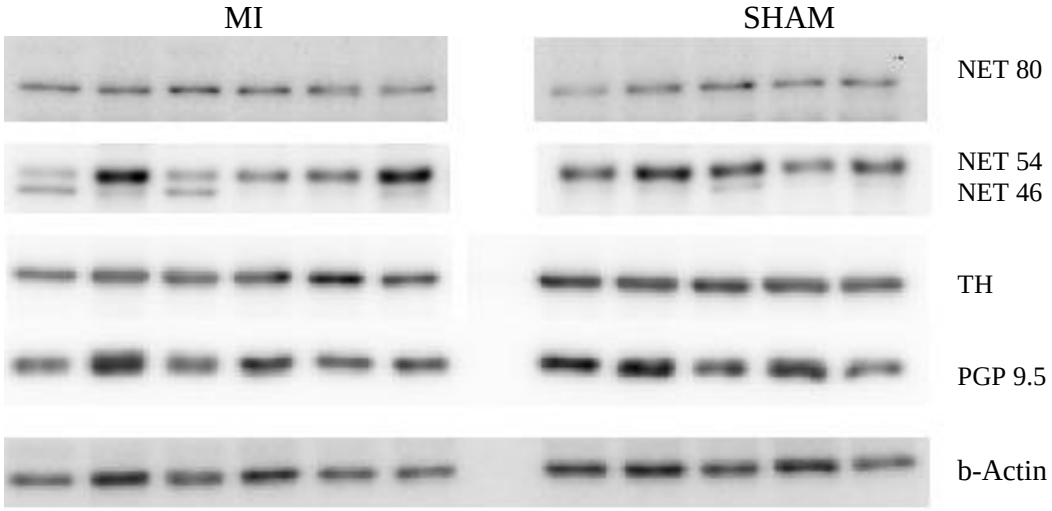

Table R5. TH, NET and PGP 9.5 protein content in RSG at 1, 4 and 12 wks post MI.

	PGP 9.5/ β-Actin		TH/ β-Actin		Total NET/ β-Actin	
	Sham	MI	Sham	MI	Sham	MI
1 wk	1.85±0.09	1.64±0.19	1.89 ± 0.24	1.92 ± 0.10	0.32 ± 0.06	0.37 ± 0.03
4 wks	0.50±0.05	0.62±0.07	1.03 ± 0.26	0.71±0.13	1.09 ± 0.14	0.98 ± 0.12
12 wks	5.11 ±0.21	5.17±0.24	5.92 ± 0.36	6.34 ± 0.47	4.39 ±0.65	5.06 ± 1.05

	NET 46/ β-Actin		NET 54/ β-Actin		NET 80/ β-Actin	
	Sham	MI	Sham	MI	Sham	MI
1 wk	0.11 ± 0.02	0.13 ± 0.01	0.09 ± 0.02	0.09 ± 0.01	0.12 ±0.02	0.14 ± 0.02
4 wks	0.57 ±0.06	0.53 ± 0.05	0.32 ±0.02	0.31 ±0.03	0.19 ± 0.05	0.15±0.05
12 wks	0.93 ±0.02	1.15 ± 0.24	3.22±0.43	3.26±0.42	0.36±0.06	0.44±0.03

Data = mean ±SE, n= 4 - 6/group. * $p < 0.05$, *vs. sham*

3.1.2. Left ventricle (area above ligation).

No significant changes in PGP 9.5 mRNA content were found in the base of the LV (Table R6), but protein content in rats post MI was significantly increased twofold at one wk post MI, and ~ 60% at 4 wks post MI (Fig R12-15; Table R7). At 12 wks post MI changes in PGP 9.5 protein expression were no longer present (Fig R13, R16).

No changes in TH mRNA were found at all three post-MI time points, but NET mRNA was significantly increased 2 fold in MI rats at 1 and 12 wks post MI, and tended to be increased (p=0.2) 2 fold at 4 wks post MI (Fig R12; Table R6). Protein expression of TH and various forms of NET was not affected by the MI condition.

Figure R12. TH, NET and PGP 9.5 mRNA in LV above the ligation at 1, 4 and 12 wks post MI.

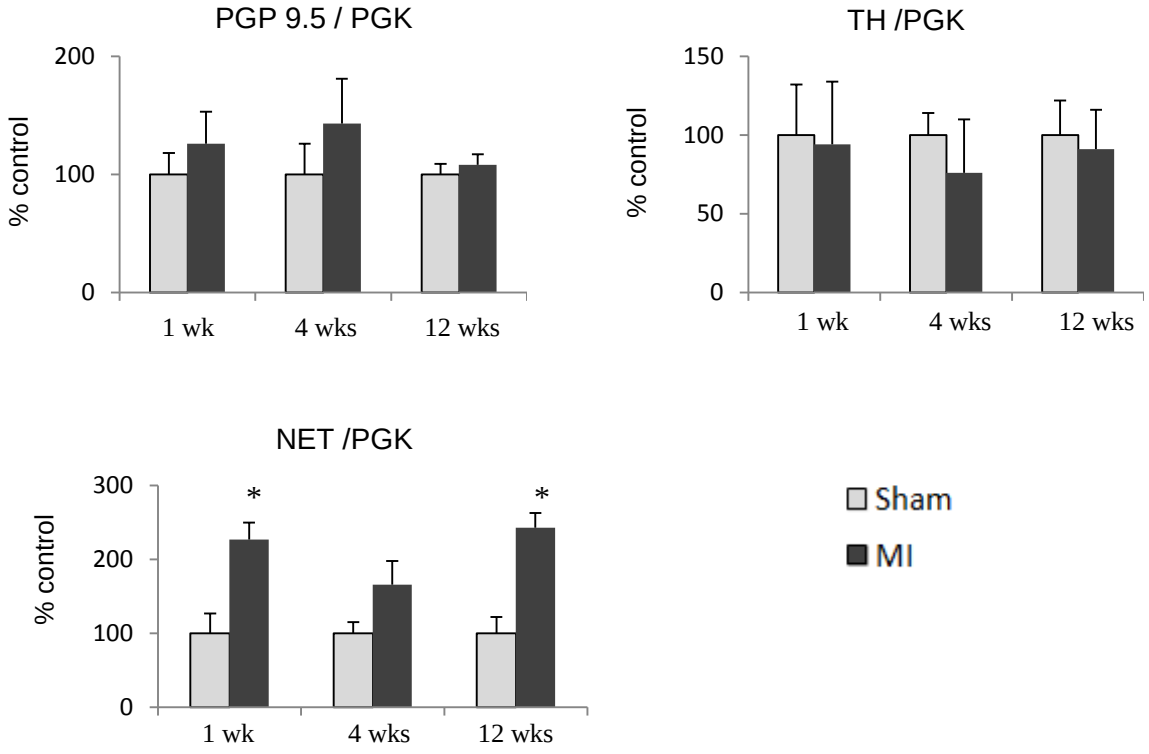

PGP 9.5, TH and NET mRNA expression was normalized to PGK. Data is shown as percentage of control group (100%). Data = mean ± SE, n = 8 - 10/group. * *P < 0.05, vs. sham*

Table R6. TH, NET and PGP 9.5 mRNA in LV at 1, 4 and 12 wks post MI.

	PGP 9.5/PGK * 10^{-3}		TH/PGK * 10^{-4}		NET/PGK * 10^{-4}	
	Sham	MI	Sham	MI	Sham	MI
1 wk	1.22± 0.22	1.54 ±0.42	1.60±0.51	1.50±0.60	1.38±0.37	**3.14±0.73***
4 wks	1.13 ± 0.30	1.62 ± 0.63	1.71±0.23	1.28±0.43	1.19±0.45	1.98±0.64
12 wks	2.26 ± 0.21	2.45 ± 0.21	0.56 ± 0.12	0.51 ± 0.13	0.89 ±0.20	**2.17± 0.45***

Data = mean ±SE, n= 6 - 10/group. * *$p < 0.05$, vs. sham*

Figure R13. TH, NET and PGP 9.5 proteins in LV above ligation at 1, 4 and 12 wks post MI.

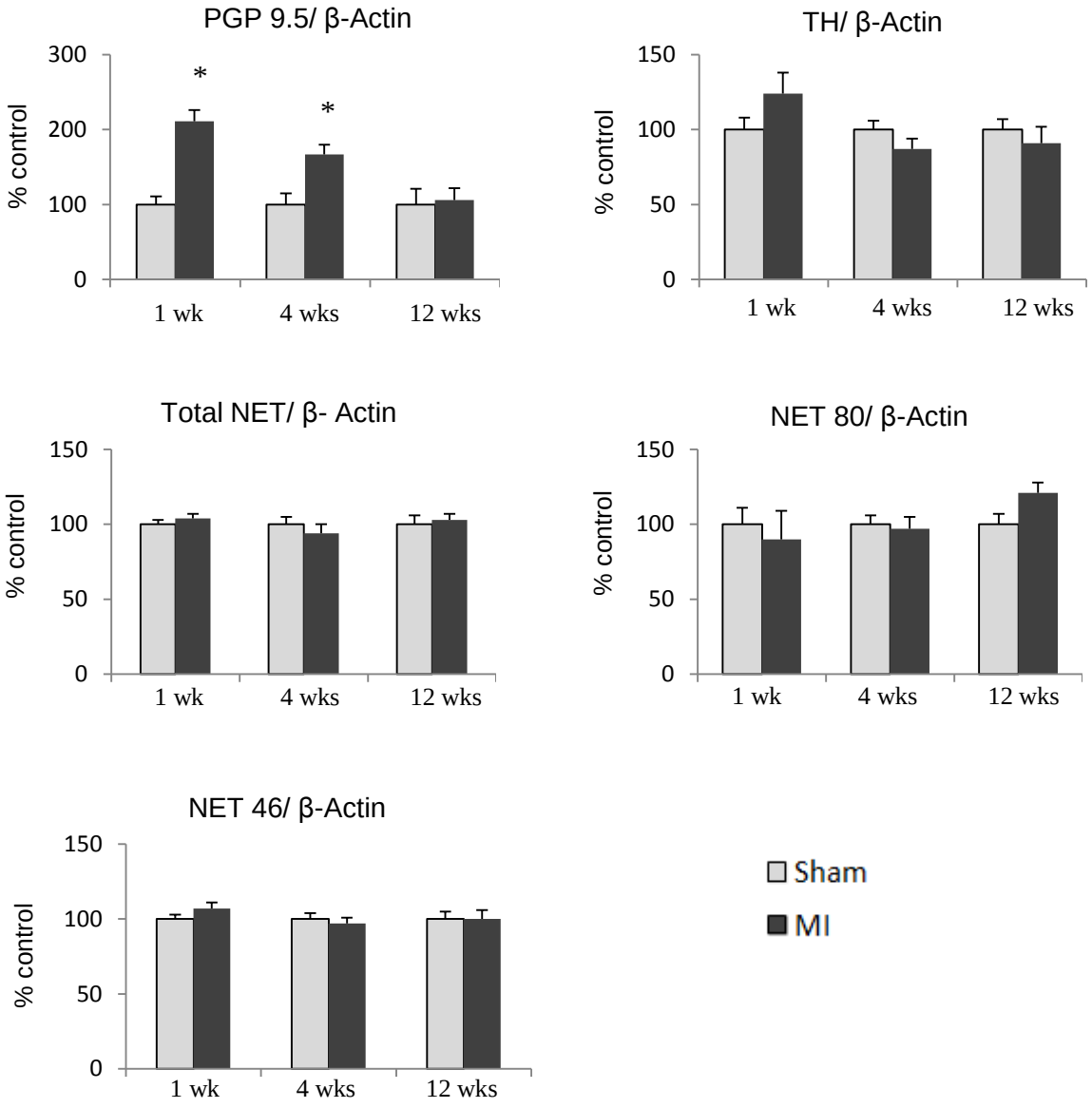

TH, NET and PGP 9.5 proteins were normalized to β-Actin. Various forms of NET expression are shown separately: 46 kDa native protein, partially glycosylated 54 kDa protein, active fully glycosylated 80 kDa protein and total NET. Data is shown as percentage of control group (100%). Data = mean ±SE, n=5 - 8/group. * $p < 0.05$, *vs. sham*

Figure R14. Western blot from the LV above the ligation showing TH, NET, PGP 9.5 and β-Actin proteins at 1 wk post MI.

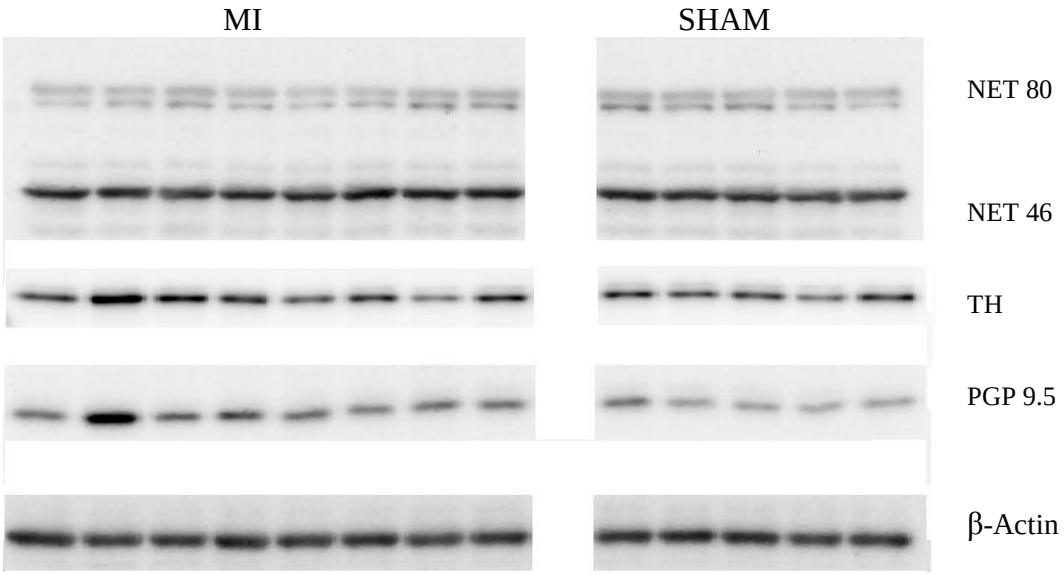

Figure R15. Western blot from the LV above the ligation showing TH, NET, PGP 9.5 and β-Actin proteins at 4 wks post MI.

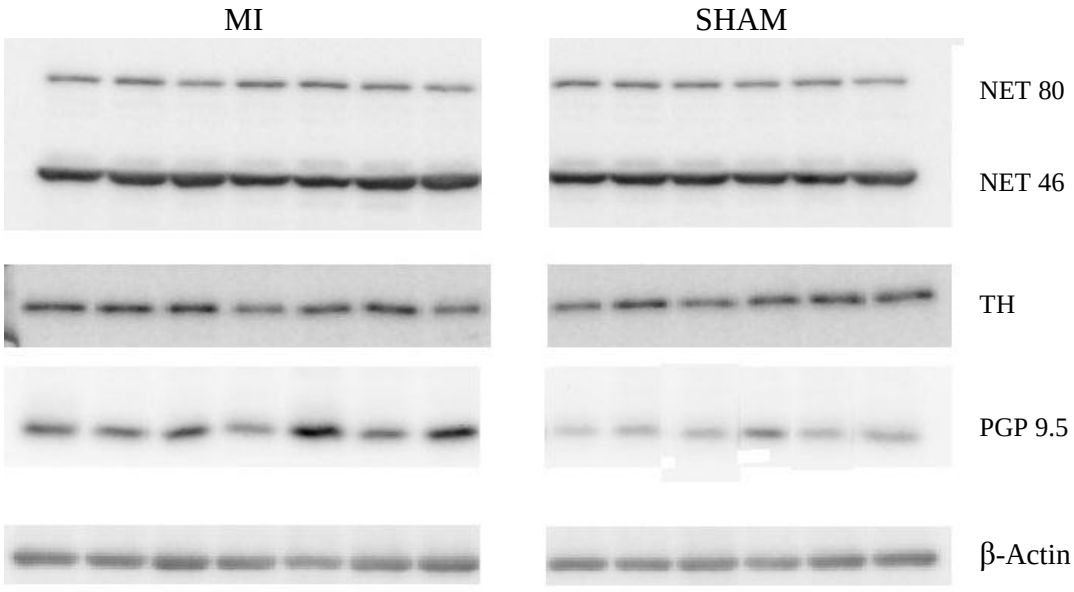

Figure R16. Western blot from the LV above the ligation showing TH, NET, PGP 9.5 and β-Actin proteins at 12 wks post MI.

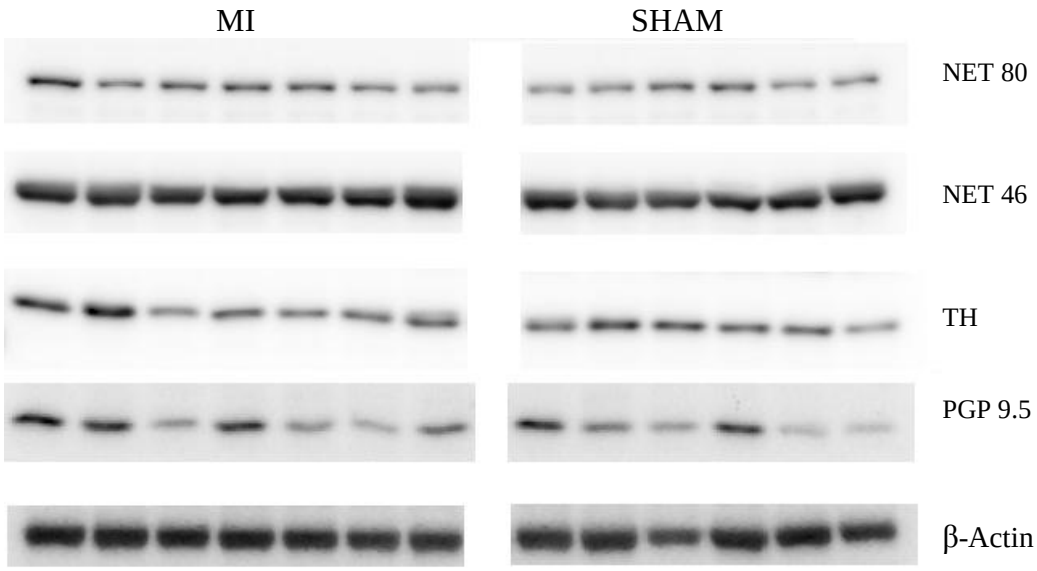

Table R7. TH, NET and PGP 9.5 protein expression in the base of the LV above the ligation post MI.

	PGP 9.5/ β-Actin		TH/ β-Actin		Total NET/ β-Actin	
	Sham	MI	Sham	MI	Sham	MI
1 wk	0.92 ± 0.10	**1.94 ± 0.30***	3.65 ± 0.30	4.51 ± 0.62	3.22 ± 0.10	3.36 ± 0.10
4 wks	0.61 ± 0.09	**1.00 ± 0.13***	1.90 ± 0.11	1.65 ± 0.12	2.30 ± 0.12	2.15 ± 0.12
12 wks	1.12 ± 0.24	1.19 ± 0.19	20.22±1.54	18.69±2.00	6.42 ± 0.36	6.63 ±0.26

	NET 46/ β-Actin		NET 80/ β-Actin	
	Sham	MI	Sham	MI
1 wk	2.45 ± 0.08	2.63 ± 0.09	0.80 ± 0.09	0.72 ± 0.14
4 wks	1.64 ± 0.07	1.59 ± 0.06	0.64 ± 0.04	0.62 ± 0.05
12 wks	4.98 ± 0.27	4.99 ± 0.27	1.36 ± 0.10	1.65 ± 0.12

Data = mean ±SE, n=5-8/group. * $p < 0.05$, *vs. sham*

3.1.3. Right ventricle

PGP 9.5 mRNA content was unaltered in the RV at 1 and 4 wks post MI, but significantly decreased ~ 2 fold at 12 wks post MI (Fig R17, Table R8). In contrast, PGP 9.5 protein expression was significantly increased twofold at one week post MI, and ~ 60% at four weeks post MI (Fig. R18-20; Table R9). No changes in PGP 9.5 protein expression were present at 12 wks post MI (Fig R21).

TH and NET mRNA levels and protein content were unaltered at all post MI time points.

Figure R17. TH, NET and PGP 9.5 mRNA in RV at 1, 4 and 12 wks post MI.

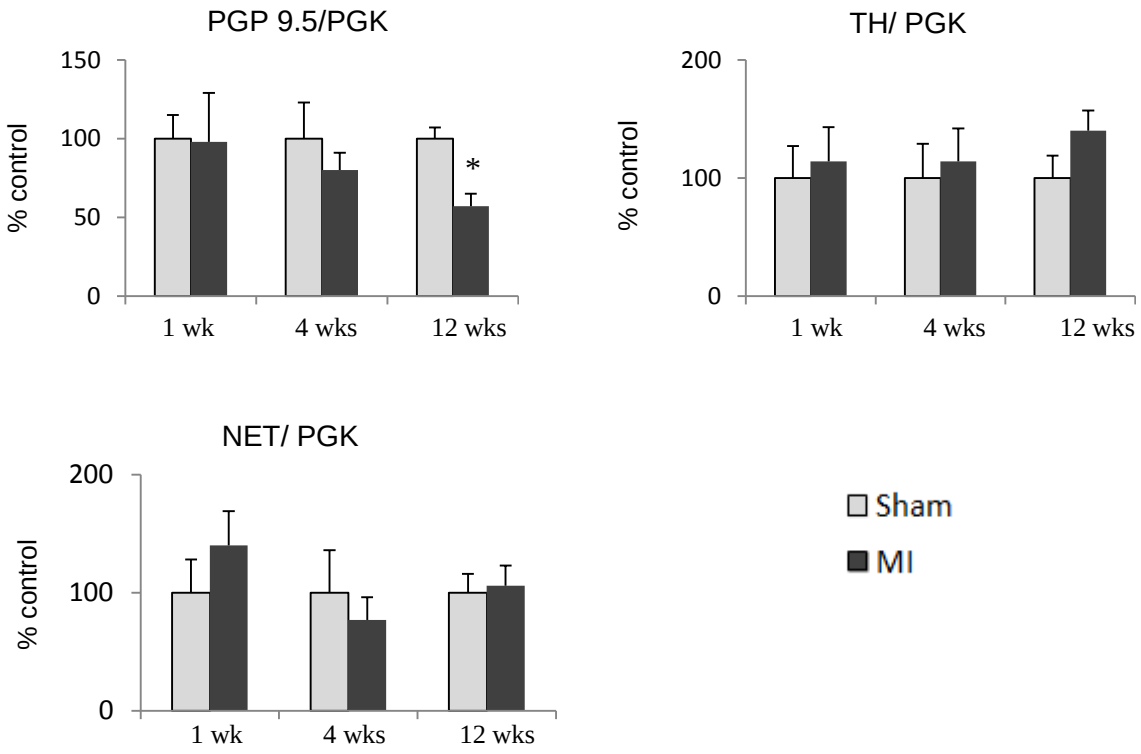

PGP 9.5, TH and NET mRNA expression was normalized to PGK. Data is shown as percentage of control group (100%).Data = mean ±SE, n=6 - 10/group. * *p < 0.05, vs. sham*

Table R8. TH, NET and PGP 9.5 mRNA in RV at 1, 4 and 12 wks post MI.

	PGP 9.5/PGK * 10^{-3}		TH/PGK * 10^{-4}		NET/PGK * 10^{-4}	
	Sham	MI	Sham	MI	Sham	MI
1 wk	0.65 ± 0.10	0.64 ± 0.20	0.75 ± 0.20	0.86 ± 0.25	0.61±0.17	0.85 ± 0.25
4 wks	1.11 ± 0.25	0.89 ± 0.10	0.88 ± 0.26	1.00 ± 0.28	1.23 ± 0.45	0.95 ± 0.18
12 wks	1.50 ± 0.10	**0.86 ±0.07***	0.58 ± 0.11	0.81 ± 0.14	1.02 ± 0.16	1.08 ± 0.19

Data = mean ±SE, n= 6 - 10/group. * *p < 0.05, vs. sham*

Figure R18. TH, NET and PGP 9.5 proteins in RV at 1, 4 and 12 wks post MI.

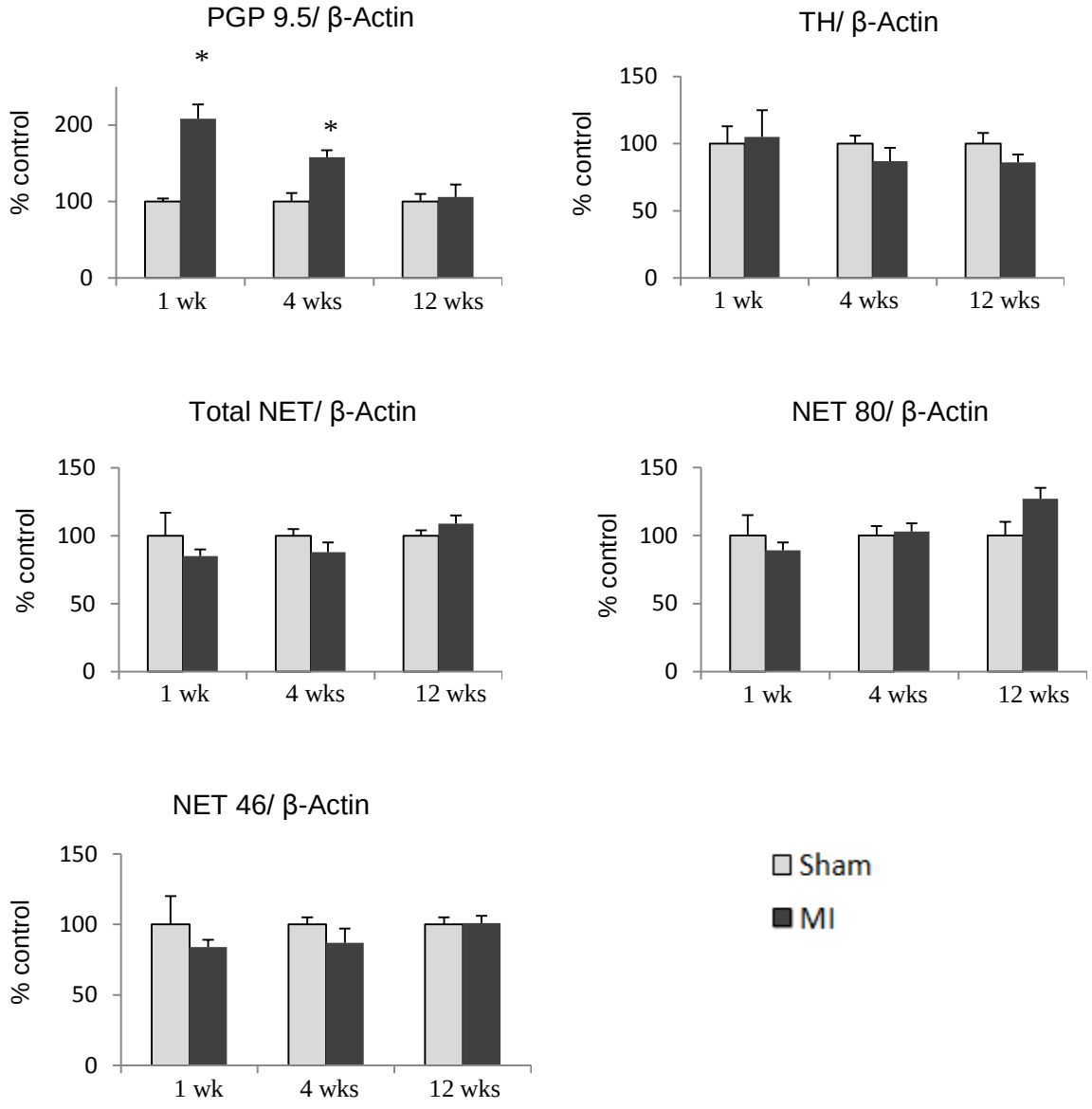

TH, NET and PGP 9.5 proteins were normalized to β-Actin. Various forms of NET expression are shown separately: 46 kDa native protein, partially glycosylated 54 kDa protein, active fully glycosylated 80 kDa protein and total NET. Data is shown as percentage of control group (100%). Data = mean ±SE, n=5 - 8/group. * $p < 0.05$, *vs. sham*

Figure R19. Western blot from the RV showing TH, NET, PGP 9.5 and β-Actin proteins at 1 wk post MI.

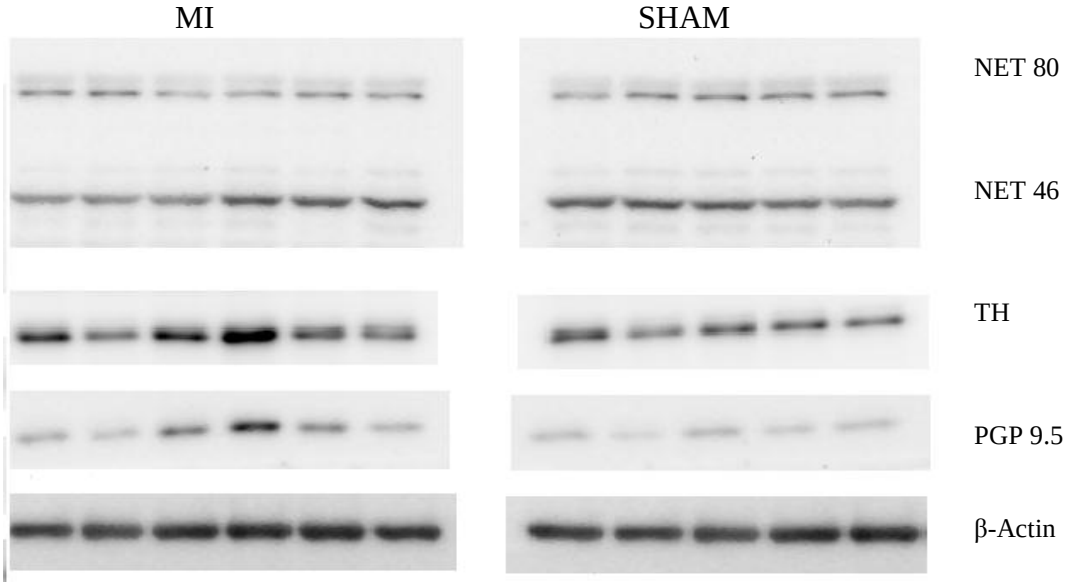

Figure R20. Western blot from the RV showing TH, NET, PGP 9.5 and β-Actin proteins at 4 wks post MI.

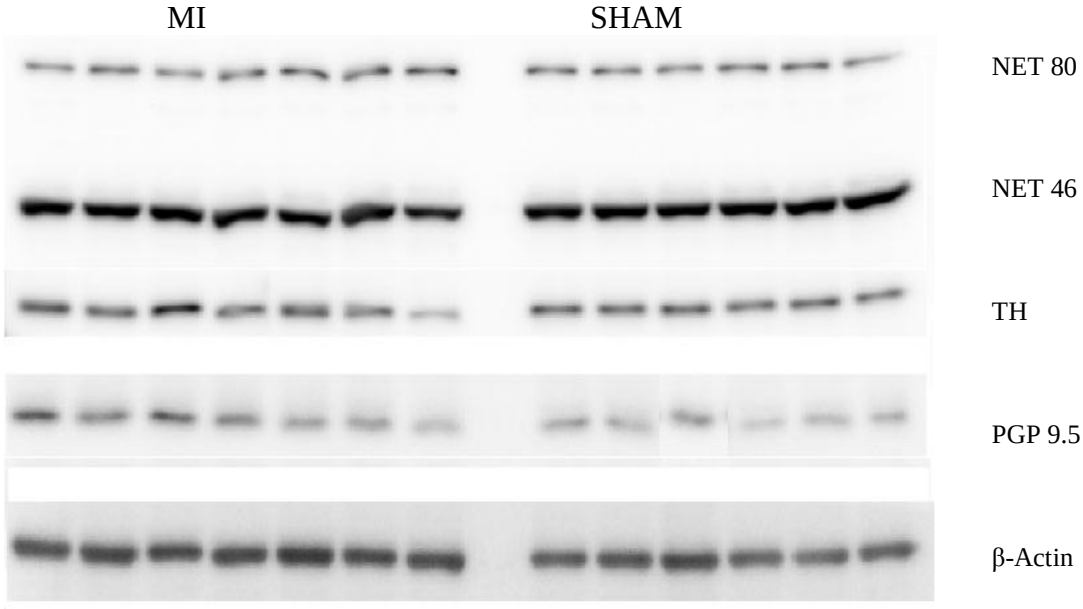

Figure R21. Western blot from the RV showing TH, NET, PGP 9.5 and β-Actin proteins at 12 wks post MI.

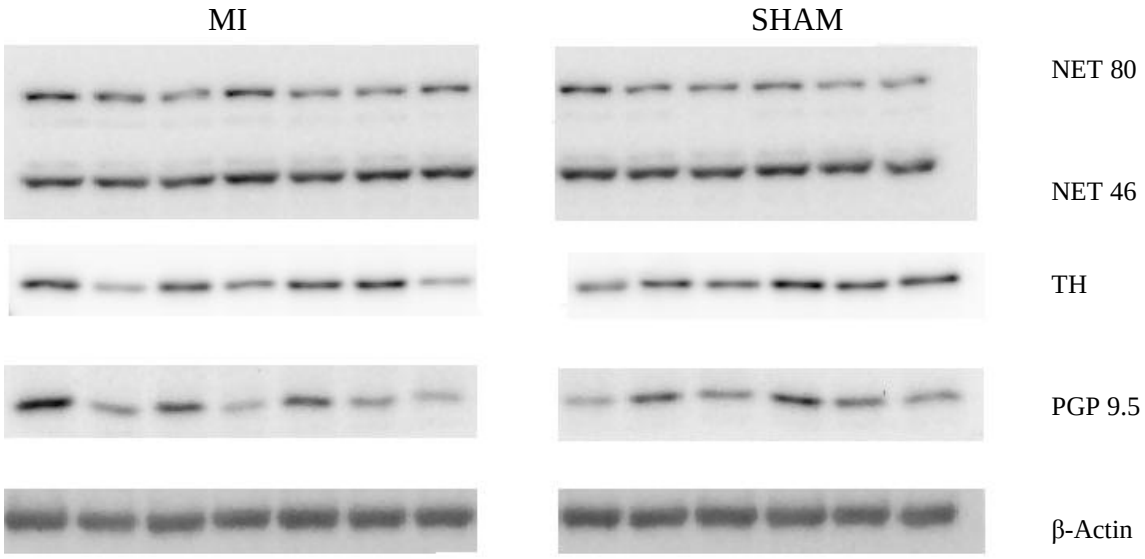

Table R9. TH, NET and PGP 9.5 protein expression in the base of the RV above the ligation post MI.

	PGP 9.5/β-Actin		TH/ β-Actin		Total NET/ β-Actin	
	Sham	MI	Sham	MI	Sham	MI
1 wk	0.51 ± 0.02	**1.06 ± 0.20***	3.35± 0.42	3.50±0.71	2.12 ± 0.37	1.79 ± 0.06
4 wks	1.00 ± 0.11	**1.58 ± 0.15***	3.43 ± 0.20	2.97 ± 0.30	9.50 ± 0.47	8.4 ± 0.58
12 wks	1.86 ± 0.19	1.97 ± 0.32	4.87 ± 0.37	4.19 ± 0.53	0.97 ±0.04	1.06 ± 0.06

	NET 46/ β-Actin		NET 80/ β-Actin	
	Sham	MI	Sham	MI
1 wk	1.52±0.31	1.27 ± 0.05	0.55 ± 0.08	0.49 ± 0.03
4 wks	6.93 ± 0.22	6.00 ± 0.60	2.34 ± 0.17	2.38 ± 0.14
12 wks	0.67 ± 0.01	0.68 ± 0.02	0.30 ± 0.03	0.38 ± 0.03

Data = mean ±SE, n=6-7/group. * $p < 0.05$, *vs. sham*

3.1.4. Summary of main findings.

1) PGP 9.5: There is a significant 2 fold increase in PGP 9.5 protein expression in the base of the LV and the RV at 1 and 4 wks post MI, which is no longer present at 12 wks post MI. In LSG, RSG and the RV there is a significant 2 fold decrease in PGP 9.5 mRNA at 12 wks post MI.

2) NET: There is a significant 2.5 fold increase in NET mRNA in the base of the LV at 1 and 12 wks post MI, and a tendency towards increase at 4 wks post MI.

3) TH: There are no significant changes in TH mRNA and protein in the heart and SG.

3.2. Origin of NET, TH and PGP 9.5 mRNA and proteins in the LV.

PGP 9.5, TH and NET mRNA content in the LV was markedly lower than that in the neurons of stellate ganglia (Table R10). At 1 wk post bilateral stellate ganglionectomy (SGX) no significant changes in PGP 9.5 and NET mRNA were observed in the LV, whereas TH mRNA was significantly increased by 50% (Fig R22, Table R11). Western blotting showed a significant 50% decrease in PGP 9.5 protein content, and a marked 90% decrease in TH protein content. No significant differences were found in NET 80 kDa, NET 46 kDa and total NET protein expression (Fig R23-24, Table R12).

Table R10. TH, NET and PGP 9.5 mRNA in the LV and LSG of sham rats.

PGP 9.5/PGK		TH/PGK		NET/PGK	
LSG	LV* 10^{-3}	LSG	LV* 10^{-4}	LSG	LV* 10^{-4}
3.82±0.35	1.22± 0.22	1.15 ± 0.12	1.60±0.51	1.55 ± 0.22	1.38±0.37

Data = mean ±SE, n= 6-8/group.

Table R11. TH, NET and PGP 9.5 mRNA in the LV at 1 wk post bilateral SGX.

PGP 9.5/PGK * 10^{-3}		TH/PGK * 10^{-4}		NET/PGK * 10^{-4}	
Sham	SGX	Sham	SGX	Sham	SGX
0.49 ± 0.09	0.44 ± 0.08	0.26 ± 0.04	**0.42 ± 0.04***	0.53 ±0.14	0.73 ± 0.19

Data = mean ±SE, n= 4 - 5/group. * *P < 0.05, vs. sham*

Figure R22. TH, NET and PGP 9.5 mRNA in LV 1 wk post bilateral SGX.

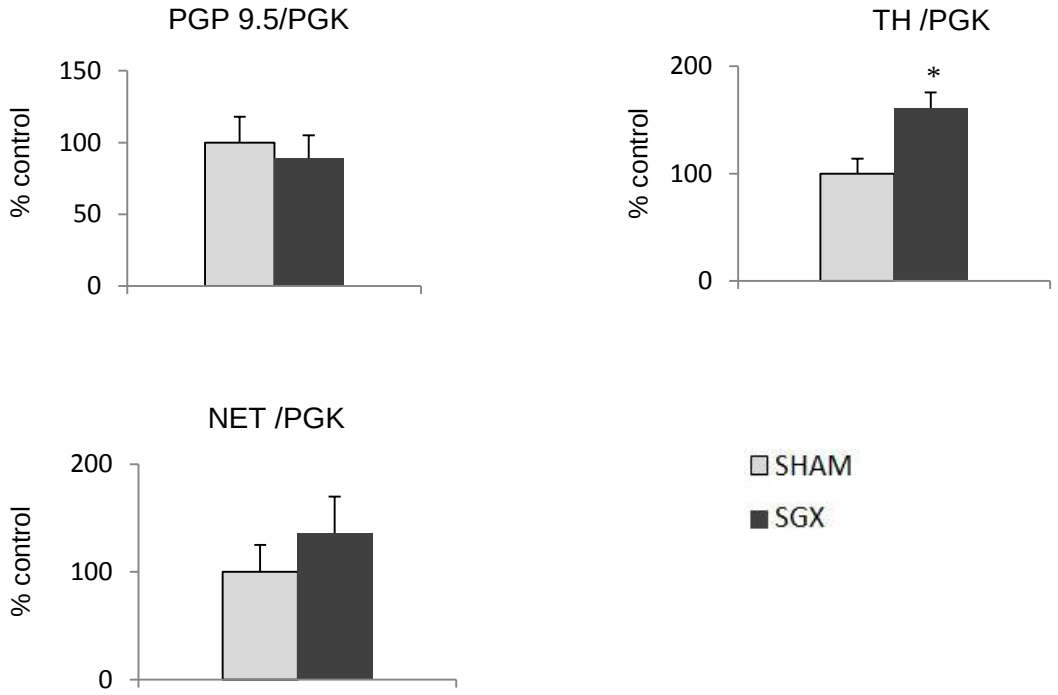

PGP 9.5, TH and NET mRNA expression was normalized to PGK. Data is shown as percentage of control group (100%). Data = mean ±SE, n=4 - 5/group. * *p < 0.05, vs. sham*

Table R12. TH, NET and PGP 9.5 proteins in the LV at 1 wk post bilateral SGX.

	PGP 9.5/β-Actin		TH/ β-Actin		Total NET/ β-Actin	
	Sham	SGX	Sham	SGX	Sham	SGX
1 wk	0.47 ± 0.01	**0.24 ± 0.01***	0.85 ± 0.15	**0.12 ± 0.03***	3.82 ± 0.25	4.44 ±0.40

	NET 46/ β-Actin		NET 80/ β-Actin	
	Sham	SGX	Sham	SGX
1 wk	3. 94 ± 0.80	3.10 ± 0.15	0.92 ± 0.05	1.26 ± 0.14

Data = mean ±SE, n=4 - 5/group.
* *p < 0.05, vs. sham*

Figure R23. TH, NET and PGP 9.5 proteins in LV 1 wk post bilateral SGX.

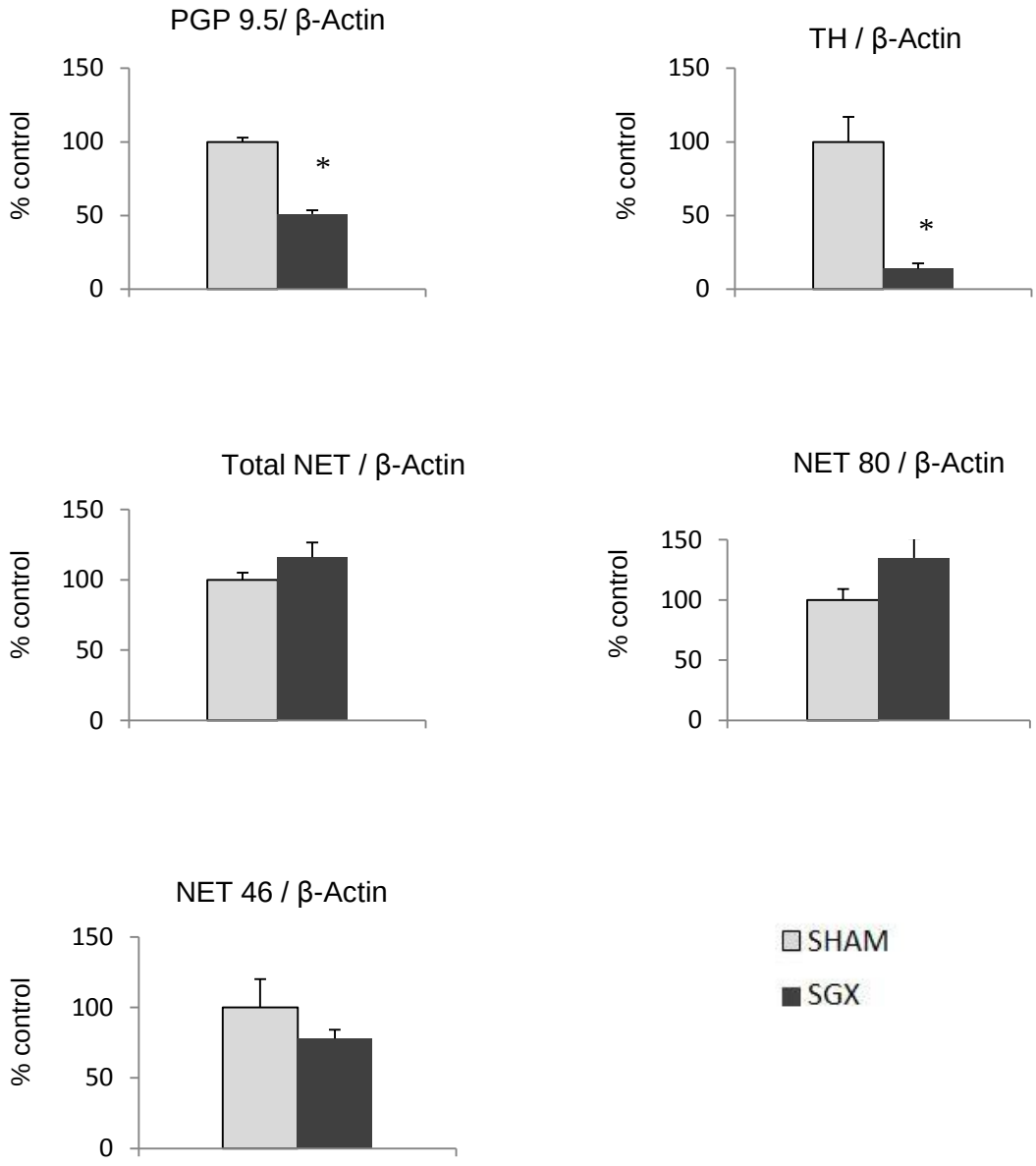

TH, NET and PGP 9.5 proteins were normalized to β-Actin. Data is shown as percentage of control group (100%). Data = mean ± SE, n = 4 - 5/group. *$p < 0.05$, *vs. sham*

Figure R24. Western blot from the LV showing TH, NET, PGP 9.5 and β-Actin proteins at 1 wk post bilateral SGX.

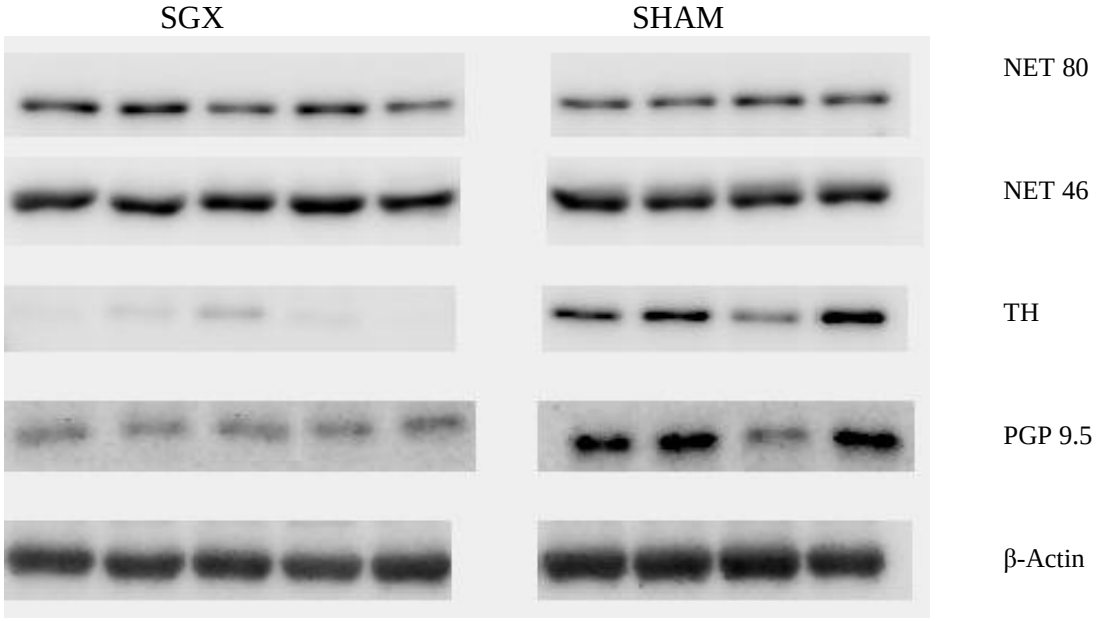

3.2.1. Summary of main findings:

At 1 wk post bilateral stellate ganglionectomy cardiac TH mRNA was significantly elevated by 50%, whereas TH protein was significantly reduced by 90%. Cardiac PGP 9.5 protein content in the heart was significantly reduced by 50%, which is notably less than the TH reduction. No significant differences were found in NET mRNA, and NET 80 kDa, NET 46 kDa and total NET protein content.

3.3. Cardiac sympathetic innervation in rats 10 days post MI. Effects of central MR blockade.

At 1 wk post MI there is a significant 2 fold increase in PGP 9.5 protein expression in the base of the LV and the RV, but no changes in TH protein expression in both ventricles. We used fluorescent immunohistochemistry to analyze the location of the increased PGP 9.5 protein and assess possible changes in cardiac sympathetic innervation. The mean infarct size was 32% of the total LV area. MI group of rats had a significant increase in LVEDP (15.5 ± 1.5 mmHg vs. 5.7 ± 0.47 mmHg in Sham), a significant decrease in LVPSP (105 ± 2.5 mmHg vs. 124 ± 1.9 mmHg MI in Sham), dP/d*t*max (5700 ± 170 mmHg⁄sec and 7280 ± 130 mmHg⁄sec MI vs. Sham) and dP/d*t*min (5320 ± 140 mmHg⁄sec and 6700 ± 115 mmHg⁄sec MI vs. Sham).

3.3.1. Cardiac sympathetic innervation in rats at 10 days post MI.

Innervation pattern in ventricles is heterogeneous, and epicardial side of the myocardium has more notable innervation density than endocardial side (Fig R25, Table R13). In sham rats at the epicardial surface PGP 9.5 showed highest nerve density with 1.10 ± 0.07 % immunoreactive area, followed closely by TH nerve density with 0.82 ± 0.08 % immunoreactive area. GAP 43 demonstrated lowest nerve fiber density with 0.51 ± 0.06 % area of positive fibers. At the endocardial surface TH, PGP 9.5 and GAP 43 nerve fiber distribution was different. TH immunoreactivity was lowest with 0.11 ± 0.01 % area of positive fibers, and PGP 9.5 and GAP 43 nerve densities were similar: 0.27 ± 0.02 % for PGP 9.5 and 0.23 ± 0.02% for GAP 43 (Table R13). In the rat heart, ventricular innervation is predominantly sympathetic, and the vast majority of nerve fibers that are positive for PGP 9.5 or GAP 43 are also positive for TH (Fig R26).

Figure R25. Representative picture of nerve fiber distribution in the base of the LV identified by PGP 9.5 immunoreactivity.

Endocardial surface **Epicardial surface**

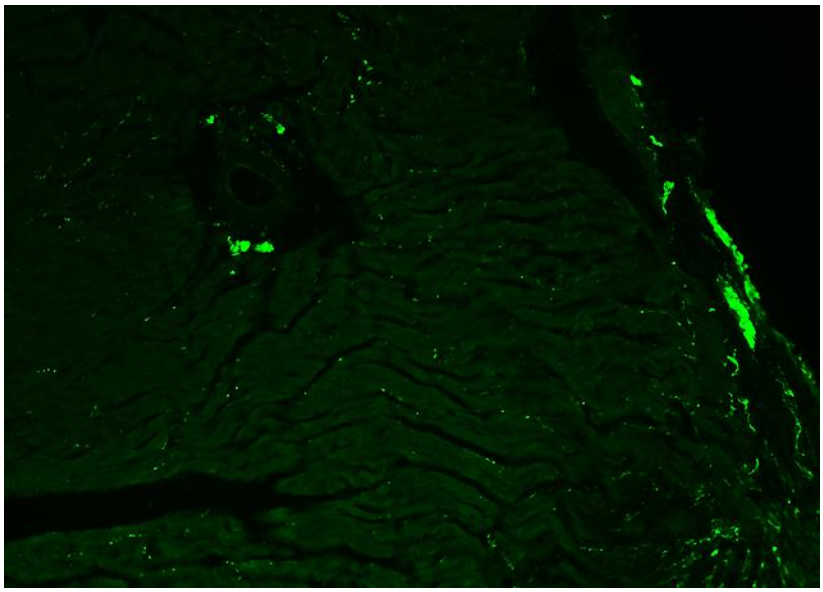

Epicardial surface of the myocardium has a more pronounced innervation density than the endocardial surface. Picture taken at 10X magnification.

The myocardium adjacent to epicardial surface had more pronounced sympathetic innervation, and thus was selected for quantification analysis in the base of the LV. Rats post MI and sham rats showed similar densities of TH, GAP 43 and PGP 9.5 positive fibers in the base of the LV, indicating that there are no notable changes in cardiac sympathetic innervation in this heart region (Fig R27-28, Table R13). In contrast, at the infarct border sympathetic hyperinnervation was observed with a 4 fold increase in GAP 43, a 2 fold increase in TH fiber density and a 50% increase in PGP 9.5 positive fibers (Fig R29-31, Table R13) when compared to nerve fiber density at the epicardial side of the LV base. When compared to very low nerve densities at the endocardial side in sham

rats, TH nerve density was increased ~15 fold, GAP 43 ~ 10 fold, and PGP 9.5 ~ 6 fold (Table R 13). In sham rats GAP 43 protein had the least amount of immunoreactive fibers in the LV, but it had the most marked increase in nerve density at the infarct border with 2.88% ± 0.23 area of positive fibers. Absolute nerve fiber density of GAP 43 was significantly higher than that of TH and PGP 9.5 at the infarct border (Fig R30). Co-localization analysis at the MI border showed that approximately 50% of fibers that are GAP 43 positive are also TH positive, and 60 -70% of fibers that are TH positive are also positive for PGP 9.5 (Fig R31).

Table R13. TH, GAP 43 and PGP 9.5 nerve fiber density at the epicardial and endocardial side in sham rats, and at the infarct border.

	% area of TH + Fibers	% area of GAP 43 + fibers	% area of PGP 9.5 + fibers
Sham, Endocardial side	0.11± 0.01	0.23 ± 0.02	0.27 ± 0.02
Sham, Epicardial side	0.82 ± 0.08	0.51 ± 0.06	1.10 ± 0.07
MI, Epicardial side (LV base)	0.90 ± 0.09	0.55 ± 0.06	1.22 ± 0.11
MI, Infarct border	**1.63 ± 0.07*†**	**2.88±0.23*†**	**1.55 ± 0.16*†**

Data = mean ±SE, n=6-7/group. * *p < 0.05, vs. sham epicardial side;* † *p < 0.05, vs. sham endocardial side*

Figure R26. PGP 9.5, GAP 43 and TH doublestaining in the base of the LV in rat post MI.

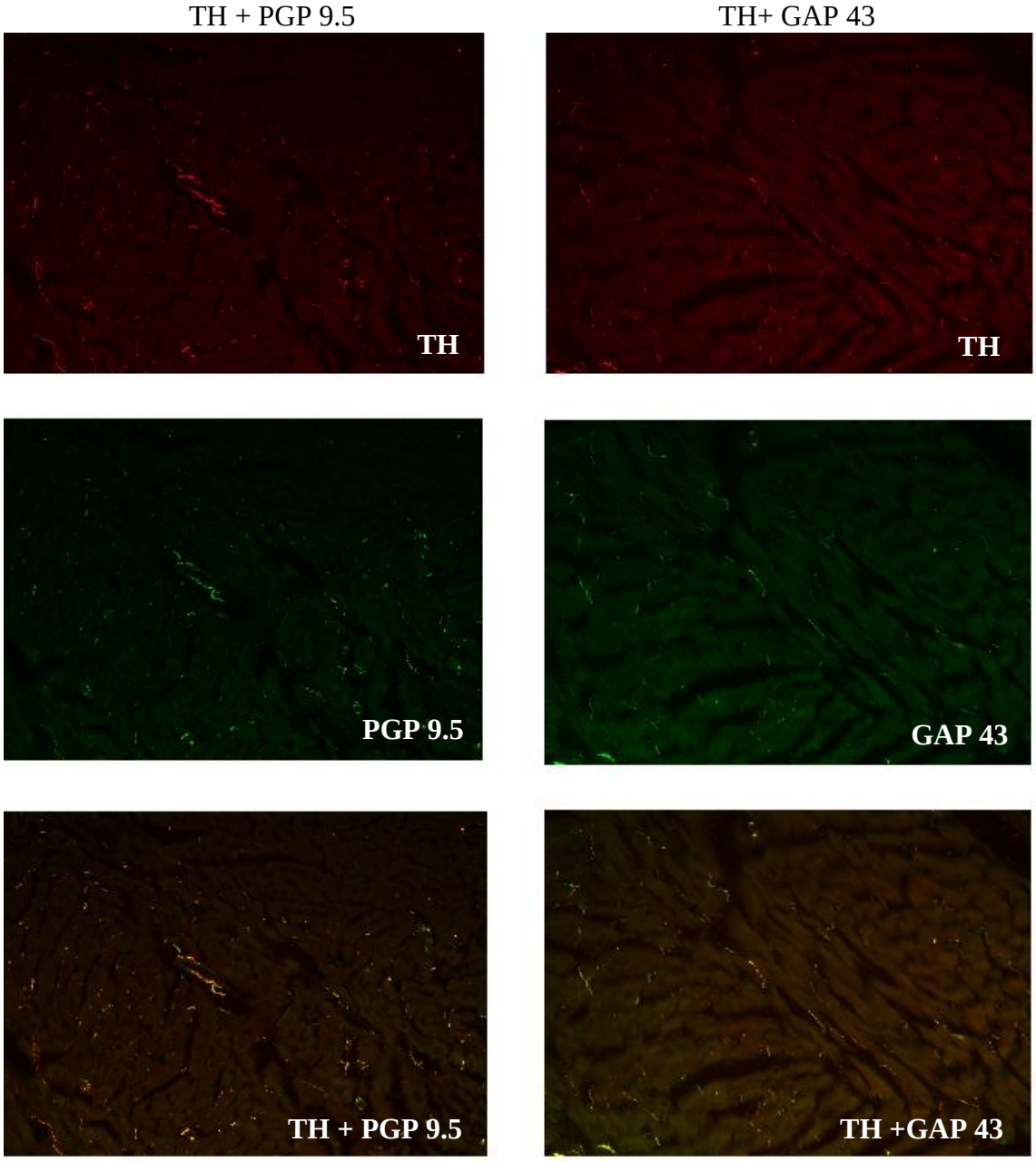

Picture taken at 20X magnification. Colocalization in sham rats has silimar pattern.

Figure R27. Quantification of TH, GAP 43 and PGP 9.5 nerve fiber density at the epicardial side of the LV base.

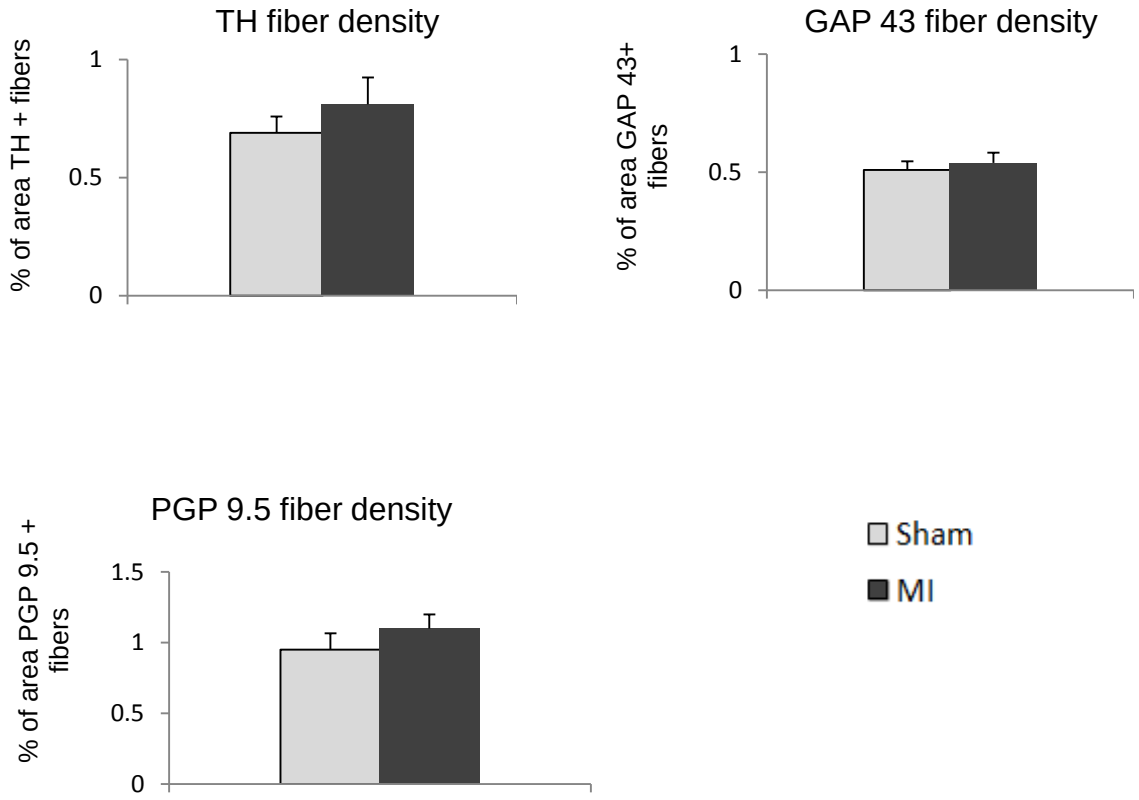

Data = mean ±SE, n=6-7/group. * *p < 0.05, vs. sham*

Figure R28. Representative picture of TH, PGP 9.5 and GAP 43 nerve fiber distribution in the base of the LV in rats post MI and in sham rats.

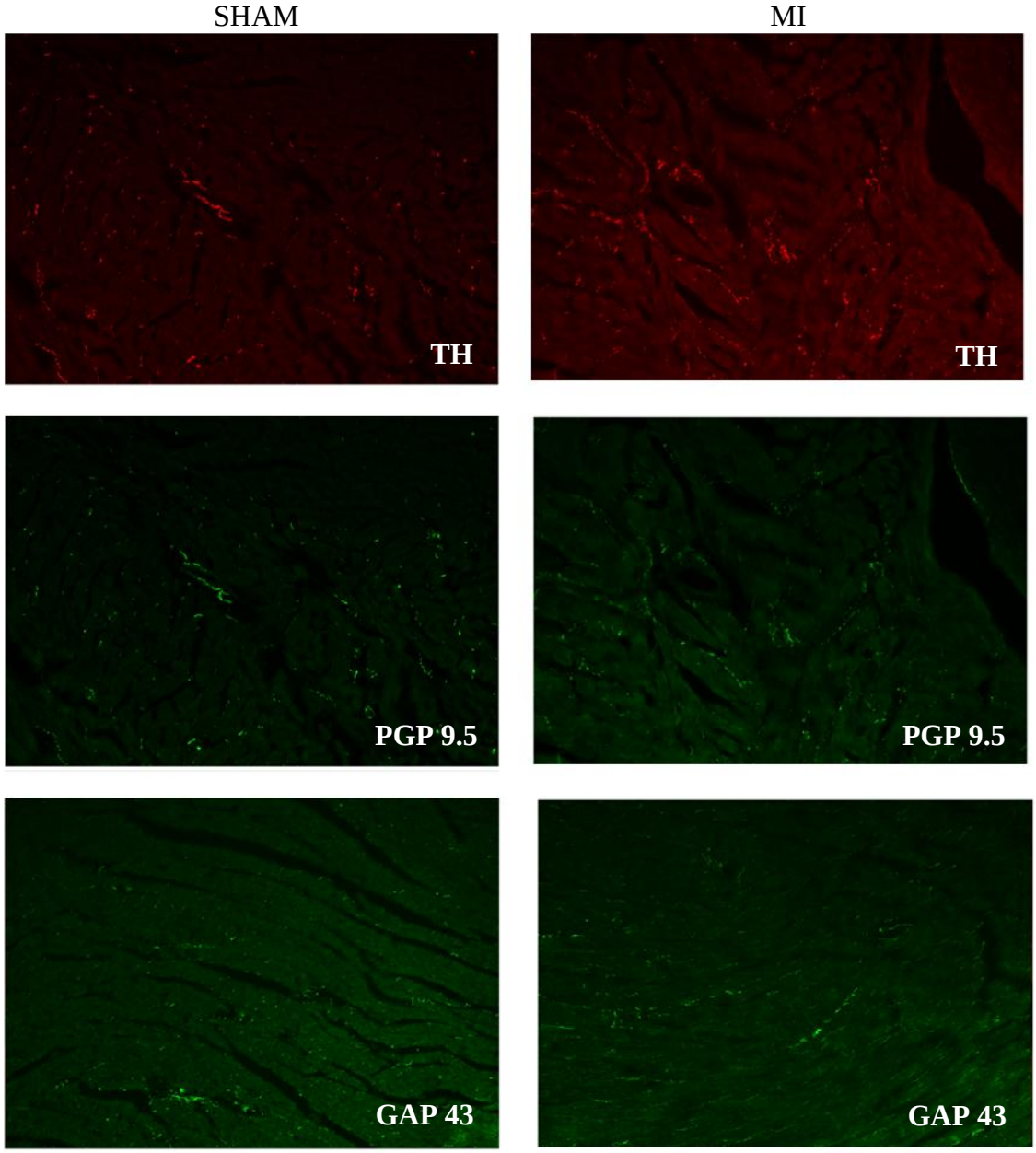

Picture taken at 20X magnification.

Figure R29. Quantification of TH, GAP 43 and PGP 9.5 nerve fiber density at the infarct border.

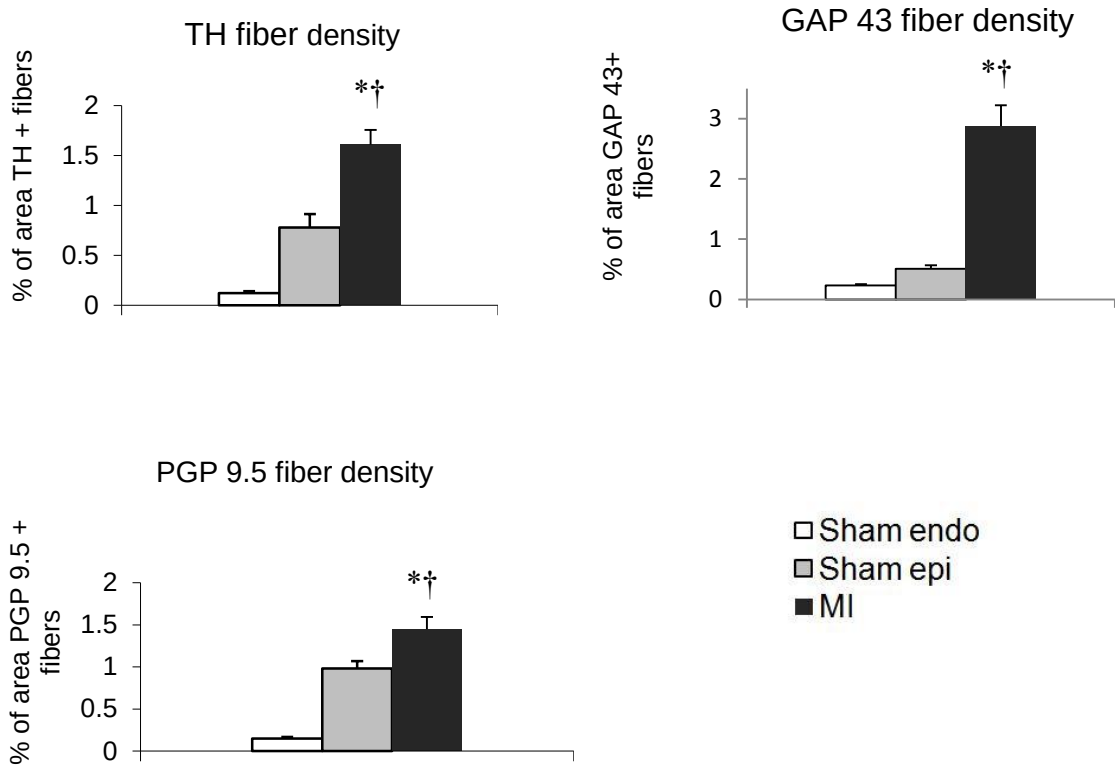

In sham, nerve densities of epicardial and endocardial myocardium are both shown. Data = mean ±SE, n=6-7/group. ** $p < 0.05$, vs. sham epi, $^{\dagger}p < 0.05$, vs. sham endo;*

Figure R30. GAP 43 vs. PGP 9.5 and TH nerve fiber density at the infarct border

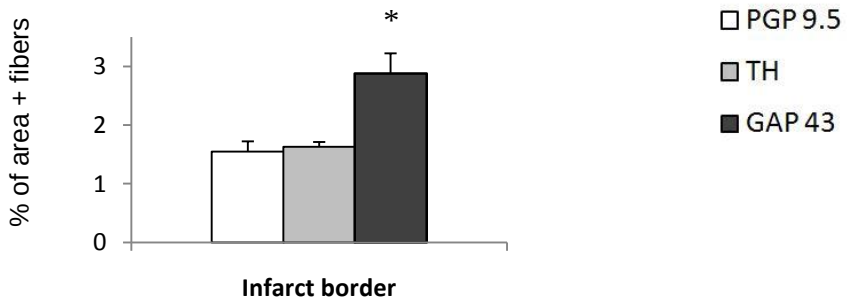

Data = mean ±SE, n=6-7/group. **p < 0.05, vs. PGP 9.5and TH*

Figure R31. PGP 9.5, GAP 43 and TH doublestaining at the infarct border.

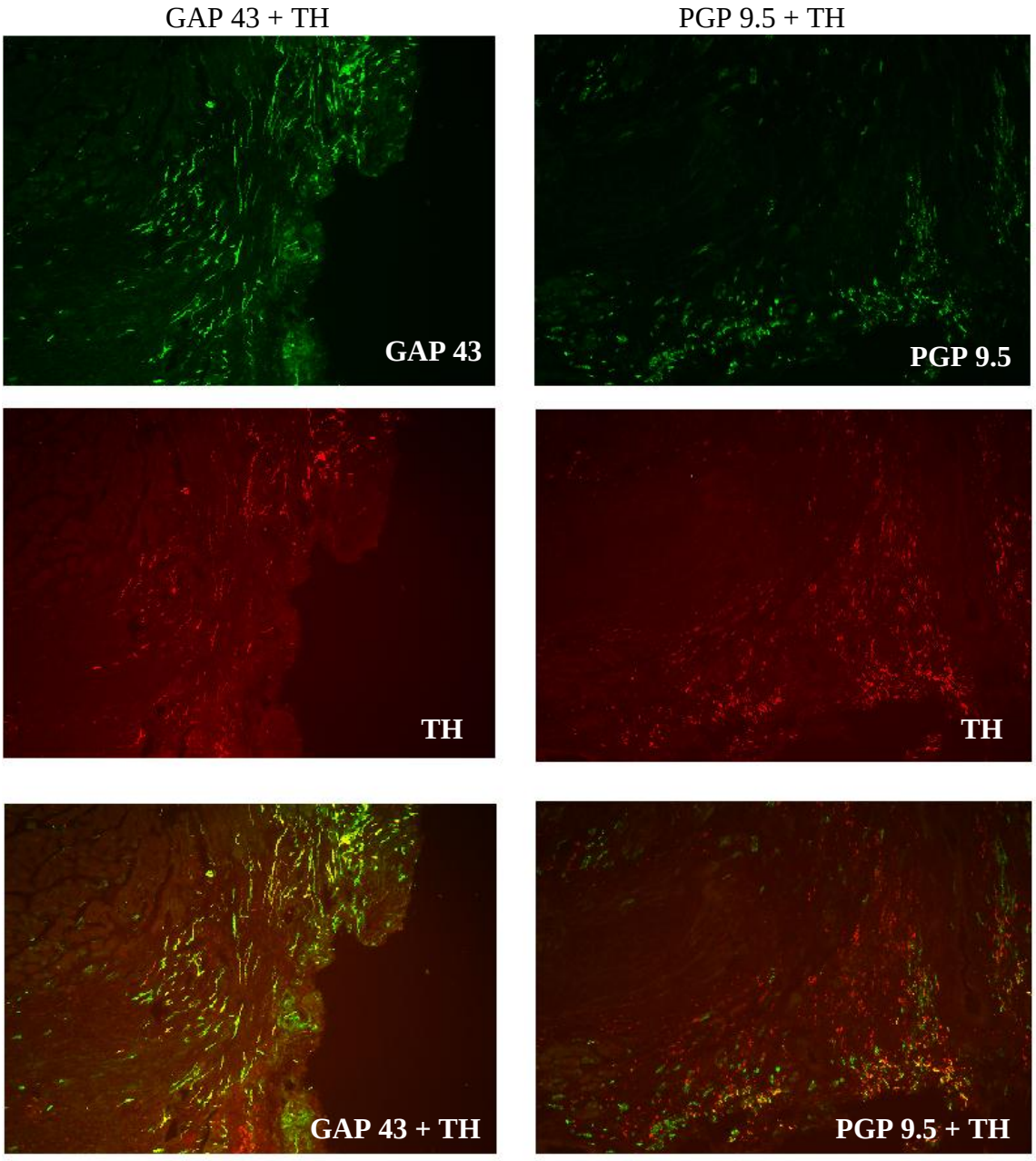

Colocalization shows that ~50 % of fibers that are GAP 43 positive are also TH positive, and ~50 % of fibers that are TH positive are also PGP 9.5 positive. Picture taken at 10X magnification.

3.3.2. Effects of central MR blockade on cardiac sympathetic hyperinnervation.

Average infarct size in the MR blocker group was 26% ± 2, and 24% ± 1 in the vehicle group (p=0.2). Compared with sham operated group, rats post MI that received icv treatment with eplerenone or vehicle had a marked decrease in EF, as well as significantly lower LVPSP, LV dP/dt max/min and higher LVEDP. LV function was depressed in MR blockade and the vehicle MI groups in a similar fashion (Fig R32).

Figure R32. LV function measured by echocardiography and Millar catheter.

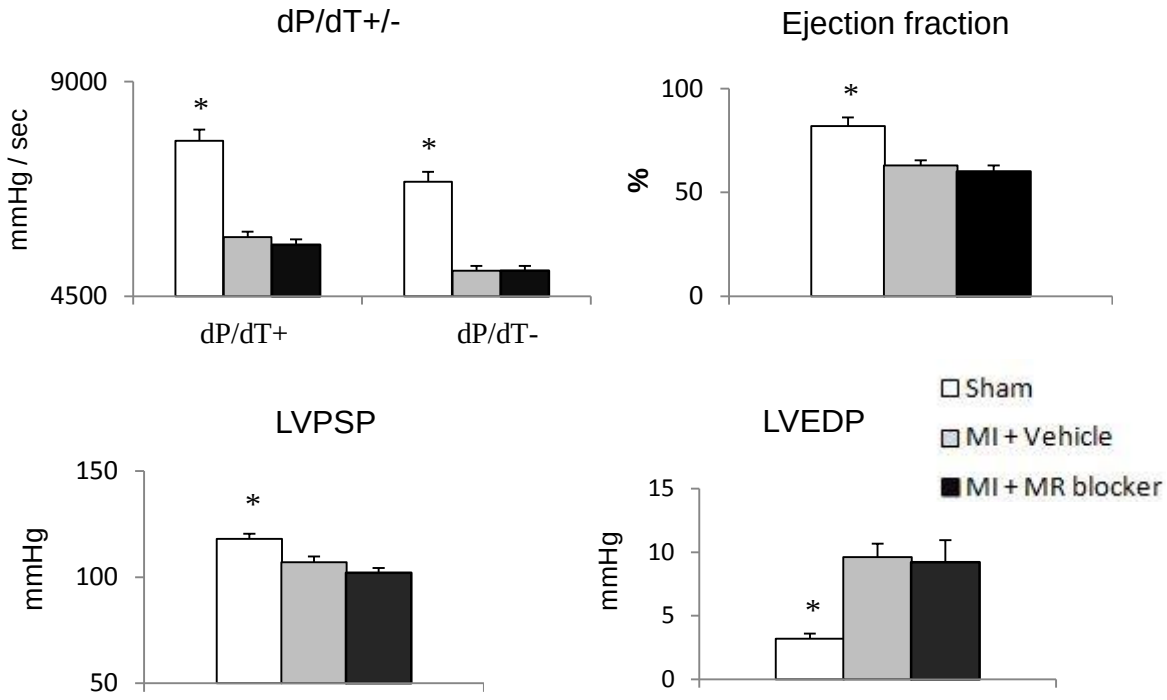

Data = mean ±SE, n= 6-7/group. * *p < 0.0001, sham vs. MI groups*

In the base of the LV we found no significant differences in the nerve fiber density of TH, GAP 43 and PGP 9.5 among the groups (Fig R33, Table R14). This is consistent with our previous study which demonstrated no changes in sympathetic innervation at the

base of the LV. At the infarct border, which is the area of maximal sympathetic hyperinnervation post MI, treatment with MR blocker significantly attenuated the increase in TH, GAP 43 and PGP 9.5 nerve densities in a similar fashion (Fig R 34, 35). The increase in TH and GAP 43 nerve fiber density was significantly attenuated ~ 3 fold, and in PGP 9.5 nerve fiber density by ~ 2 fold. When compared to innervation at the epicardial side in sham rats, TH and PGP 9.5 nerve densities at the MI border of epleronone treated rats were normalized, but GAP 43 was still 75% higher (Table R14).

Figure R33. Quantification of TH, GAP 43 and PGP 9.5 nerve fiber density at the epicardial side of the LV base.

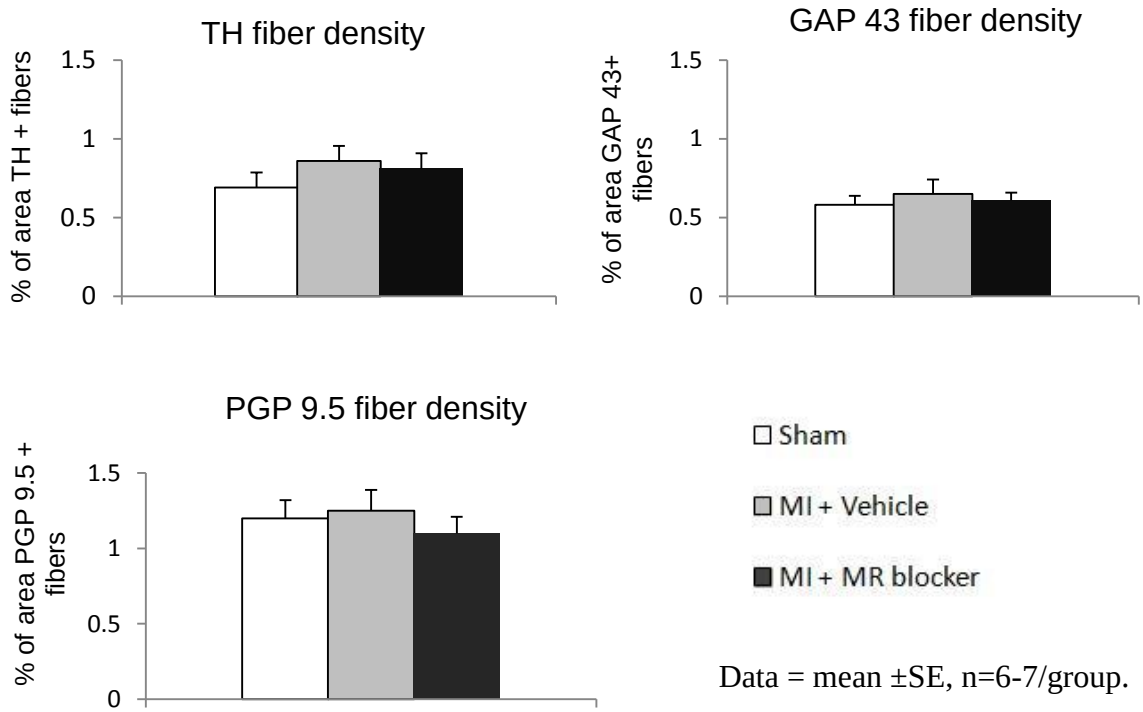

Data = mean ±SE, n=6-7/group.

Figure R34. Quantification of TH, GAP 43 and PGP 9.5 nerve fiber density at the infarct border.

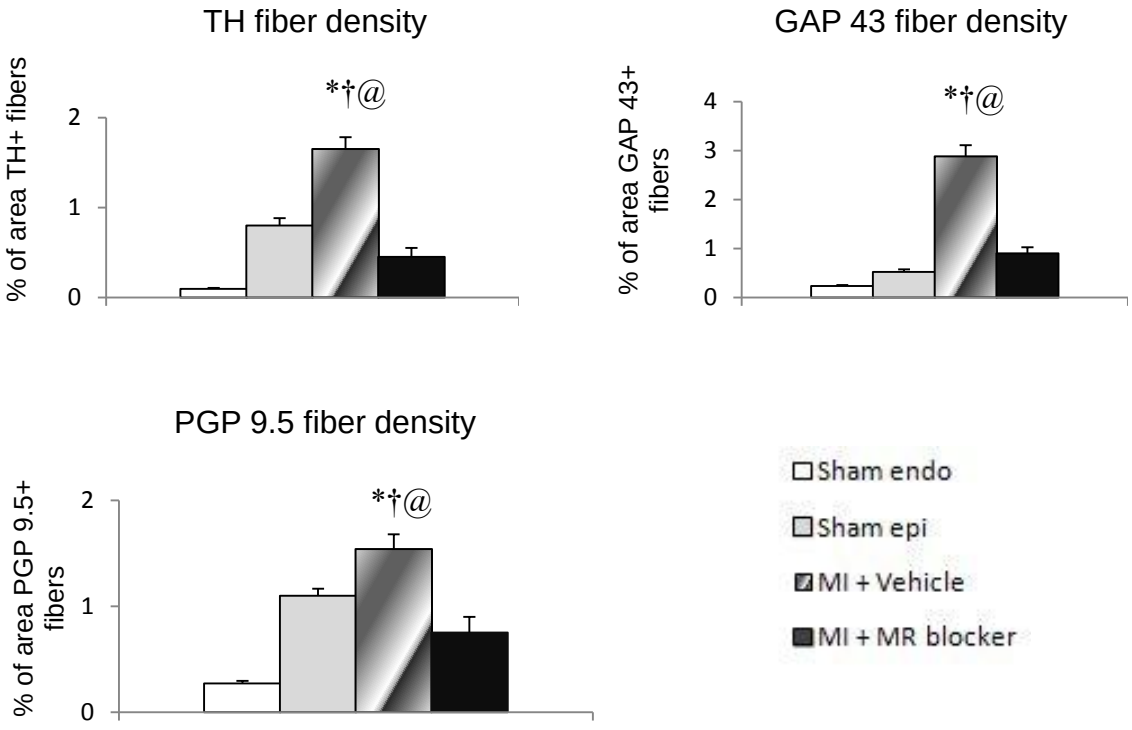

In sham, nerve densities at the epicardial and endocardial sides are both shown. Data = mean ±SE, n=6-7/group. **p < 0.05, vs. sham epi, $^{\dagger}p < 0.05$, vs. sham endo, $^{@}p < 0.05$, vs. MI + MR blocker*

Table R14. TH, GAP 43 and PGP 9.5 nerve fiber density at the infarct border.

	% area of TH + fibers	% area of GAP 43 + fibers	% area of PGP 9.5 + fibers
Sham, Endocardial side	0.11± 0.01	0.23 ± 0.02	0.27 ± 0.02
Sham, Epicardial side	0.82 ± 0.08	0.51 ± 0.06	1.10 ± 0.07
MI, Epicardial side (LV base)	0.90 ± 0.09	0.55 ± 0.06	1.22 ± 0.11
MI, Infarct border	1.63 ± 0.07*†	2.88±0.23*†	1.55 ± 0.16*†
MI + MR blocker, MI border	0.45 ± 0.10$^{@*}$	0.89 ± 0.13$^{@†*}$	0.75±0.15$^{@*}$

Data = mean ±SE, n=6-7/group. $^{*}p< 0.05$ *vs. sham endo;* $^{†}p< 0.05$ *vs. sham epi;* $^{@}p< 0.05$ *vs. MI + Vehicle.*

Figure R35. Representative picture of TH +, GAP 43 + and PGP 9.5 + nerve fiber density at the infarct border in rats post MI treated with vehicle vs. eplerenone.

MI + Vehicle

MI + MR Blocker

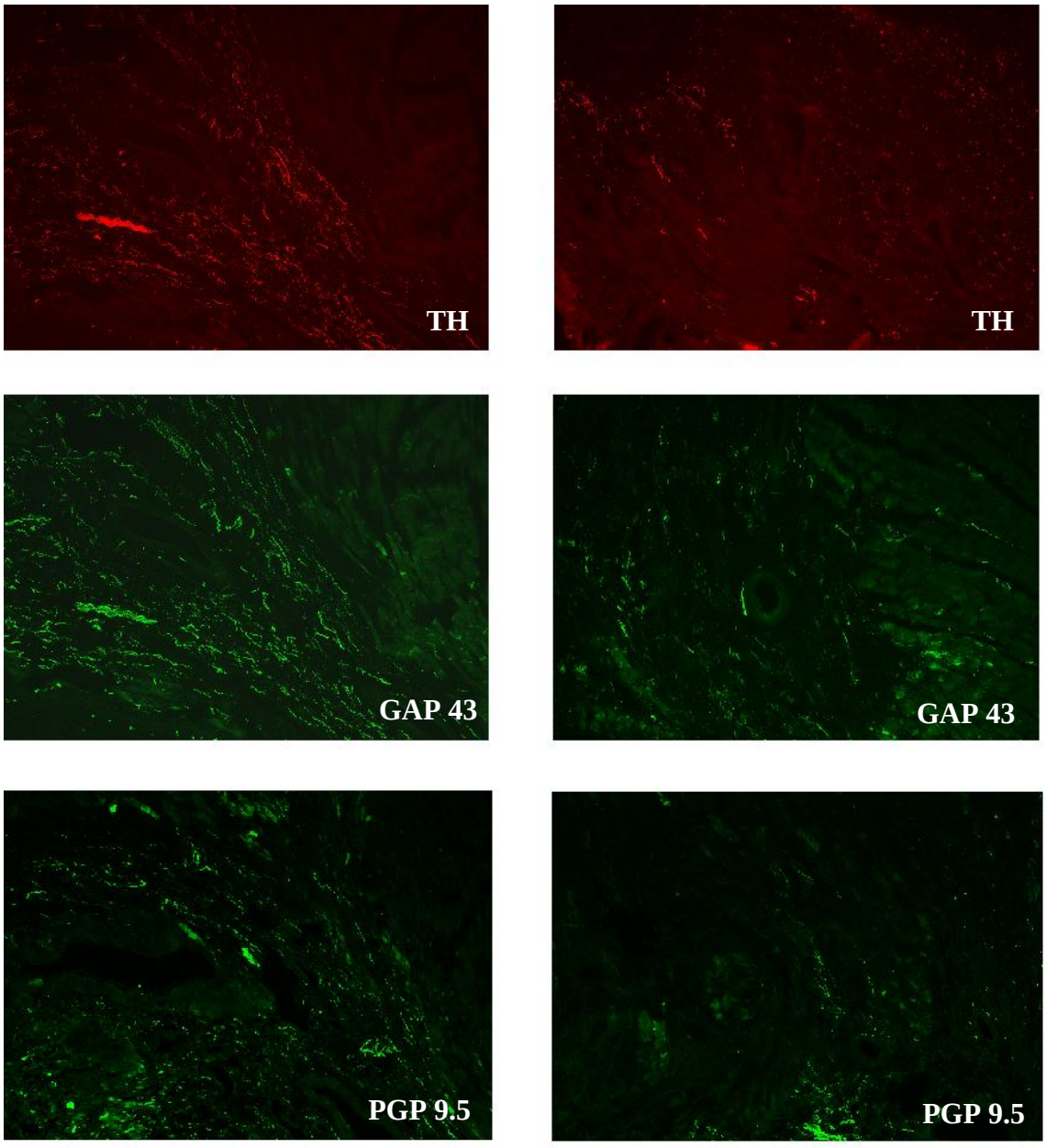

Picture taken at 10X magnification.

3.4. Extra-neuronal PGP 9.5 expression and ubiquitin-proteasome system dysfunction/activation.

3.4.1. Extra-neuronal PGP 9.5 expression.

Fluorescent immunohistochemistry was used to further study the location of the increased PGP 9.5 protein in the heart after MI. In the base of the LV, PGP 9.5 immunoreactivity was noted predominantly within cardiac nerves, but could also be appreciated in a small number of individual spindle –shaped cells. In the peri-infarct area we noticed a large number of spindle –shaped cells which resemble fibroblasts and had strong PGP 9.5 immunoreactivity, but not TH immunoreactivity (Fig R36). These cells resembled fibroblasts, so we first carried out fluorescent double-staining of LV sections from rats post MI for the PGP 9.5 protein and the fibroblast marker - vimentin protein. No co-localization between PGP 9.5 positive cells and vimentin staining was present. Vimentin positive cells surrounded PGP 9.5 positive cells, confirming their peri-infarct location (Fig R36). We then performed fluorescent double-staining of LV sections from MI rats for the PGP 9.5 protein and for alpha-sacromeric Actin protein, a specific marker for cardiomyocytes. A positive co-localization between these proteins indicates that cardiomyocytes in the peri-infarct area express PGP 9.5 at 1 wk post MI (Fig R37).

3.4.2. Ubiquitin-proteasome system dysfunction/activation.

PGP 9.5, as a deubiquitinating enzyme, can generate free mono-ubiquitin molecules, affect ubiquitin stability and prolong its half – life (Fang et al. 2010, Osaka et al. 2003), thus upregulation of PGP 9.5 expression may indicate changes in UPS activity or function. We proceeded with assessment of protein expression of GAP 43, PGP 9.5, ubiquitin and ubiquitinated proteins in the base of the LV and the peri-infarct zone.

Ubiquitinated proteins with various molecular weights were present in the LV, and the expression of most prominent ones (MW ~ 30 kDa, 40 kDa, 50 kDa, 60 kDa, 100 kDa, 250 kDa) was quantified separately.

In the base of the heart no significant differences in GAP 43 protein expression were present between the groups, but PGP 9.5 and ubiquitin protein expression was significantly increased ~ 2 fold in rats post MI. Levels of ubiquitinated proteins with MW ~ 50 kDa and 60 kDa were significantly 60-70% higher in rats post MI. No notable differences in content of ubiquitinated proteins with MW of 30, 40, 100 and 250 kDa were observed between the groups (Fig R38, R40; Table R15).

In the peri-infarct zone, similarly to the non- infarcted base of the LV, no significant differences in GAP 43 protein expression were present between the groups. In contrast, PGP 9.5 protein expression was significantly elevated ~ 6 fold, and the dramatic increase in PGP 9.5 protein content was located in the peri-infarct area of the LV where PGP 9.5 positive cells were found. The content of ubiquitin and of ubiquitinated proteins with molecular weights of 60 kDa and 250 kDa was significantly increased ~ 2 fold, but the content of ubiquitinated proteins with molecular weights of 30 kDa, 40 kDa and 100 kDa was significantly decreased ~ 2 fold in MI group (Fig R39, R41; Table R15).

Figure R36. Representative picture of TH -, Vimentin - and PGP 9.5 + cells found in the peri-infarct zone in MI rats.

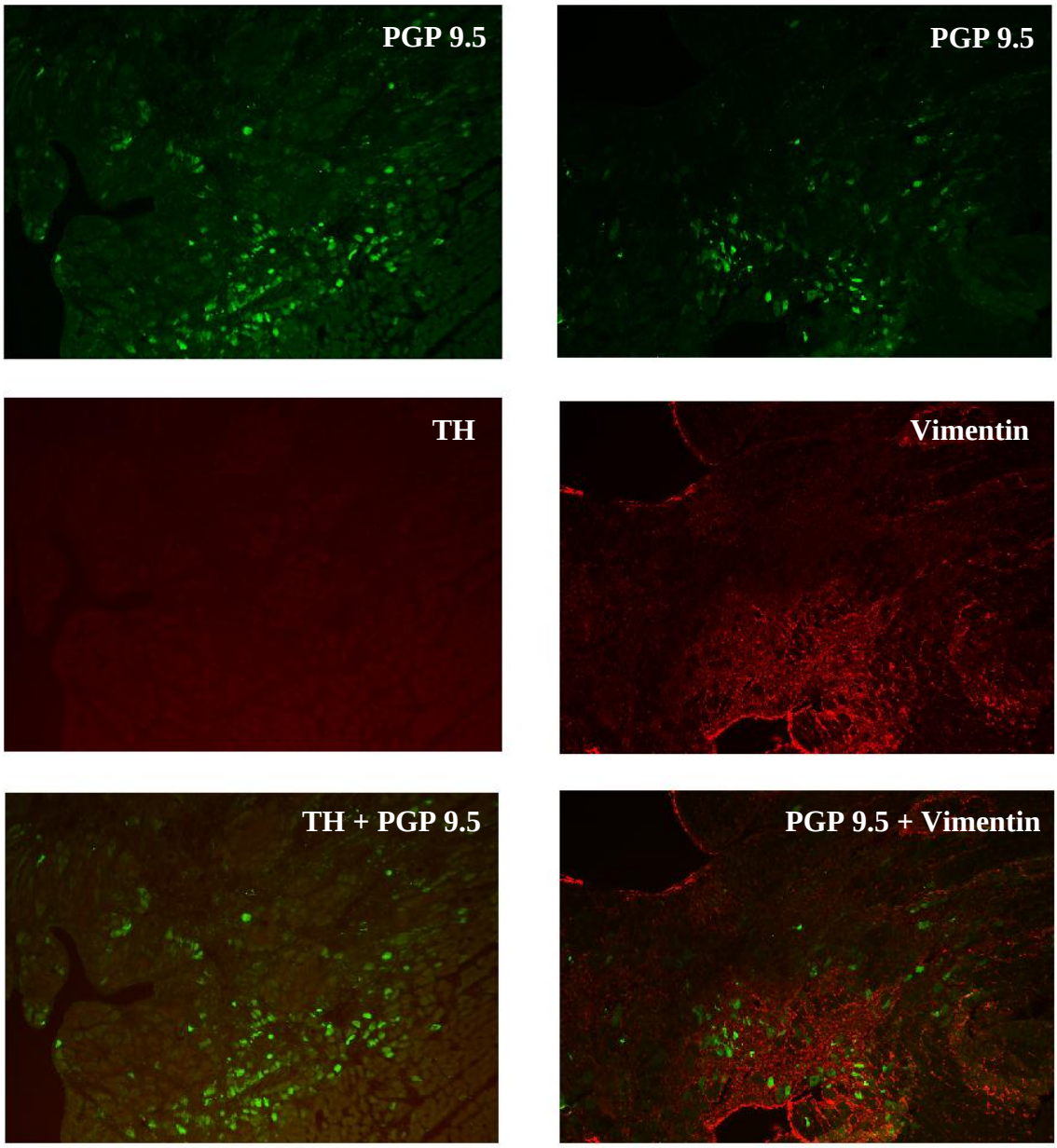

Picture taken at 10X magnification.

Figure R37. Representative picture of PGP 9.5 + cells and alpha-sarcomeric Actin immunoreactivity in the peri-infarct area.

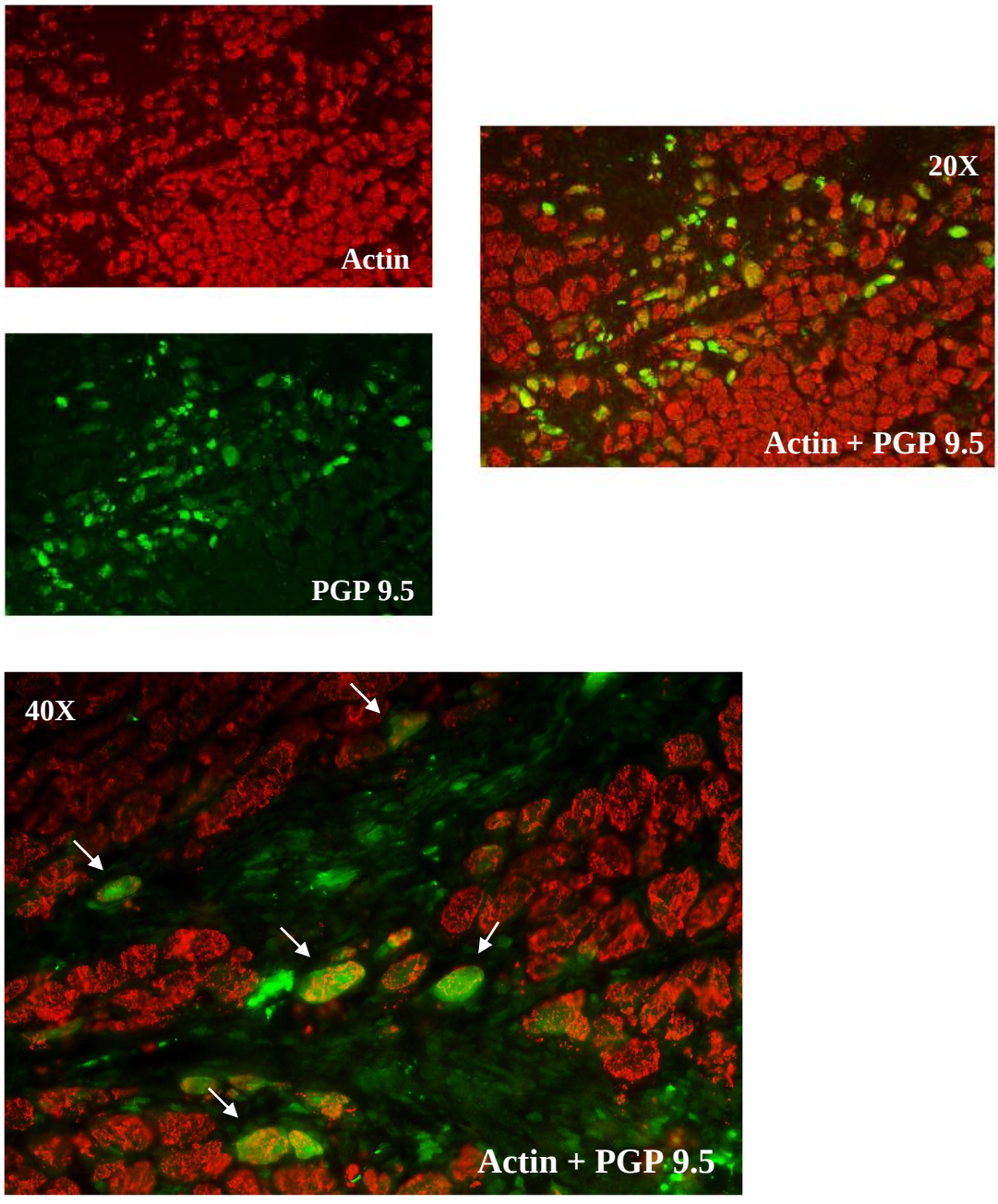

Figure R38. GAP 43, PGP 9.5, ubiquitin and ubiquitinated proteins in LV above ligation at 10 days post MI.

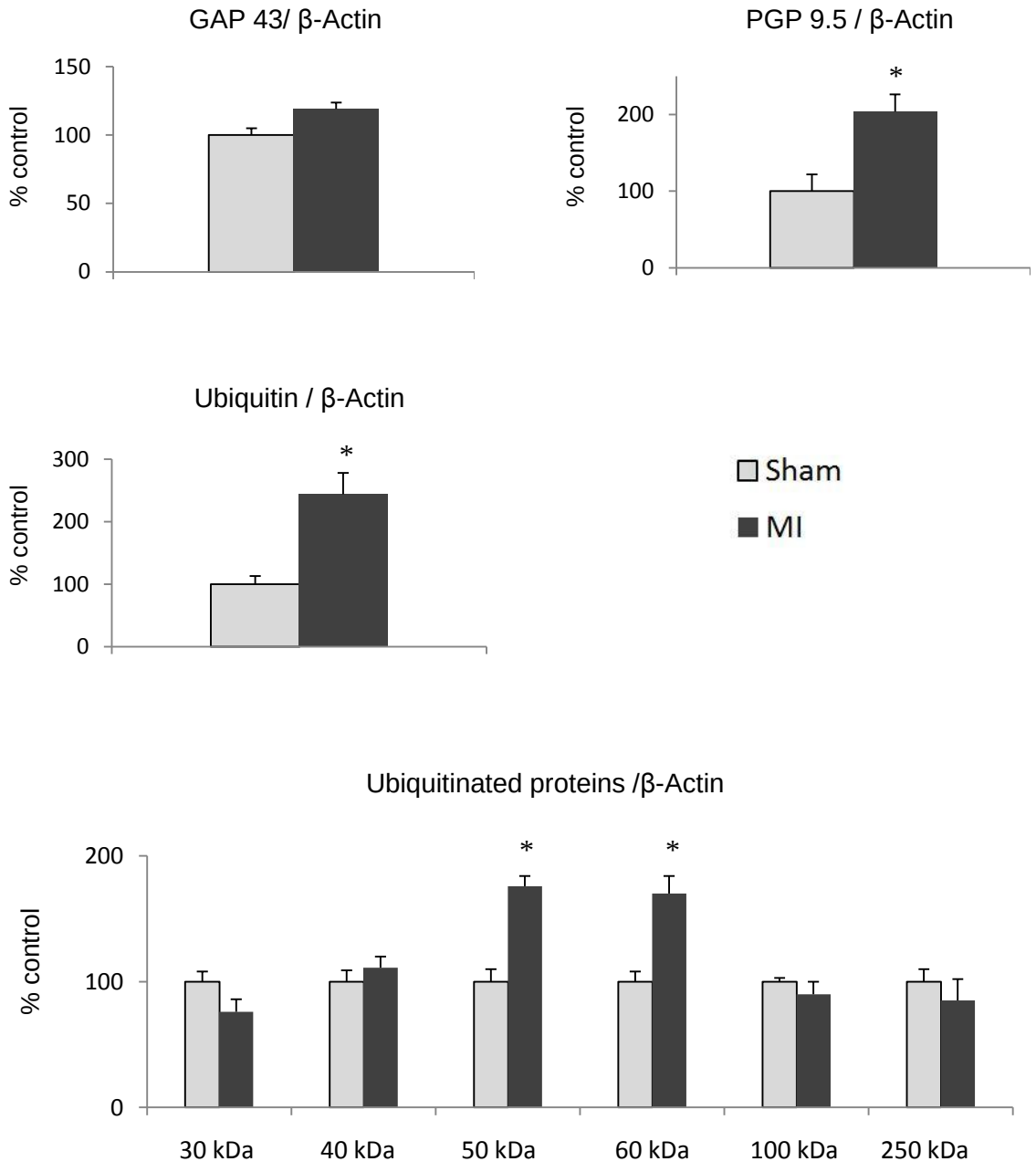

GAP 43, PGP 9.5, ubiquitin and ubiquitinated proteins were normalized to β-Actin. Ubiquitinated proteins with approximate MW of 30, 40, 50, 60, 100 and 250 kDa are shown separately. Data is shown as percentage of control group (100%). Data = mean ±SE, n= 5 - 8/group. **p < 0.05, sham vs. MI*

Figure R39. GAP 43, PGP 9.5, ubiquitin and ubiquitinated proteins in the peri-infarct zone at 10 days post MI.

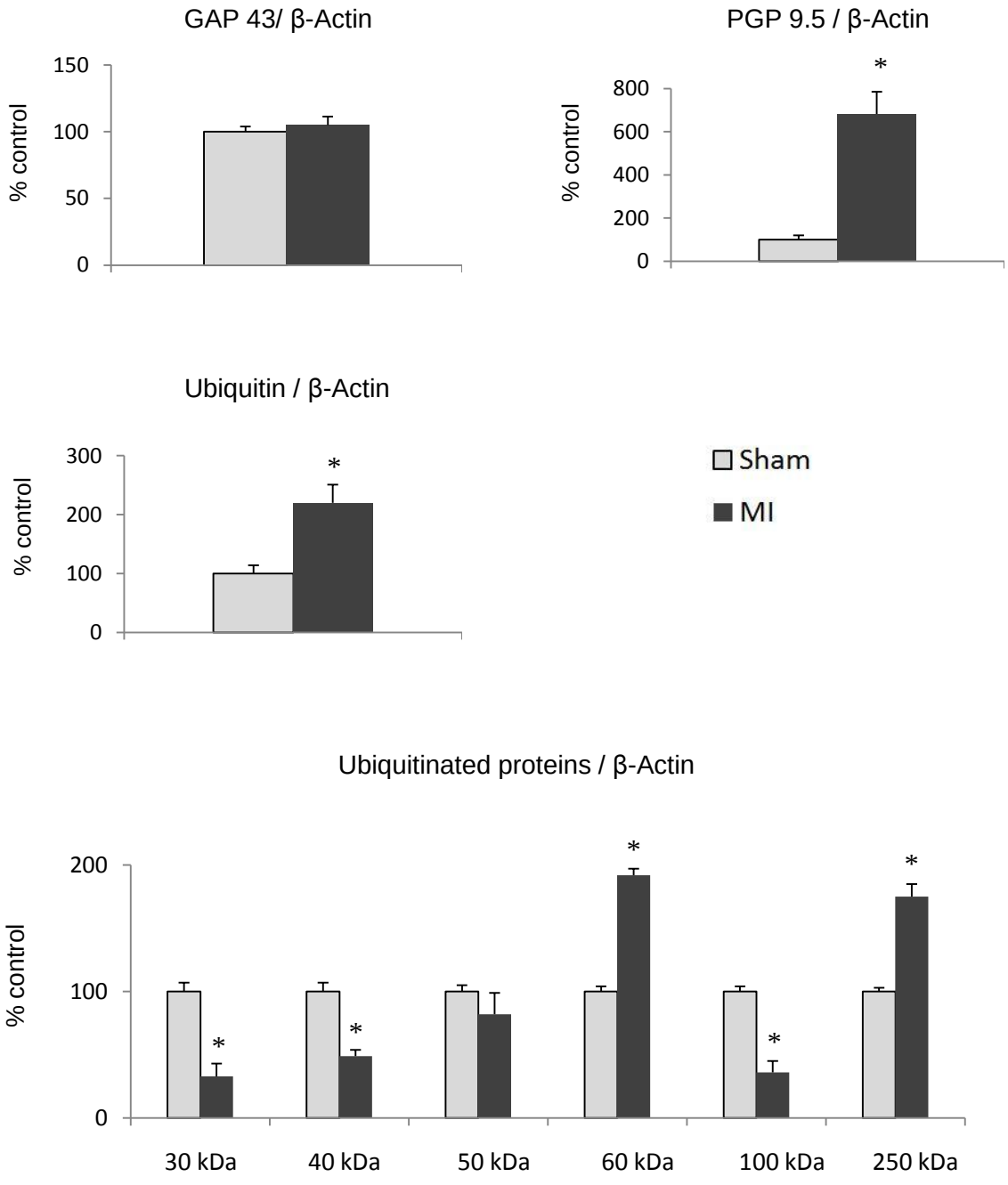

GAP 43, PGP 9.5, ubiquitin and ubiquitinated proteins were normalized to β-Actin. Ubiquitinated proteins with approximate MW of 30, 40, 50, 60, 100 and 250 kDa are shown separately. Data is shown as percentage of control group (100%). Data = mean ±SE, n= 5 - 8/group. * *p < 0.05, sham vs. MI*

Figure R40. Western blot from the LV base showing GAP 43, PGP 9.5, ubiquitin, ubiquitinated proteins and β-Actin at 10 days post MI.

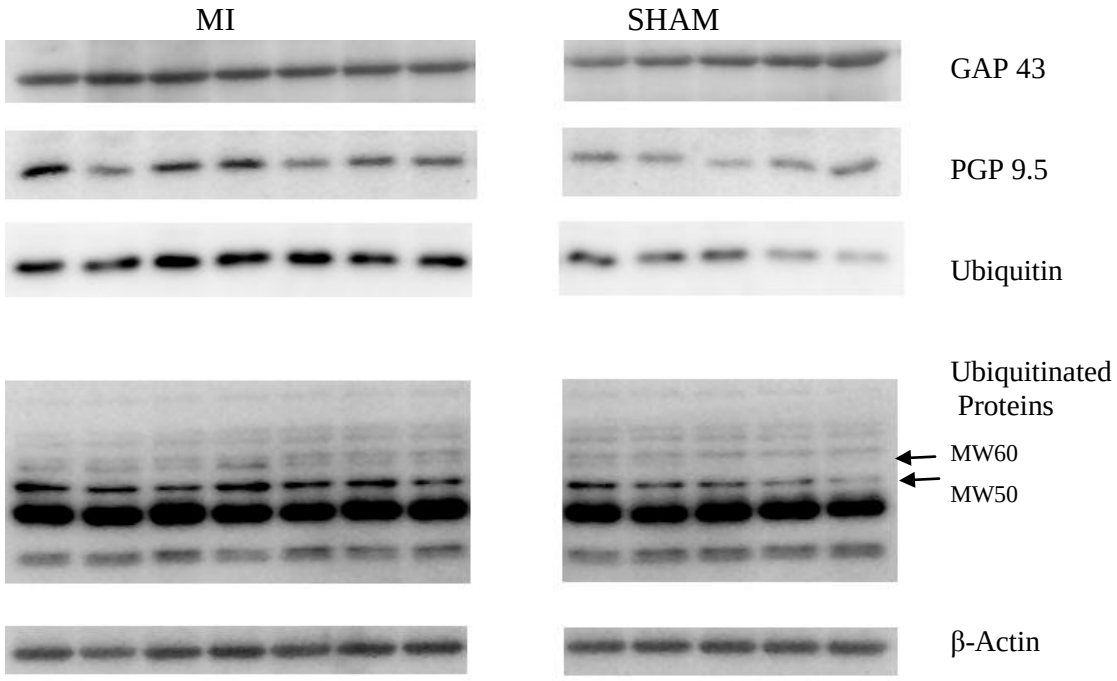

Figure R41. Western blot from the peri-infarct showing GAP 43, PGP 9.5, ubiquitin, ubiquitinated proteins and β -Actin at 10 days post MI.

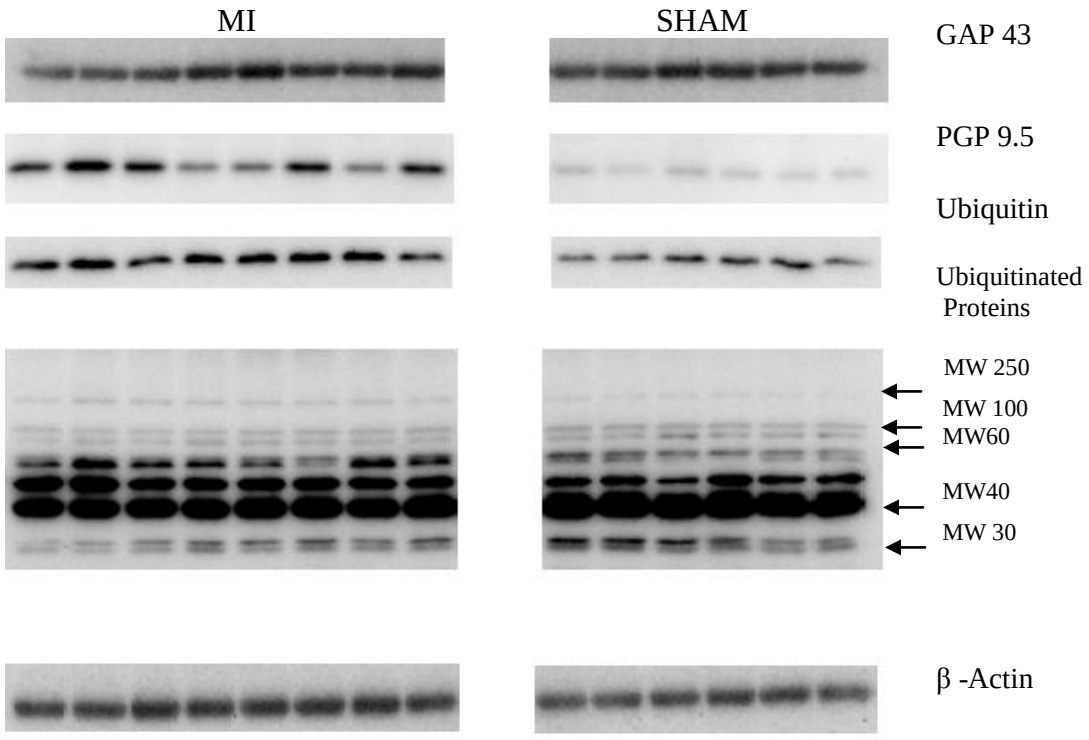

Table R15. Expression of GAP 43, PGP 9.5, ubiquitin and ubiquitinated proteins in the LV at 10 days post MI.

	LV base of the heart		Peri-infarct	
	SHAM	MI	SHAM	MI
GAP 43/β-Actin	2.35±0.20	2.82±0.08	2.17±0.07	2.26±0.13
PGP 9.5/ β-Actin	0.22±0.05	**0.39±0.03***	0.60 ±0.12	**4.10±0.62***
Ubiquitin/ β-Actin	0.77±0.11	**1.63± 0.21***	1.18±0.16	**2.60±0.36***
Ubiquitinated Protein ~30 kDa/ β-Actin	0.25±0.02	0.23±0.02	0.31±0.02	**0.10±0.01***
Ubiquitinated Protein ~40 kDa/ β-Actin	0.71±0.06	0.75±0.06	2.33±0.03	**1.12±0.06***
Ubiquitinated Protein ~50 kDa/ β-Actin	0.21±0.02	**0.33±0.03***	1.21±0.06	0.99±0.17
Ubiquitinated Protein ~60 kDa/ β-Actin * 10^{-1}	0.90± 0.07	**1.56±0.16***	0.28±0.01	**0.54±0.11***
Ubiquitinated Protein ~100 kDa/ β-Actin *10^{-1}	0.87±0.03	0.95±0.01	1.27±0.05	**0.46±0.04***
Ubiquitinated Protein ~250 kDa/ β-Actin *10^{-1}	0.20±0.02	0.22± 0.02	0.66±0.02	**1.15± 0.12***

Data = mean ±SE, n= 5 - 8/group. * *$p < 0.05$, sham vs. MI*

3.4.3. Effects of central MR blockade on PGP 9.5 and Ubiquitin expression.

No significant changes in GAP 43 protein were present among groups in the non-infarcted LV, the peri-infarct zone and in the RV. In contrast, PGP 9.5 protein expression was significantly increased ~ 2 fold in the non-infarcted LV (Fig R42-43), ~ 3 fold in the peri-infarct zone (Fig R44-45) and ~ 50% in the RV (Fig R46-47) in both MR blockade and Vehicle MI groups vs. Sham group. Ubiquitin protein was also increased significantly ~ 2 fold in the non-infarcted LV and peri-infarct zone in MR blockade and Vehicle MI groups vs. Sham group (Fig R42, R44). No significant changes in ubiquitin protein expression in the RV were observed among the groups (Fig R46). In the non-infarcted LV levels of ubiquitinated proteins with MW ~ 50 kDa and 60 kDa were significantly 60-70% higher in the MR blockade and Vehicle MI groups vs. the Sham operated group. No notable changes in content of ubiquitinated proteins with MW of 30, 40, 100 and 250 kDa were observed among the groups (Fig R42, Table R16). In the peri-infarct zone, the content of ubiquitinated proteins with molecular weights of 60 kDa and 250 kDa was significantly increased ~ 2 fold, and the content of ubiquitinated proteins with molecular weights of 30 kDa, 40 kDa and 100 kDa was significantly decreased ~ 2 fold in MR blockade and Vehicle MI groups vs. the Sham operated group (Fig R44, Table R17). There were no significant changes in the expression of GAP 43, PGP 9.5, ubiquitin and ubiquitinated proteins between the MR blockade and Vehicle MI groups in any region of the heart studied (Table R16-18).

Figure R42. GAP 43, PGP 9.5, ubiquitin and ubiquitinated proteins in LV above ligation at 10 days post MI.

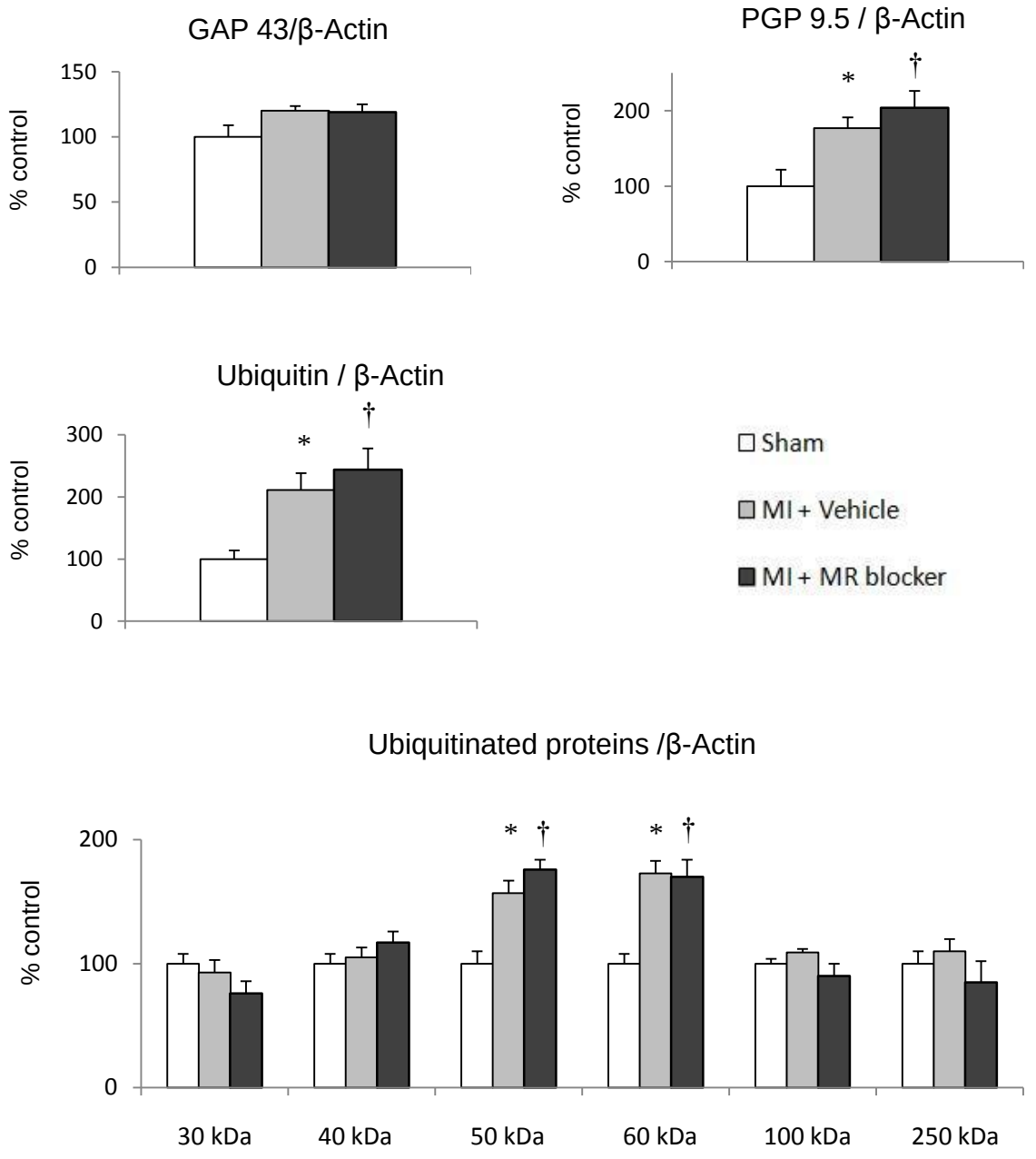

GAP 43, PGP 9.5, ubiquitin and ubiquitinated proteins were normalized to β-Actin and compared to control (sham). Ubiquitinated proteins with approximate MW of 30, 40, 50, 60, 100 and 250 kDa are shown separately. Data is shown as percentage of control group (100%). Data = mean ±SE, n= 5 - 8/group. *$p < 0.05$, *MI + Vehicle vs. sham,* $^{\dagger}p < 0.05$, *MI + MR blocker vs. sham.*

Table R16. Expression of GAP 43, PGP 9.5, ubiquitin and ubiquitinated proteins in the base of the LV above the ligation 10 days post MI.

	LV base of the heart		
	Sham	MI + Vehicle	MI + MR Blocker
GAP 43/β-Actin	2.35±0.20	2.82±0.08	2.80±0.14
PGP 9.5/ β-Actin	0.22±0.05	**0.39±0.03***	**0.45±0.05†**
Ubiquitin/ β-Actin	0.77±0.11	**1.63± 0.21***	**1.88 ± 0.25†**
Ubiquitinated Protein ~30 kDa/ β-Actin	0.25±0.02	0.23±0.02	0.19 ± 0.02
Ubiquitinated Protein ~40 kDa/ β-Actin	0.71±0.06	0.75±0.06	0.83±0.07
Ubiquitinated Protein ~50 kDa/ β-Actin	0.21±0.02	**0.33±0.03***	**0.37±0.03†**
Ubiquitinated Protein ~60 kDa/ β-Actin * 10^{-1}	0.90± 0.07	**1.56±0.16***	**1.53±0.21†**
Ubiquitinated Protein ~100 kDa/ β-Actin *10^{-1}	0.87±0.03	0.95±0.01	0.78±0.08
Ubiquitinated Protein ~250 kDa/ β-Actin *10^{-1}	0.20±0.02	0.22± 0.02	0.17±0.03

Data = mean ±SE, n= 5 - 8/group. **p < 0.05, MI + Vehicle vs. sham, †p < 0.05, MI + MR blocker vs. sham.*

Figure R43. Western blot from the LV base showing GAP 43, PGP 9.5, ubiquitin, ubiquitinated proteins and β-Actin at 10 days post MI.

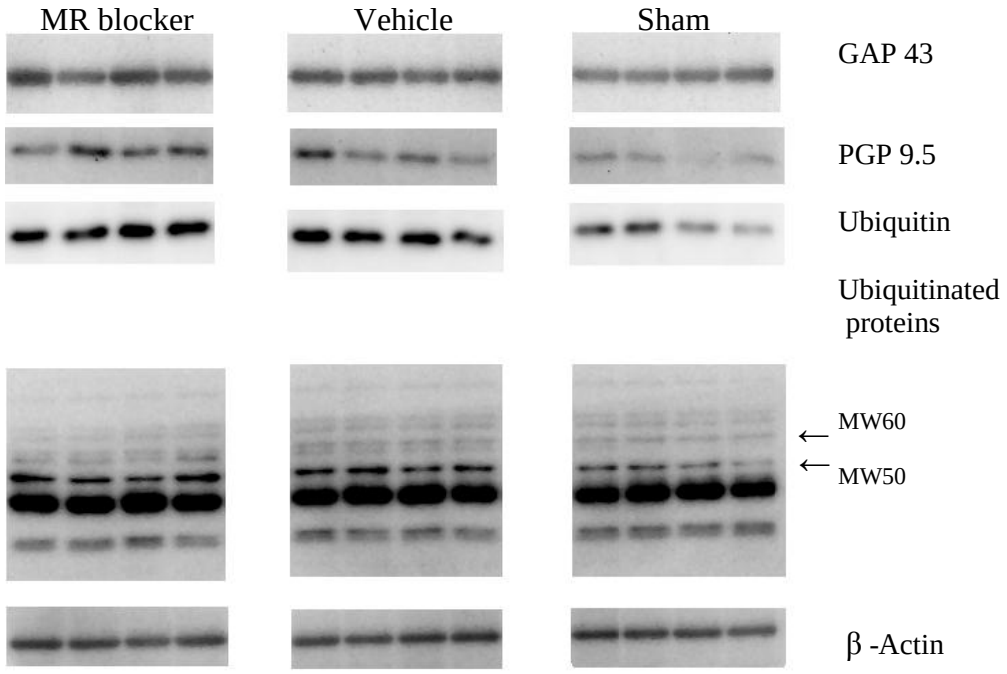

Figure R44. GAP 43, PGP 9.5, ubiquitin and ubiquitinated proteins in peri-infarct area at 10 days post MI.

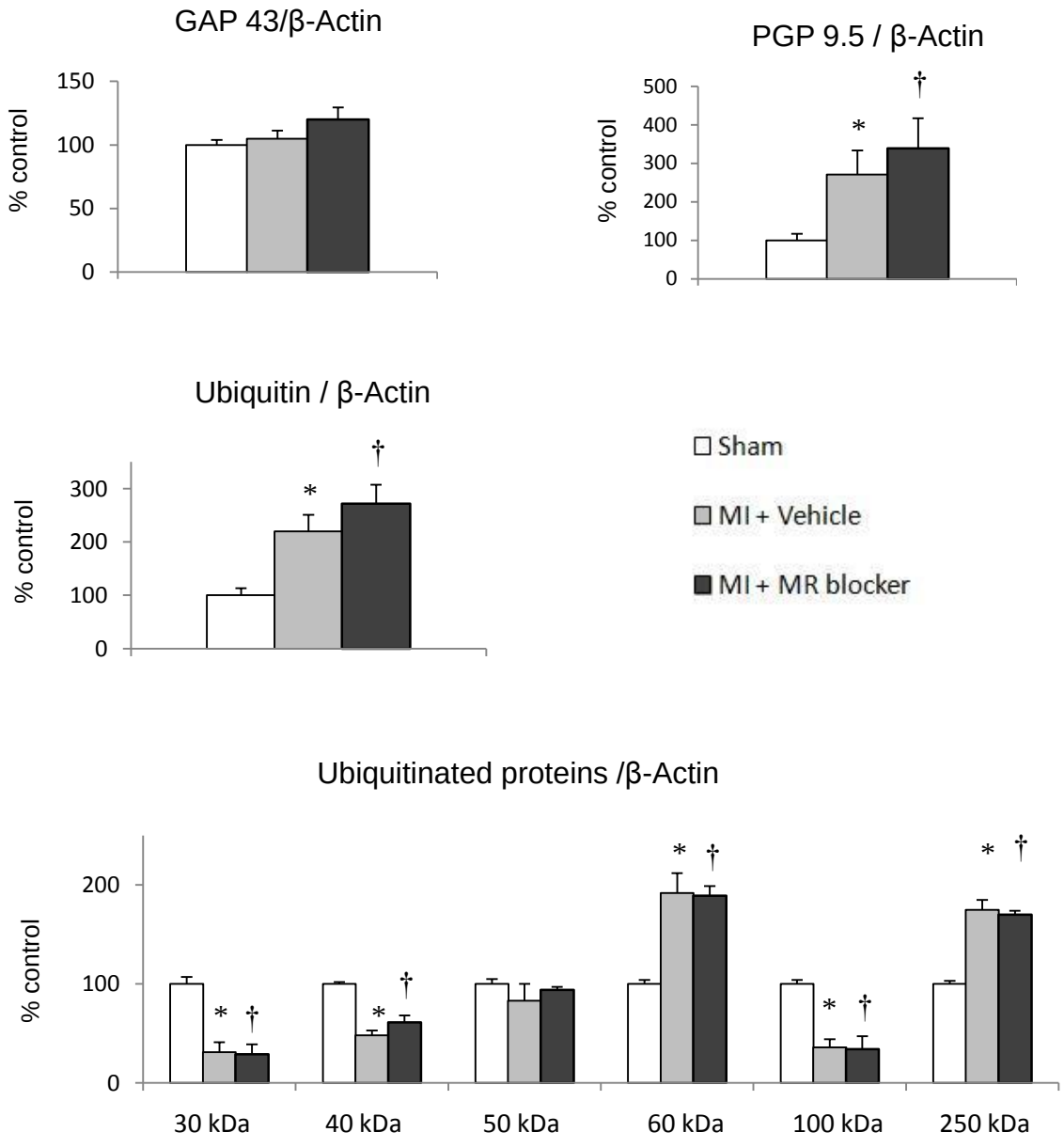

GAP 43, PGP 9.5, ubiquitin and ubiquitinated proteins were normalized to β-Actin and compared to control (sham). Ubiquitinated proteins with approximate MW of 30, 40, 50, 60, 100 and 250 kDa are shown separately. Data is shown as percentage of control group (100%). Data = mean ±SE, n= 5 - 8/group. **p < 0.05, MI + Vehicle vs. sham, †p < 0.05, MI + MR blocker vs. sham.*

Table R17. Expression of GAP 43, PGP 9.5, ubiquitin and ubiquitinated proteins in the peri-infarct at 10 days post MI.

	Peri-infarct		
	Sham	MI + Vehicle	MI + MR Blocker
GAP 43/β-Actin	2.17±0.07	2.26±0.13	2.62±0.20
PGP 9.5/ β-Actin	0.28±0.05	**0.76±0.18***	**0.95±0.22**†
Ubiquitin/ β-Actin	1.18±0.16	**2.60±0.36***	**3.22±0.44**†
Ubiquitinated Protein ~30 kDa/ β-Actin	0.31±0.02	**0.10±0.01***	**0.09±0.01**†
Ubiquitinated Protein ~40 kDa/ β-Actin	2.33±0.03	**1.12±0.06***	**1.42±0.09**†
Ubiquitinated Protein ~50 kDa/ β-Actin	1.21±0.06	0.99±0.17	1.13±0.02
Ubiquitinated Protein ~60 kDa/ β-Actin	0.28±0.01	**0.54±0.11***	**0.53±0.05**†
Ubiquitinated Protein ~100 kDa/ β-Actin $*10^{-1}$	1.27±0.05	**0.46±0.04***	**0.44±0.06**†
Ubiquitinated Protein ~250 kDa/ β-Actin $*10^{-2}$	0.66±0.02	**1.15± 0.12***	**1.12 ± 0.03**†

Data = mean ±SE, n= 5 - 8/group. *$^{*}p < 0.05$, MI + Vehicle vs. sham, $^{\dagger}p < 0.05$, MI + MR blocker vs. sham.*

Figure R45. Western blot from the peri-infarct showing GAP 43, PGP 9.5, ubiquitin, ubiquitinated proteins and β -Actin at 10 days post MI.

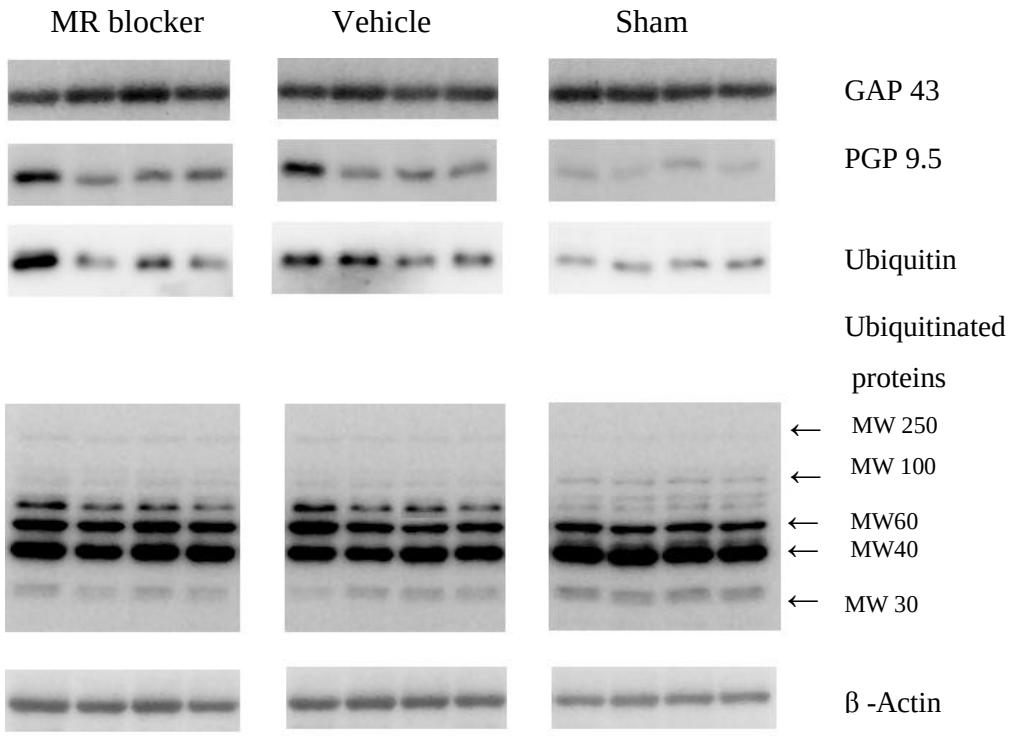

Figure R46. GAP 43, PGP 9.5, ubiquitin and ubiquitinated proteins in the RV.

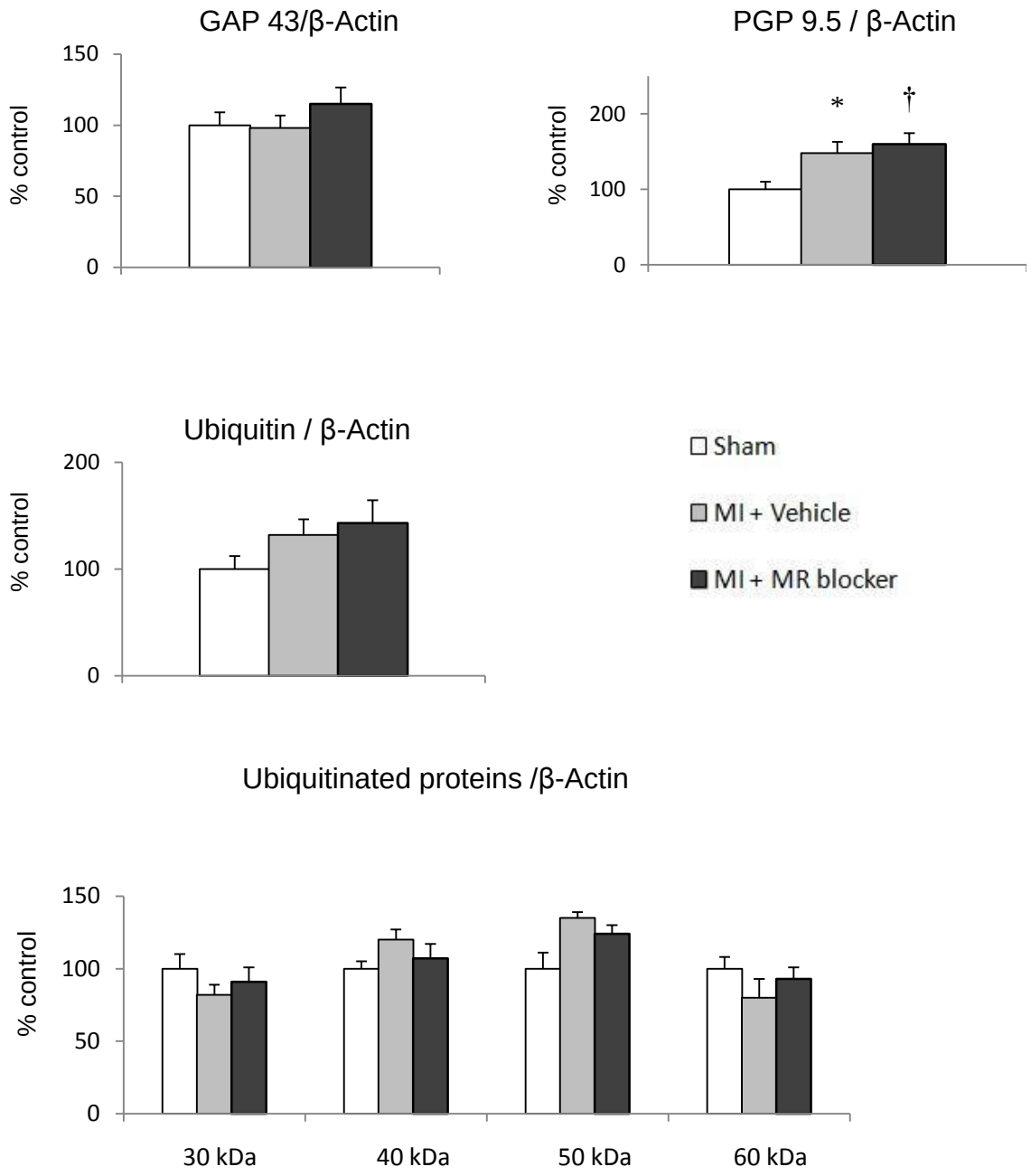

GAP 43, PGP 9.5, ubiquitin and ubiquitinated proteins were normalized to β-Actin and compared to control (sham). Ubiquitinated proteins with approximate MW of 30, 40, 50, 60 kDa are shown separately. Data is shown as percentage of control group (100%). Data = mean ±SE, n= 5 - 8/group. **p< 0.05, MI + Vehicle vs. sham, †p < 0.05, MI + MR blocker vs. sham.*

Table R18. Expression of GAP 43, PGP 9.5, ubiquitin and ubiquitinated proteins in the RV at 10 days post MI.

	RV		
	Sham	MI + Vehicle	MI + MR blocker
GAP 43/β-Actin	1.55±0.14	1.52±0.13	1.75± 0.18
PGP 9.5/ β-Actin	0.23 ± 0.02	**0.34 ± 0.03***	**0.37 ± 0.03**†
Ubiquitin/ β-Actin	4.12 ± 0.51	5.45 ± 0.59	5.91 ± 0.91
Ubiquitinated Protein ~30 kDa/ β-Actin	0.34±0.03	0.28±0.02	0.31±0.03
Ubiquitinated Protein ~40 kDa/ β-Actin	1.12±0.05	1.29±0.09	1.20 ± 0.11
Ubiquitinated Protein ~50 kDa/ β-Actin	1.25±0.14	1.69±0.07	1.55±0.09
Ubiquitinated Protein ~100 kDa/ β-Actin * 10^{-1}	3.15±0.26	2.46±0.32	2.95±0.22

Data = mean ±SE, n= 5 - 8/group. *$^{*}p < 0.05$, MI + Vehicle vs. sham, $^{\dagger}p < 0.05$, MI + MR blocker vs. sham.*

Figure R47. Western blot from the RV showing GAP 43, PGP 9.5, ubiquitin, ubiquitinated proteins and β -Actin at 10 days post MI.

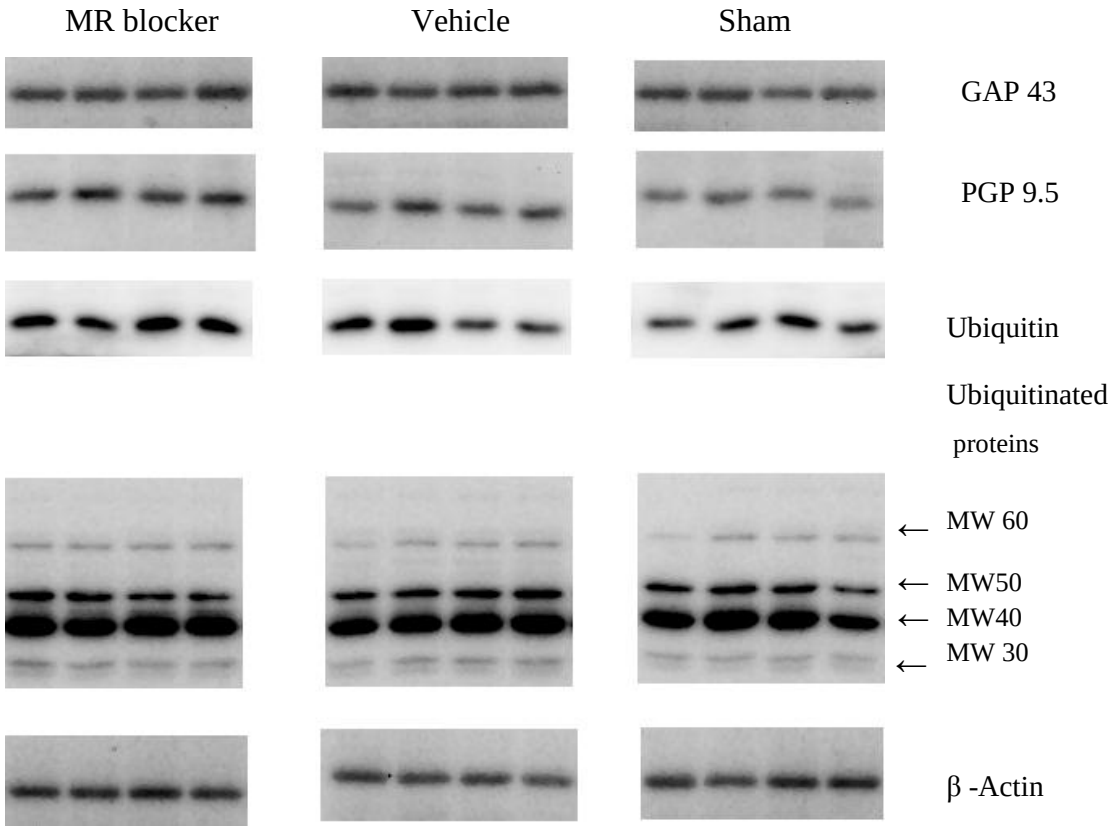

4. Discussion

4.1. Summary of main findings

The present study shows as novel finding that in rats post MI central treatment with eplerenone markedly attenuates cardiac sympathetic hyperinnervation at the infarct border. The time course of TH, NET and PGP 9.5 expression in the non-infarcted LV and RV showed a selective 2 fold increase in only PGP 9.5 protein content at 1 wk post MI, a 60% increase at 4 wks post MI, and no change at 12 wks. TH and NET were located only within cardiac sympathetic nerves. PGP 9.5 was expressed in both sympathetic axons and cardiomyocytes in the peri-infarct zone after the MI, and associated with increased ubiquitin expression.

4.2. Time course of TH, NET and PGP 9.5 expression

No changes in TH and NET mRNA and protein content in stellate ganglia were found at 1, 4 and 12 wks in rats post MI. At 12 wks post MI, in the left stellate ganglia the content of highly glycosylated NET protein with MW 80kDa was increased by 2 fold. No changes in PGP 9.5 mRNA content were noted at 1 and 4 wks post MI, whereas at 12 wks post MI PGP 9.5 mRNA was significantly decreased ~ 2 fold in both left and right stellate ganglia, but with no parallel changes in the protein level of PGP 9.5. No notable changes in TH and NET proteins in the non-infarcted base of the LV and in the RV were found. NET mRNA, however, was significantly increased by 2 fold at 1 and 12 wks post MI in the LV.

To our knowledge, the time course of TH, NET and PGP 9.5 expression in the heart and stellate ganglia has not been assessed previously in rats after permanent coronary

artery ligation. Parrish et al. (2008) reported a significant 2 fold increase of TH and NET mRNA in stellate ganglia, and a 2 fold increase of TH and NET proteins in the base of heart in rats at 1 wk post ischaemia-reperfusion. One explanation for these different findings is that ischaemia-reperfusion may affect TH and NET expression in a different fashion than the permanent MI model. The choice of normalization control could also affect results. PGP 9.5 was used as the only control by Parrish et al. (2008) to normalize TH and NET expression for variations in innervation. When glyceraldehyde 3-phosphate dehydrogenase was utilized as a control, no changes in TH and NET mRNA were found in the stellate ganglia of mice 1 wk post ischaemia-reperfusion (Parrish et al. 2010). PGP 9.5 gene expression can be notably downregulated by oxidative stress (Shen et al. 2006), and reactive oxygen species (ROS) generation is increased during ischaemia-reperfusion injury (Raedschelders et al. 2012). Oxidative stress can also be induced by Ang II, which can increase the NAD(P)H-dependent superoxide anion production and intracellular generation of ROS (Wei et al. 2008). The latter mechanism may be involved in the observed 2 fold decrease of PGP 9.5 mRNA in stellate ganglia and in the RV at 12 wks post MI, since plasma levels of Ang II are persistently elevated in rats post MI (Leenen et al. 1999a).

In addition to plasma Ang II, increased local Ang II levels could be a potential stimulus to trigger a selective upregulation of NET mRNA at 1 and 12 wks post MI in the base of the LV. Incubation of neuronal cultures with Ang II in vitro induces a 5 fold increase in NET mRNA levels (Lu et al. 1996). In rats a significant 2 fold increase in LV Ang II levels was found in the acute post MI state lasting 3-7 days after the MI (Leenen et al. 1999a, Silvestre et al. 1999). Thus, an increase in plasma and cardiac Ang II levels

may be responsible for the observed change in NET mRNA content in the LV above the ligation in the acute and chronic state post MI in rats.

NET mRNA levels in the heart are very low (see Results, table R10), which likely explains why an increase in local mRNA did not affect cardiac native NET 46 kDa protein levels. At 12 wks post MI an increased content of highly glycosylated NET protein was noted with MW 80kDa in left stellate ganglia. The increase in 80 kDa form of NET suggests that NET activity post MI in rats can be regulated via post-translational mechanisms, such as glycosylation. Highly glycosylated NET with MW 80 and 54 kDa show increased protein stability, surface trafficking and transport activity in comparison with unglycosylated NET with MW 46 kDa (Melikian et al. 1996).

Absence of changes in TH expression in rats post MI does not exclude increased TH activity mediated by other mechanisms, such as TH phosphorylation. TH phosphorylation at Ser40 can maintain TH activation for over 48 hours, suggesting that TH phosphorylation can be involved in prolonged regulation of TH activity (Bobrovskaya et al. 2007).

4.3. Origin of NET, TH and PGP 9.5 mRNA and proteins in the heart.

PGP 9.5, TH and NET mRNA and proteins in the heart may be locally expressed by intracardiac ganglia of the intrinsic nervous system, or be synthesized by neurons of stellate ganglia and then be sent to the heart via anterograde axonal transport. PGP 9.5, TH and NET mRNA levels in the LV were markedly lower than those in the neurons of stellate ganglia. This finding suggests that if local mRNA is translated into functional

proteins, they are not likely to markedly influence the total cardiac levels of PGP 9.5, TH and NET proteins in the heart.

To identify the origin of cardiac TH, NET and PGP 9.5 mRNA and proteins we performed bilateral stellate ganglionectomy in rats and after 1 wk assessed TH, NET and PGP 9.5 mRNA and protein content in the heart. At 1 wk post bilateral stellate ganglionectomy no significant changes in PGP 9.5 and NET mRNA were observed in the LV, whereas TH mRNA was significantly increased by 50%. This finding indicates that cardiac PGP 9.5, TH and NET mRNA all predominantly represent local expression in the LV. The source of expression is likely to be intracardiac ganglia, since multiple studies described PGP 9.5, TH and NET immunoreactive neurons and SIF cells in the rodent heart (Hoard et al. 2008, Richardson et al. 2003, Slavikova et al. 2003).

In contrast, in the LV 1 wk post bilateral stellate ganglionectomy TH protein content was markedly reduced by 90%, PGP 9.5 protein was reduced by 50%, but no significant changes were found in NET protein expression. This is consistent with the study by Pardini et al. (1989), who reported that in rats cardiac NE content is decreased ~ 90% 1 wk post bilateral stellate ganglionectomy. Since cardiac levels of TH protein decrease dramatically post ganglionectomy, a local 2 fold increase in TH mRNA likely indicates a compensatory increase provided either by intrinsic cardiac neurons or SIF cells. No notable changes in NET protein content post ganglionectomy suggest that NET protein has a relatively long half-life and/or capacity to regulate protein activity via increased protein stability. No in vivo studies have been done to assess NET half-life, but studies that assessed other monoamine transporters using irreversible transporter inhibitors

reported that dopamine and serotonin transporters have a relatively long half live of 2 and 3.5 days respectively (Kimmel et al. 2003, Vicentic et al. 1999).

After ganglionectomy PGP 9.5 content in the heart was reduced by 50%, which is markedly less than that of TH. Since cardiac ventricles lack parasympathetic innervation (Oh et al. 2006), these findings can not be attributed to the presence of PGP 9.5 in parasympathetic axons. PGP 9.5 protein half life was established to be around 2 days (Thao et al. 2012), so one should expect ~ 90% reduction in the protein levels after 7 days post ganglionectomy. Possible explanations for the observed finding could be presence of compensatory mechanisms which increase the stability of PGP 9.5 protein, or possible extra-neuronal PGP 9.5 protein expression in the LV. PGP 9.5 mRNA levels in the heart are also notably higher than those of TH and NET, which could indicate an additional source of mRNA synthesis.

These findings suggest that cardiac TH, NET and PGP mRNA are expressed in the heart locally, likely by the intrinsic ganglia or SIF cells, but most of cardiac TH protein is produced in the stellate ganglia and then transported to the heart. This is consistent with other studies which identified stellate ganglia as the main source of cardiac sympathetic innervation (Pardini et al. 1989, Yasunaga and Nosaka 1979). Since levels of cardiac NET, TH and PGP 9.5 mRNA are very low, they are not likely to markedly contribute to total cardiac protein levels, suggesting that PGP 9.5 and NET proteins are likely to be transported from stellate ganglia as well. Extra-neuronal expression of PGP 9.5 protein in the heart, however, remains a possibility and requires further investigation.

4.4. Cardiac sympathetic innervation

In the present study, cardiac sympathetic hyperinnervation was apparent at the infarct border with a 4 fold increase in GAP 43, a 2 fold increase in TH, and a 50% increase in PGP 9.5 nerve densities when compared to the epicardial side of the LV base in sham rats. When sympathetic hyperinnervation of the infarct border was compared with the endocardial side of the heart, increases in nerve densities were more pronounced. In contrast, in the non-infarcted base of the LV no significant changes in nerve densities were observed. This pattern is consistent with several studies which also described sympathetic hyperinnervation predominantly at the infarct border/peri-infarct area in rats at this time point post MI (Hasan et al. 2006, Li et al. 2004, Wernli et al. 2009). Sympathetic nerve density in the non-infarcted LV may increase later post MI, as most studies in rats described it at 4 weeks post MI (Lee et al. 2012, Lee et al. 2010, Yuan et al. 2009).

Our results show that central treatment with the MR blocker eplerenone at 5 ug/day for 9 days post MI markedly attenuates the increase in nerve density at the infarct border for TH, GAP 43 and in PGP 9.5. Central MR blockade decreases various parameters of sympathetic hyperactivity and improves cardiac functioning in rats post MI (Huang and Leenen 2005, Lal et al. 2004). The effect of central mechanisms on CSA post MI has not been evaluated yet, but it is reasonable to expect that central MR blockade also inhibits CSA. These findings suggest that CSNA may play an important role in development of sympathetic hyperinnervation post MI. In normal dogs subthreshold electrical stimulation of left stellate ganglia induces nerve sprouting and increases nerve density in the heart. In dogs post MI similar stimulation for 1 month promotes sympathetic hyperinnervation

and increases nerve density to a larger extent than NGF infusion in the left stellate ganglia (Swissa et al. 2004).

Central MR blockade may also decrease cardiac sympathetic hyperinnervation post MI by other mechanisms, such as by affecting NGF expression/function, or by decreasing the level of inflammation or oxidative stress. NGF belongs to the family of neurotrophins, along with neurotrophin-3, 4/5 and brain-derived neurotrophic factor. Pronounced NGF release and overexpression occurs within hours post MI at the infarct site and at the infarct border, and to a lesser extent in the non-infarcted LV (Oh et al. 2006, Zhou et al. 2004). Hasan et al. (2006) showed that macrophages and myofibroblasts at the infarct border zone express NGF at 7 to14 days post MI, and macrophage depletion with liposomes containing clodronate markedly reduces cardiac sympathetic hyperinnervation (Wernli et al. 2009). Inflammatory cells post MI may contribute to the cardiac source of NGF post MI, but other sources of expression may contribute as well, since macrophages appear at the scar region at 4^{th} day post MI (Naresh et al. 2012), yet the increase of NGF protein and mRNA at the infarct and peri-infarct region occurs within first hours and peaks at 3 days post MI (Oh et al. 2006, Zhou et al. 2004).

Chronically post MI oxidative stress and ROS originating from xanthine oxidase, NADPH oxidases, mitochondria and nitric oxide synthase may promote hyperinnervation in the remote regions of the heart (Lee et al. 2011). Superoxide and nitric oxide can trigger NGF expression upregulation via its by-product, peroxynitrite (Vargas et al. 2004). Inhibition of xanthine oxidase and subsequent superoxide production by allopurinol for 4 wks post MI decreased cardiac sympathetic nerve fiber density in the

remote myocardium by 2 fold. Treatment with N-acetylcysteine, a precursor of free radial scavenger glutathione, for 4 wks post MI also decreased cardiac sympathetic nerve fiber density in the remote regions by 3 fold.

Central MR blockade may potentially decrease oxidative stress and ROS formation in the heart via its effects on circulatory and cardiac RAAS. Our group demonstrated that chronic icv treatment with spironolactone for 6 wks prevents MI induced increase in serum aldosterone concentration (Lal et al. 2004). Icv infusion of Fab fragments to block brain "ouabain" for 4 wks notably attenuates increases in angiotensin-converting enzymes and AT_1 receptor density in the LV post MI (Tan et al. 2004). These findings suggest that chronically post MI sympathetic hyperactivity activates circulatory and cardiac RAAS. Ang II can induce oxidative stress in the heart by increasing NAD(P)H-dependent superoxide anion production and intracellular generation of ROS (Wei et al. 2008). Whether effects of central MR blockade on RAAS and ROS formation post MI could be a potential mechanism for decreasing cardiac sympathetic hyperinnervation post MI is yet to be investigated.

4.5. Extra-neuronal PGP 9.5 expression and ubiquitin proteasome system activation

In the base of the LV, PGP 9.5 immunoreactivity was noted predominantly within cardiac nerves, but could also be appreciated in a small number of individual spindle – shaped cells. In the peri-infarct area we noticed a large number of spindle –shaped cells which resemble fibroblasts and had strong PGP 9.5 immunoreactivity, but not TH immunoreactivity. However, no colocalization between PGP 9.5 positive cells and fibroblast marker - vimentin protein was present. Vimentin positive cells surrounded PGP

9.5 positive cells, confirming their peri-infarct location. In contrast, PGP 9.5 protein and alpha-sarcomeric Actin protein showed positive co-localization indicating that cardiomyocytes in the peri-infarct area express PGP 9.5. These findings indicate that after the MI cardiomyocytes change expression profile and upregulate PGP 9.5 expression. This is in agreement with Western blotting results, which showed a selective significant 6 fold increase in PGP 9.5 protein in the peri-infarct zone, and a 2 fold increase in the non-infarcted base of the heart. Content of other neuronal proteins, such as NET, GAP 43 and TH remained analtered. These changes appear to take place early post MI, since no changes in PGP 9.5 protein levels were found at 12 wks post MI. At one wk post MI myofibroblasts synthesizing NGF and brain-derived neurotrophic factor, along with neural stem cells, astrocytes and oligodendrocytes have been described in the scar (Drapeau et al. 2005, Hasan et al. 2006). Synthesis and local secretion of neurotrophic proteins by these cells may be a potential trigger for PGP 9.5 expression by cardiomyocytes post MI.

Our analysis of ubiquitinated proteins in the peri-infarct area demonstrated that expression ubiquitin and of ubiquitinated proteins with approximate MW of 60 kDa and 250 kDa was significantly increased ~ 2 fold, but expression of ubiquitinated proteins with approximate MW of 30 kDa, 40 kDa and 100 kDa was significantly decreased ~ 2 fold in the MI group. PGP 9.5, also referred to as ubiquitin carboxyl-terminal hydrolase L1 (UCH-L1), has several important roles associated with the ubiquitin protein. By hydrolyzing a peptide bond between ubiquitin and target protein, UCH-L1 generates a free mono-ubiquitin molecule available for next UPS catalytic cycle (Fang et al. 2010). It alsostabilizes mono-ubiquitin, which ensures its stability and elongates its half – life

(Osaka et al. 2003). Our results show that expression of ubiquitin in the peri-infarct proximity is increased ~2 fold, which is likely due to PGP 9.5 expression upregulation. Notably upregulated cardiac UCH-L1 and ubiquitin expression was also reported in a RV hypertrophy and failure rodent model (Rajagopalan et al. 2013). Weekes et al. (2003) described cardiac PGP 9.5 immunoreactivity in hearts from patients with severe dilated cardiomyopathy, which associated with accumulation of ubiquitinated proteins. Further studies are needed to identify the actual ubiquitinated proteins and the cellular processes involved, which likely represent the extensive remodeling early post-MI.

4.6. Conclusions

In summary, the present study demonstrates that in rats post MI central MR blockade markedly attenuates cardiac sympathetic hyperinnervation, and suggests that CSNA is likely to be involved in development of hyperinnervation. Cardiac sympathetic hyperactivity and sympathetic hyperinnervation have been implicated in ventricular arrhythmias and sudden cardiac death post-MI (Chen et al. 2001, Jardine et al. 2007), and one may speculate that central MR blockade can improve early post MI morbidity and mortality. The EPHESUS trial demonstrated a significant decrease in the incidence of cardiac arrhythmias and sudden cardiac deaths in patients post MI treated with eplerenone (Pitt et al. 2003). It is possible that eplerenone's central actions can decrease CSA and/or hyperinnervation post MI, contributing to this beneficial action.

4.7 Limitations

In the present study CSNA was not measured, but icv treatment with eplerenone is expected to attenuate CSNA since it prevents generalized sympathetic hyperactivity post MI. Assessment of effects of central MR blockade on other mechanisms involved in sympathetic hyperinnervation such as NGF, inflammation and oxidative stress would strengthen the study.

4.8 Future studies

Future studies should assess effects of central MR blockade on cardiac NGF expression in rats at 10 days post MI.

References

Abdi S and Yang Z (2005). A novel technique for experimental stellate ganglion block in rats. *Anesth Analg,* **101**, 561-565, table of contents.

Basu S, Sinha SK, Shao Q, Ganguly PK, and Dhalla NS (1996). Neuropeptide Y modulation of sympathetic activity in myocardial infarction. *J Am Coll Cardiol,* **27**, 1796-1803.

Biguet NF, Rittenhouse AR, Mallet J, and Zigmond RE (1989). Preganglionic nerve stimulation increases mRNA levels for tyrosine hydroxylase in the rat superior cervical ganglion. *Neurosci Lett,* **104**, 189-194.

Birmingham MK, Sar M, and Stumpf WE (1984). Localization of aldosterone and corticosterone in the central nervous system, assessed by quantitative autoradiography. *Neurochem Res,* **9**, 333-350.

Bisognano JD, Weinberger HD, Bohlmeyer TJ, Pende A, Raynolds MV, Sastravaha A, Roden R, Asano K, Blaxall BC, Wu SC, Communal C, Singh K, Colucci W, Bristow MR, and Port DJ (2000). Myocardial-directed overexpression of the human beta(1)-adrenergic receptor in transgenic mice. *J Mol Cell Cardiol,* **32**, 817-830.

Blakely RD and Bauman AL (2000). Biogenic amine transporters: regulation in flux. *Curr Opin Neurobiol,* **10**, 328-336.

Bobrovskaya L, Gilligan C, Bolster EK, Flaherty JJ, Dickson PW, and Dunkley PR (2007). Sustained phosphorylation of tyrosine hydroxylase at serine 40: a novel mechanism for maintenance of catecholamine synthesis. *J Neurochem,* **100**, 479-489.

Brown AM (1967). Excitation of afferent cardiac sympathetic nerve fibres during myocardial ischaemia. *J Physiol,* **190**, 35-53.

Brum PC, Rolim N., Bakurau A.N., and Medeiros A. (2006). Neurohormonal activation in heart failure: the role of adrenergic receptors. *Anais da Academia Brasileira de Ciências,* **78**, 485-503.

Bulteau AL, Lundberg KC, Humphries KM, Sadek HA, Szweda PA, Friguet B, and Szweda LI (2001). Oxidative modification and inactivation of the proteasome during coronary occlusion/reperfusion. *J Biol Chem,* **276**, 30057-30063.

Burgi K, Cavalleri MT, Alves AS, Britto LR, Antunes VR, and Michelini LC (2011). Tyrosine hydroxylase immunoreactivity as indicator of sympathetic activity: simultaneous evaluation in different tissues of hypertensive rats. *Am J Physiol Regul Integr Comp Physiol,* **300**, R264-271.

Cao JM, Chen LS, KenKnight BH, Ohara T, Lee MH, Tsai J, Lai WW, Karagueuzian HS, Wolf PL, Fishbein MC, and Chen PS (2000). Nerve sprouting and sudden cardiac death. *Circ Res,* **86**, 816-821.

Chen LS, Zhou S, Fishbein MC, and Chen PS (2007). New perspectives on the role of autonomic nervous system in the genesis of arrhythmias. *J Cardiovasc Electrophysiol,* **18**, 123-127.

Chen PS, Chen LS, Cao JM, Sharifi B, Karagueuzian HS, and Fishbein MC (2001). Sympathetic nerve sprouting, electrical remodeling and the mechanisms of sudden cardiac death. *Cardiovasc Res,* **50**, 409-416.

Colucci WS, Sawyer DB, Singh K, and Communal C (2000). Adrenergic overload and apoptosis in heart failure: implications for therapy. *J Card Fail,* **6**, 1-7.

Communal C, Singh K, Sawyer DB, and Colucci WS (1999). Opposing effects of beta(1)- and beta(2)-adrenergic receptors on cardiac myocyte apoptosis : role of a pertussis toxin-sensitive G protein. *Circulation,* **100**, 2210-2212.

Costanzo LS**.** *Physiology*. Philadelphia: Saunders, 2002.

Crick SJ, Sheppard M.N., Ho S.Y., and Anderson R.H. *Neural supply of the heart*. Totowa, New Jersey: Humana press Inc., 2000.

Davern PJ and Head GA (2007). Fos-related antigen immunoreactivity after acute and chronic angiotensin II-induced hypertension in the rabbit brain. *Hypertension,* **49**, 1170-1177.

Drapeau J, El-Helou V, Clement R, Bel-Hadj S, Gosselin H, Trudeau LE, Villeneuve L, and Calderone A (2005). Nestin-expressing neural stem cells identified in the scar following myocardial infarction. *J Cell Physiol,* **204**, 51-62.

Du XJ, Fang L, Gao XM, Kiriazis H, Feng X, Hotchkin E, Finch AM, Chaulet H, and Graham RM (2004). Genetic enhancement of ventricular contractility protects against pressure-overload-induced cardiac dysfunction. *J Mol Cell Cardiol,* **37**, 979-987.

Dunkley PR, Bobrovskaya L, Graham ME, von Nagy-Felsobuki EI, and Dickson PW (2004). Tyrosine hydroxylase phosphorylation: regulation and consequences. *J Neurochem,* **91**, 1025-1043.

Eiden LE, Schafer MK, Weihe E, and Schutz B (2004). The vesicular amine transporter family (SLC18): amine/proton antiporters required for vesicular accumulation and regulated exocytotic secretion of monoamines and acetylcholine. *Pflugers Arch,* **447**, 636-640.

El-Helou V, Proulx C, Gosselin H, Clement R, Mimee A, Villeneuve L, and Calderone A (2008). Dexamethasone treatment of post-MI rats attenuates sympathetic innervation of the infarct region. *J Appl Physiol,* **104**, 150-156.

Esler M, Jennings G, Lambert G, Meredith I, Horne M, and Eisenhofer G (1990). Overflow of catecholamine neurotransmitters to the circulation: source, fate, and functions. *Physiol Rev,* **70**, 963-985.

Esler M and Kaye D (2000). Measurement of sympathetic nervous system activity in heart failure: the role of norepinephrine kinetics. *Heart Fail Rev,* **5**, 17-25.

Fang Y, Fu D, and Shen XZ (2010). The potential role of ubiquitin c-terminal hydrolases in oncogenesis. *Biochim Biophys Acta,* **1806**, 1-6.

Fitzpatrick PF (2000). The aromatic amino acid hydroxylases. *Adv Enzymol Relat Areas Mol Biol,* **74**, 235-294.

Forsgren S, Moravec M, and Moravec J (1990). Catecholamine-synthesizing enzymes and neuropeptides in rat heart epicardial ganglia; an immunohistochemical study. *Histochem J,* **22**, 667-676.

Francis J, Weiss RM, Wei SG, Johnson AK, Beltz TG, Zimmerman K, and Felder RB (2001). Central mineralocorticoid receptor blockade improves volume regulation and reduces sympathetic drive in heart failure. *Am J Physiol Heart Circ Physiol,* **281**, H2241-2251.

Gabor A and Leenen FH (2009). Mechanisms in the PVN mediating local and central sodium-induced hypertension in Wistar rats. *Am J Physiol Regul Integr Comp Physiol,* **296**, R618-630.

Ganguly PK, Dhalla KS, Shao Q, Beamish RE, and Dhalla NS (1997). Differential changes in sympathetic activity in left and right ventricles in congestive heart failure after myocardial infarction. *Am Heart J,* **133**, 340-345.

Gauthier C, Langin D, and Balligand JL (2000). Beta3-adrenoceptors in the cardiovascular system. *Trends Pharmacol Sci,* **21**, 426-431.

Geerling JC, Kawata M, and Loewy AD (2006). Aldosterone-sensitive neurons in the rat central nervous system. *J Comp Neurol,* **494**, 515-527.

Glickman MH and Ciechanover A (2002). The ubiquitin-proteasome proteolytic pathway: destruction for the sake of construction. *Physiol Rev,* **82**, 373-428.

Gomez-Sanchez EP (2010). The mammalian mineralocorticoid receptor: tying down a promiscuous receptor. *Exp Physiol,* **95**, 13-18.

Gordon SL, Quinsey NS, Dunkley PR, and Dickson PW (2008). Tyrosine hydroxylase activity is regulated by two distinct dopamine-binding sites. *J Neurochem,* **106**, 1614-1623.

Gordon SL, Webb JK, Shehadeh J, Dunkley PR, and Dickson PW (2009). The low affinity dopamine binding site on tyrosine hydroxylase: the role of the N-terminus and in situ regulation of enzyme activity. *Neurochem Res,* **34**, 1830-1837.

Graham LN, Smith PA, Stoker JB, Mackintosh AF, and Mary DA (2002). Time course of sympathetic neural hyperactivity after uncomplicated acute myocardial infarction. *Circulation,* **106**, 793-797.

Groll M and Huber R (2003). Substrate access and processing by the 20S proteasome core particle. *Int J Biochem Cell Biol,* **35**, 606-616.

Habecker BA, Willison BD, Shi X, and Woodward WR (2006). Chronic depolarization stimulates norepinephrine transporter expression via catecholamines. *J Neurochem,* **97**, 1044-1051.

Haider N, Baliga RR, Chandrashekhar Y, and Narula J (2010). Adrenergic excess, hNET1 down-regulation, and compromised mIBG uptake in heart failure poverty in the presence of plenty. *JACC Cardiovasc Imaging,* **3**, 71-75.

Hasan W, Jama A, Donohue T, Wernli G, Onyszchuk G, Al-Hafez B, Bilgen M, and Smith PG (2006). Sympathetic hyperinnervation and inflammatory cell NGF synthesis following myocardial infarction in rats. *Brain Res,* **1124**, 142-154.

Hayashi M, Tsutamoto T, Wada A, Tsutsui T, Ishii C, Ohno K, Fujii M, Taniguchi A, Hamatani T, Nozato Y, Kataoka K, Morigami N, Ohnishi M, Kinoshita M, and Horie M (2003). Immediate administration of mineralocorticoid receptor antagonist spironolactone prevents post-infarct left ventricular remodeling associated with suppression of a marker of myocardial collagen synthesis in patients with first anterior acute myocardial infarction. *Circulation,* **107**, 2559-2565.

Hoard JL, Hoover DB, Mabe AM, Blakely RD, Feng N, and Paolocci N (2008). Cholinergic neurons of mouse intrinsic cardiac ganglia contain noradrenergic enzymes, norepinephrine transporters, and the neurotrophin receptors tropomyosin-related kinase A and p75. *Neuroscience,* **156**, 129-142.

Hoover DB, Isaacs ER, Jacques F, Hoard JL, Page P, and Armour JA (2009). Localization of multiple neurotransmitters in surgically derived specimens of human atrial ganglia. *Neuroscience,* **164**, 1170-1179.

Huang BS, Ahmadi S, Ahmad M, White RA, and Leenen FH (2010). Central neuronal activation and pressor responses induced by circulating ANG II: role of the brain aldosterone-"ouabain" pathway. *Am J Physiol Heart Circ Physiol,* **299**, H422-430.

Huang BS and Leenen FH (2005). Blockade of brain mineralocorticoid receptors or Na+ channels prevents sympathetic hyperactivity and improves cardiac function in rats post-MI. *Am J Physiol Heart Circ Physiol,* **288**, H2491-2497.

Huang BS and Leenen FH (2009). The brain renin-angiotensin-aldosterone system: a major mechanism for sympathetic hyperactivity and left ventricular remodeling and dysfunction after myocardial infarction. *Curr Heart Fail Rep,* **6**, 81-88.

Huang BS and Leenen FH (1996). Sympathoexcitatory and pressor responses to increased brain sodium and ouabain are mediated via brain ANG II. *Am J Physiol,* **270**, H275-280.

Huang BS, White RA, Ahmad M, Tan J, Jeng AY, and Leenen FH (2009). Central infusion of aldosterone synthase inhibitor attenuates left ventricular dysfunction and remodelling in rats after myocardial infarction. *Cardiovasc Res,* **81**, 574-581.

Huang BS, Yuan B, and Leenen FH (2000). Chronic blockade of brain "ouabain" prevents sympathetic hyper-reactivity and impairment of acute baroreflex resetting in rats with congestive heart failure. *Can J Physiol Pharmacol,* **78**, 45-53.

Jansen AS, Wessendorf MW, and Loewy AD (1995). Transneuronal labeling of CNS neuropeptide and monoamine neurons after pseudorabies virus injections into the stellate ganglion. *Brain Res,* **683**, 1-24.

Jardine DL, Charles CJ, Ashton RK, Bennett SI, Whitehead M, Frampton CM, and Nicholls MG (2005). Increased cardiac sympathetic nerve activity following acute myocardial infarction in a sheep model. *J Physiol,* **565**, 325-333.

Jardine DL, Charles CJ, Frampton CM, and Richards AM (2007). Cardiac sympathetic nerve activity and ventricular fibrillation during acute myocardial infarction in a conscious sheep model. *Am J Physiol Heart Circ Physiol,* **293**, H433-439.

Jewitt DE, Reid D, Thomas M, Mercer CJ, Valori C, and Shillingford JP (1969). Free noradrenaline and adrenaline excretion in relation to the development of cardiac arrhythmias and heart-failure in patients with acute myocardial infarction. *Lancet,* **1**, 635-641.

Jugdutt BI, Idikio H, and Uwiera RR (2007). Angiotensin receptor blockade and angiotensin-converting-enzyme inhibition limit adverse remodeling of infarct zone collagens and global diastolic dysfunction during healing after reperfused ST-elevation myocardial infarction. *Mol Cell Biochem,* **303**, 27-38.

Kang CS, Chen CC, Lin CC, Chang NC, and Lee TM (2009). Effect of ATP-sensitive potassium channel agonists on sympathetic hyperinnervation in postinfarcted rat hearts. *Am J Physiol Heart Circ Physiol,* **296**, H1949-1959.

Kasama S, Toyama T, Sumino H, Kumakura H, Takayama Y, Minami K, Ichikawa S, Matsumoto N, Sato Y, and Kurabayashi M (2011). Prognostic value of cardiac

sympathetic nerve activity evaluated by [123I]m-iodobenzylguanidine imaging in patients with ST-segment elevation myocardial infarction. *Heart,* **97**, 20-26.

Kasper DL, Braunwald E., Fauci A., Hausker S.L., Longo D.L., and J.L. J**.** *Principles of Internal Medicine 16th edition*. New York: McGraw-Hill Companies, Inc, 2005.

Kaumann AJ and Molenaar P (1997). Modulation of human cardiac function through 4 beta-adrenoceptor populations. *Naunyn Schmiedebergs Arch Pharmacol,* **355**, 667-681.

Kaye DM, Lambert GW, Lefkovits J, Morris M, Jennings G, and Esler MD (1994). Neurochemical evidence of cardiac sympathetic activation and increased central nervous system norepinephrine turnover in severe congestive heart failure. *J Am Coll Cardiol,* **23**, 570-578.

Kilbourne EJ, Nankova BB, Lewis EJ, McMahon A, Osaka H, Sabban DB, and Sabban EL (1992). Regulated expression of the tyrosine hydroxylase gene by membrane depolarization. Identification of the responsive element and possible second messengers. *J Biol Chem,* **267**, 7563-7569.

Kimmel HL, Carroll FI, and Kuhar MJ (2003). Withdrawal from repeated cocaine alters dopamine transporter protein turnover in the rat striatum. *J Pharmacol Exp Ther,* **304**, 15-21.

Kimura K, Ieda M, and Fukuda K (2012). Development, maturation, and transdifferentiation of cardiac sympathetic nerves. *Circ Res,* **110**, 325-336.

Klabunde RE**.** *Cardiovascular physiology concepts*. Philadelphia: Lippincott Williams & Wilkins, 2005.

Klimaschewski L, Kummer W, and Heym C (1996). Localization, regulation and functions of neurotransmitters and neuromodulators in cervical sympathetic ganglia. *Microsc Res Tech,* **35**, 44-68.

Kolettis TM, Agelaki MG, Baltogiannis GG, Vlahos AP, Mourouzis I, Fotopoulos A, and Pantos C (2007). Comparative effects of acute vs. chronic oral amiodarone treatment during acute myocardial infarction in rats. *Europace,* **9**, 1099-1104.

Kumer SC and Vrana KE (1996). Intricate regulation of tyrosine hydroxylase activity and gene expression. *J Neurochem,* **67**, 443-462.

Lal A, Veinot JP, and Leenen FH (2004). Critical role of CNS effects of aldosterone in cardiac remodeling post-myocardial infarction in rats. *Cardiovasc Res,* **64**, 437-447.

Lee TM, Chen CC, Chung TH, and Chang NC (2012). Effect of sildenafil on ventricular arrhythmias in post-infarcted rat hearts. *Eur J Pharmacol,* **690**, 124-132.

Lee TM, Chen CC, and Hsu YJ (2011). Differential effects of NADPH oxidase and xanthine oxidase inhibition on sympathetic reinnervation in postinfarct rat hearts. *Free Radic Biol Med,* **50**, 1461-1470.

Lee TM, Lai PY, and Chang NC (2010). Effect of N-acetylcysteine on sympathetic hyperinnervation in post-infarcted rat hearts. *Cardiovasc Res,* **85**, 137-146.

Leenen FH (1999). Cardiovascular consequences of sympathetic hyperactivity. *Can J Cardiol,* **15 Suppl A**, 2A-7A.

Leenen FH, Skarda V, Yuan B, and White R (1999a). Changes in cardiac ANG II postmyocardial infarction in rats: effects of nephrectomy and ACE inhibitors. *Am J Physiol,* **276**, H317-325.

Leenen FH, Yuan B, and Huang BS (1999b). Brain "ouabain" and angiotensin II contribute to cardiac dysfunction after myocardial infarction. *Am J Physiol*, **277**, H1786-1792.

Lemire I, Ducharme A, Tardif JC, Poulin F, Jones LR, Allen BG, Hebert TE, and Rindt H (2001). Cardiac-directed overexpression of wild-type alpha1B-adrenergic receptor induces dilated cardiomyopathy. *Am J Physiol Heart Circ Physiol*, **281**, H931-938.

Li W, Knowlton D, Van Winkle DM, and Habecker BA (2004). Infarction alters both the distribution and noradrenergic properties of cardiac sympathetic neurons. *Am J Physiol Heart Circ Physiol*, **286**, H2229-2236.

Lin F, Owens WA, Chen S, Stevens ME, Kesteven S, Arthur JF, Woodcock EA, Feneley MP, and Graham RM (2001). Targeted alpha(1A)-adrenergic receptor overexpression induces enhanced cardiac contractility but not hypertrophy. *Circ Res*, **89**, 343-350.

Lind RW, Swanson LW, and Ganten D (1984). Angiotensin II immunoreactivity in the neural afferents and efferents of the subfornical organ of the rat. *Brain Res*, **321**, 209-215.

Lindley TE, Doobay MF, Sharma RV, and Davisson RL (2004). Superoxide is involved in the central nervous system activation and sympathoexcitation of myocardial infarction-induced heart failure. *Circ Res*, **94**, 402-409.

Liu Y, Fallon L, Lashuel HA, Liu Z, and Lansbury PT, Jr. (2002). The UCH-L1 gene encodes two opposing enzymatic activities that affect alpha-synuclein degradation and Parkinson's disease susceptibility. *Cell*, **111**, 209-218.

Lorentz CU, Alston EN, Belcik T, Lindner JR, Giraud GD, and Habecker BA (2010). Heterogeneous ventricular sympathetic innervation, altered beta-adrenergic receptor expression, and rhythm instability in mice lacking the p75 neurotrophin receptor. *Am J Physiol Heart Circ Physiol*, **298**, H1652-1660.

Lu D, Yu K, Paddy MR, Rowland NE, and Raizada MK (1996). Regulation of norepinephrine transport system by angiotensin II in neuronal cultures of normotensive and spontaneously hypertensive rat brains. *Endocrinology*, **137**, 763-772.

Lujan HL, Palani G, Chen Y, Peduzzi JD, and Dicarlo SE (2009). Targeted ablation of cardiac sympathetic neurons reduces resting, reflex and exercise-induced sympathetic activation in conscious rats. *Am J Physiol Heart Circ Physiol*, **296**, H1305-1311.

Malliani A, Schwartz PJ, and Zanchetti A (1969). A sympathetic reflex elicited by experimental coronary occlusion. *Am J Physiol*, **217**, 703-709.

Mandela P and Ordway GA (2006). The norepinephrine transporter and its regulation. *J Neurochem*, **97**, 310-333.

McAlpine HM, Morton JJ, Leckie B, Rumley A, Gillen G, and Dargie HJ (1988). Neuroendocrine activation after acute myocardial infarction. *Br Heart J*, **60**, 117-124.

McCulloch RI, Daubner SC, and Fitzpatrick PF (2001). Effects of substitution at serine 40 of tyrosine hydroxylase on catecholamine binding. *Biochemistry*, **40**, 7273-7278.

Melikian HE, Ramamoorthy S, Tate CG, and Blakely RD (1996). Inability to N-glycosylate the human norepinephrine transporter reduces protein stability, surface trafficking, and transport activity but not ligand recognition. *Mol Pharmacol*, **50**, 266-276.

Mircoli L, Fedele L, Benetti M, Bolla GB, Radaelli A, Perlini S, and Ferrari AU (2002). Preservation of the baroreceptor heart rate reflex by chemical sympathectomy in experimental heart failure. *Circulation*, **106**, 866-872.

Moore KL and Dalley AF**.** *Clinically oriented anatomy*. Philadelphia: Lippincott Williams and Wilkins, 1999.

Myslivecek J and Trojan S (2003). Regulation of adrenoceptors and muscarinic receptors in the heart. *Gen Physiol Biophys*, **22**, 3-14.

Naresh NK, Xu Y, Klibanov AL, Vandsburger MH, Meyer CH, Leor J, Kramer CM, French BA, and Epstein FH (2012). Monocyte and/or macrophage infiltration of heart after myocardial infarction: MR imaging by using T1-shortening liposomes. *Radiology*, **264**, 428-435.

Oh YS, Jong AY, Kim DT, Li H, Wang C, Zemljic-Harpf A, Ross RS, Fishbein MC, Chen PS, and Chen LS (2006). Spatial distribution of nerve sprouting after myocardial infarction in mice. *Heart Rhythm*, **3**, 728-736.

Oikonomidis DL, Tsalikakis DG, Baltogiannis GG, Tzallas AT, Xourgia X, Agelaki MG, Megalou AJ, Fotopoulos A, Papalois A, Kyriakides ZS, and Kolettis TM (2010). Endothelin-B receptors and ventricular arrhythmogenesis in the rat model of acute myocardial infarction. *Basic Res Cardiol*, **105**, 235-245.

Olerud JE, Chiu DS, Usui ML, Gibran NS, and Ansel JC (1998). Protein gene product 9.5 is expressed by fibroblasts in human cutaneous wounds. *J Invest Dermatol*, **111**, 565-572.

Omland T, Aarsland T, Aakvaag A, Lie RT, and Dickstein K (1993). Prognostic value of plasma atrial natriuretic factor, norepinephrine and epinephrine in acute myocardial infarction. *Am J Cardiol*, **72**, 255-259.

Ordway GA, Jia W, Li J, Zhu MY, Mandela P, and Pan J (2005). Norepinephrine transporter function and desipramine: residual drug effects versus short-term regulation. *J Neurosci Methods*, **143**, 217-225.

Osaka H, Wang YL, Takada K, Takizawa S, Setsuie R, Li H, Sato Y, Nishikawa K, Sun YJ, Sakurai M, Harada T, Hara Y, Kimura I, Chiba S, Namikawa K, Kiyama H, Noda M, Aoki S, and Wada K (2003). Ubiquitin carboxy-terminal hydrolase L1 binds to and stabilizes monoubiquitin in neuron. *Hum Mol Genet*, **12**, 1945-1958.

Packer M (1992). The neurohormonal hypothesis: a theory to explain the mechanism of disease progression in heart failure. *J Am Coll Cardiol*, **20**, 248-254.

Pardini BJ, Lund DD, and Schmid PG (1989). Organization of the sympathetic postganglionic innervation of the rat heart. *J Auton Nerv Syst*, **28**, 193-201.

Parrish DC, Alston EN, Rohrer H, Nkadi P, Woodward WR, Schutz G, and Habecker BA (2010). Infarction-induced cytokines cause local depletion of tyrosine hydroxylase in cardiac sympathetic nerves. *Exp Physiol*, **95**, 304-314.

Parrish DC, Gritman K, Van Winkle DM, Woodward WR, Bader M, and Habecker BA (2008). Postinfarct sympathetic hyperactivity differentially stimulates expression of tyrosine hydroxylase and norepinephrine transporter. *Am J Physiol Heart Circ Physiol*, **294**, H99-H106.

Patel KP, Zhang K, and Carmines PK (2000). Norepinephrine turnover in peripheral tissues of rats with heart failure. *Am J Physiol Regul Integr Comp Physiol,* **278**, R556-562.

Patterson AJ, Zhu W, Chow A, Agrawal R, Kosek J, Xiao RP, and Kobilka B (2004). Protecting the myocardium: a role for the beta2 adrenergic receptor in the heart. *Crit Care Med,* **32**, 1041-1048.

Pitt B, Remme W, Zannad F, Neaton J, Martinez F, Roniker B, Bittman R, Hurley S, Kleiman J, and Gatlin M (2003). Eplerenone, a selective aldosterone blocker, in patients with left ventricular dysfunction after myocardial infarction. *N Engl J Med,* **348**, 1309-1321.

Powell SR and Divald A (2010). The ubiquitin-proteasome system in myocardial ischaemia and preconditioning. *Cardiovasc Res,* **85**, 303-311.

Raedschelders K, Ansley DM, and Chen DD (2012). The cellular and molecular origin of reactive oxygen species generation during myocardial ischemia and reperfusion. *Pharmacol Ther,* **133**, 230-255.

Rajagopalan V, Zhao M, Reddy S, Fajardo G, Wang X, Dewey S, Gomes AV, and Bernstein D (2013). Altered ubiquitin-proteasome signaling in right ventricular hypertrophy and failure. *Am J Physiol Heart Circ Physiol,* **305**, H551-562.

Ramchandra R, Hood SG, Watson AM, Allen AM, and May CN (2012). Central angiotensin type 1 receptor blockade decreases cardiac but not renal sympathetic nerve activity in heart failure. *Hypertension,* **59**, 634-641.

Randall WC and Rohse WG (1956). The augmentor action of the sympathetic cardiac nerves. *Circ Res,* **4**, 470-475.

Richardson RJ, Grkovic I, and Anderson CR (2003). Immunohistochemical analysis of intracardiac ganglia of the rat heart. *Cell Tissue Res,* **314**, 337-350.

Rittenhouse AR and Zigmond RE (1990). Nerve stimulation in vivo acutely increases tyrosine hydroxylase activity in the superior cervical ganglion and its end organs. *Brain Res,* **524**, 156-159.

Rodriguez JE, Schisler JC, Patterson C, and Willis MS (2009). Seek and destroy: the ubiquitin----proteasome system in cardiac disease. *Curr Hypertens Rep,* **11**, 396-405.

Rundqvist B, Elam M, Bergmann-Sverrisdottir Y, Eisenhofer G, and Friberg P (1997). Increased cardiac adrenergic drive precedes generalized sympathetic activation in human heart failure. *Circulation,* **95**, 169-175.

Salvatore MF, Garcia-Espana A, Goldstein M, Deutch AY, and Haycock JW (2000). Stoichiometry of tyrosine hydroxylase phosphorylation in the nigrostriatal and mesolimbic systems in vivo: effects of acute haloperidol and related compounds. *J Neurochem,* **75**, 225-232.

Salvatore MF, Waymire JC, and Haycock JW (2001). Depolarization-stimulated catecholamine biosynthesis: involvement of protein kinases and tyrosine hydroxylase phosphorylation sites in situ. *J Neurochem,* **79**, 349-360.

San Mauro MP, Patronelli P., Spinelli P., Cordero A., Covello D., and Gorgostiaga J.A. (2009). Nerves of the heart: a comprehensive review with a clinical point of view. *Neuroanatomy,* **8**, 28-31.

Savchenko V, Sung U, and Blakely RD (2003). Cell surface trafficking of the antidepressant-sensitive norepinephrine transporter revealed with an ectodomain antibody. *Mol Cell Neurosci,* **24**, 1131-1150.

Schwartz PJ and Stone HL (1979). Effects of unilateral stellectomy upon cardiac performance during exercise in dogs. *Circ Res,* **44**, 637-645.

Schwenke DO, Tokudome T, Kishimoto I, Horio T, Shirai M, Cragg PA, and Kangawa K (2008). Early ghrelin treatment after myocardial infarction prevents an increase in cardiac sympathetic tone and reduces mortality. *Endocrinology,* **149**, 5172-5176.

Shen H, Sikorska M, Leblanc J, Walker PR, and Liu QY (2006). Oxidative stress regulated expression of ubiquitin Carboxyl-terminal Hydrolase-L1: role in cell survival. *Apoptosis,* **11**, 1049-1059.

Shen JZ and Young MJ (2012). Corticosteroids, heart failure, and hypertension: a role for immune cells? *Endocrinology*, **153**, 5692-5700.

Shi Z, Chen AD, Xu Y, Chen Q, Gao XY, Wang W, and Zhu GQ (2009). Long-term administration of tempol attenuates postinfarct ventricular dysfunction and sympathetic activity in rats. *Pflugers Arch,* **458**, 247-257.

Silvestre JS, Heymes C, Oubenaissa A, Robert V, Aupetit-Faisant B, Carayon A, Swynghedauw B, and Delcayre C (1999). Activation of cardiac aldosterone production in rat myocardial infarction: effect of angiotensin II receptor blockade and role in cardiac fibrosis. *Circulation,* **99**, 2694-2701.

Simpson P (1983). Norepinephrine-stimulated hypertrophy of cultured rat myocardial cells is an alpha 1 adrenergic response. *J Clin Invest,* **72**, 732-738.

Singh K, Xiao L, Remondino A, Sawyer DB, and Colucci WS (2001). Adrenergic regulation of cardiac myocyte apoptosis. *J Cell Physiol,* **189**, 257-265.

Slavikova J, Kuncova J, Reischig J, and Dvorakova M (2003). Catecholaminergic neurons in the rat intrinsic cardiac nervous system. *Neurochem Res,* **28**, 593-598.

Soeki T, Kishimoto I, Schwenke DO, Tokudome T, Horio T, Yoshida M, Hosoda H, and Kangawa K (2008). Ghrelin suppresses cardiac sympathetic activity and prevents early left ventricular remodeling in rats with myocardial infarction. *Am J Physiol Heart Circ Physiol*, **294**, H426-432.

Sohns W, van Veen TA, and van der Heyden MA (2010). Regulatory roles of the ubiquitin-proteasome system in cardiomyocyte apoptosis. *Curr Mol Med,* **10**, 1-13.

Spiegel K, Kremer NE, and Kessler JA (1989). Differences in the effects of membrane depolarization on levels of preprosomatostatin mRNA and tyrosine hydroxylase mRNA in rat sympathetic neurons in vivo and in culture. *Brain Res Mol Brain Res*, **5**, 23-29.

Sung U, Apparsundaram S, Galli A, Kahlig KM, Savchenko V, Schroeter S, Quick MW, and Blakely RD (2003). A regulated interaction of syntaxin 1A with the antidepressant-sensitive norepinephrine transporter establishes catecholamine clearance capacity. *J Neurosci*, **23**, 1697-1709.

Swissa M, Zhou S, Gonzalez-Gomez I, Chang CM, Lai AC, Cates AW, Fishbein MC, Karagueuzian HS, Chen PS, and Chen LS (2004). Long-term subthreshold electrical stimulation of the left stellate ganglion and a canine model of sudden cardiac death. *J Am Coll Cardiol,* **43**, 858-864.

Tan J, Wang H, and Leenen FH (2004). Increases in brain and cardiac AT1 receptor and ACE densities after myocardial infarct in rats. *Am J Physiol Heart Circ Physiol*, **286**, H1665-1671.

Thao DT, An PN, Yamaguchi M, and LinhThuoc T (2012). Overexpression of ubiquitin carboxyl terminal hydrolase impairs multiple pathways during eye development in Drosophila melanogaster. *Cell Tissue Res*, **348**, 453-463.

Torabi A, Cleland JG, Khan NK, Loh PH, Clark AL, Alamgir F, Caplin JL, Rigby AS, and Goode K (2008). The timing of development and subsequent clinical course of heart failure after a myocardial infarction. *Eur Heart J*, **29**, 859-870.

Toth A, Nickson P, Qin LL, and Erhardt P (2006). Differential regulation of cardiomyocyte survival and hypertrophy by MDM2, an E3 ubiquitin ligase. *J Biol Chem*, **281**, 3679-3689.

Tsuyuki RT, Shibata MC, Nilsson C, and Hervas-Malo M (2003). Contemporary burden of illness of congestive heart failure in Canada. *Can J Cardiol*, **19**, 436-438.

Tu JV, Nardi L, Fang J, Liu J, Khalid L, and Johansen H (2009). National trends in rates of death and hospital admissions related to acute myocardial infarction, heart failure and stroke, 1994-2004. *CMAJ*, **180**, E118-125.

Unger T, Rascher W, Schuster C, Pavlovitch R, Schomig A, Dietz R, and Ganten D (1981). Central blood pressure effects of substance P and angiotensin II: role of the sympathetic nervous system and vasopressin. *Eur J Pharmacol*, **71**, 33-42.

Vahid-Ansari F and Leenen FH (1998). Pattern of neuronal activation in rats with CHF after myocardial infarction. *Am J Physiol*, **275**, H2140-2146.

van Veldhuisen DJ, van Gilst WH, de Smet BJ, de Graeff PA, Scholtens E, Buikema H, Girbes AR, Wesseling H, and Lie KI (1994). Neurohumoral and hemodynamic effects of ibopamine in a rat model of chronic myocardial infarction and heart failure. *Cardiovasc Drugs Ther*, **8**, 245-250.

Vargas MR, Pehar M, Cassina P, Estevez AG, Beckman JS, and Barbeito L (2004). Stimulation of nerve growth factor expression in astrocytes by peroxynitrite. *In Vivo*, **18**, 269-274.

Vicentic A, Battaglia G, Carroll FI, and Kuhar MJ (1999). Serotonin transporter production and degradation rates: studies with RTI-76. *Brain Res*, **841**, 1-10.

Vracko R, Thorning D, and Frederickson RG (1990). Fate of nerve fibers in necrotic, healing, and healed rat myocardium. *Lab Invest*, **63**, 490-501.

Wallis D, Watson A., and Mo N. (1996). Cardiac neurons of autonomic ganglia. *Microscopy research and technique*, **35**, 69-79.

Wallukat G (2002). The beta-adrenergic receptors. *Herz*, **27**, 683-690.

Wang H, Huang BS, Ganten D, and Leenen FH (2004). Prevention of sympathetic and cardiac dysfunction after myocardial infarction in transgenic rats deficient in brain angiotensinogen. *Circ Res*, **94**, 843.

Wang H, Huang BS, and Leenen FH (2003). Brain sodium channels and ouabainlike compounds mediate central aldosterone-induced hypertension. *Am J Physiol Heart Circ Physiol*, **285**, H2516-2523.

Weekes J, Morrison K, Mullen A, Wait R, Barton P, and Dunn MJ (2003). Hyperubiquitination of proteins in dilated cardiomyopathy. *Proteomics*, **3**, 208-216.

Wehrwein EA, Parker LM, Wright AA, Spitsbergen JM, Novotny M, Babankova D, Swain GM, Habecker BA, and Kreulen DL (2008). Cardiac norepinephrine transporter protein expression is inversely correlated to chamber norepinephrine content. *Am J Physiol Regul Integr Comp Physiol,* **295**, R857-863.

Wei SG, Yu Y, Zhang ZH, Weiss RM, and Felder RB (2008). Angiotensin II-triggered p44/42 mitogen-activated protein kinase mediates sympathetic excitation in heart failure rats. *Hypertension,* **52**, 342-350.

Weihe E, Schutz B, Hartschuh W, Anlauf M, Schafer MK, and Eiden LE (2005). Coexpression of cholinergic and noradrenergic phenotypes in human and nonhuman autonomic nervous system. *J Comp Neurol,* **492**, 370-379.

Wernli G, Hasan W, Bhattacherjee A, van Rooijen N, and Smith PG (2009). Macrophage depletion suppresses sympathetic hyperinnervation following myocardial infarction. *Basic Res Cardiol,* **104**, 681-693.

Westcott KV, Huang BS, and Leenen FH (2009). Brain renin-angiotensin-aldosterone system and ventricular remodeling after myocardial infarct: a review. *Can J Physiol Pharmacol,* **87**, 979-988.

Woodcock EA, Du XJ, Reichelt ME, and Graham RM (2008). Cardiac alpha 1-adrenergic drive in pathological remodelling. *Cardiovasc Res,* **77**, 452-462.

Xiao RP, Zhu W, Zheng M, Cao C, Zhang Y, Lakatta EG, and Han Q (2006). Subtype-specific alpha1- and beta-adrenoceptor signaling in the heart. *Trends Pharmacol Sci,* **27**, 330-337.

Xie P, Guo S, Fan Y, Zhang H, Gu D, and Li H (2009). Atrogin-1/MAFbx enhances simulated ischemia/reperfusion-induced apoptosis in cardiomyocytes through degradation of MAPK phosphatase-1 and sustained JNK activation. *J Biol Chem,* **284**, 5488-5496.

Yasunaga K and Nosaka S (1979). Cardiac sympathetic nerves in rats: anatomical and functional features. *Jpn J Physiol,* **29**, 691-705.

Yuan MJ, Huang CX, Tang YH, Wang X, Huang H, Chen YJ, and Wang T (2009). A novel peptide ghrelin inhibits neural remodeling after myocardial infarction in rats. *Eur J Pharmacol,* **618**, 52-57.

Zhang C, Xu Z, He XR, Michael LH, and Patterson C (2005). CHIP, a cochaperone/ubiquitin ligase that regulates protein quality control, is required for maximal cardioprotection after myocardial infarction in mice. *Am J Physiol Heart Circ Physiol,* **288**, H2836-2842.

Zhang W, Huang BS, and Leenen FH (1999). Brain renin-angiotensin system and sympathetic hyperactivity in rats after myocardial infarction. *Am J Physiol,* **276**, H1608-1615.

Zhang Y and Cheng Z (2000). Sympathetic inhibition with clonidine prolongs survival in experimental chronic heart failure. *Int J Cardiol,* **73**, 157-162; discussion 163-154.

Zhang ZH, Francis J, Weiss RM, and Felder RB (2002). The renin-angiotensin-aldosterone system excites hypothalamic paraventricular nucleus neurons in heart failure. *Am J Physiol Heart Circ Physiol,* **283**, H423-433.

Zhou S, Chen LS, Miyauchi Y, Miyauchi M, Kar S, Kangavari S, Fishbein MC, Sharifi B, and Chen PS (2004). Mechanisms of cardiac nerve sprouting after myocardial infarction in dogs. *Circ Res,* **95**, 76-83.

Zhu GQ, Gao L, Patel KP, Zucker IH, and Wang W (2004). ANG II in the paraventricular nucleus potentiates the cardiac sympathetic afferent reflex in rats with heart failure. *J Appl Physiol,* **97**, 1746-1754.

Zigmond RE, Chalazonitis A, and Joh T (1980). Preganglionic nerve stimulation increases the amount of tyrosine hydroxylase in the rat superior cervical ganglion. *Neurosci Lett*, **20**, 61-65.